Structure, Reactivity, and Growth Pathways of Metallocarbohedrenes M_8C_{12} and Transition Metal/Carbon Clusters and Nanocrystals: A Challenge to Computational Chemistry

Marie-Madeleine Rohmer† and Marc Bénard*,†

Laboratoire de Chimie Quantique, UMR 7551 CNRS and Université Louis Pasteur, F-67000 Strasbourg, France

Josep-M. Poblet†

Departament de Quimica Fisica, Universitat Rovira i Virgili, E-43005 Tarragona, Spain

Received April 12, 1999

Contents

I. Introduction: Fullerenes, Metallocarbohedrenes, and the Magic of the 12 Pentagons

Nature has in store a limited number of favorite shapes that are continuously rediscovered in unrelated fields. The honeycomb structures belong to that category. Made of planar hexagonal tiles, they get curved with a disclination of 60° as soon as one hexagon is replaced by a pentagon. As a consequence of Euler's theorem, they give rise to a perfectly closed architecture when the total number of "missing vertices" amounts to 12 in the whole structure.[1] The impact of the fullerene discovery[2] on the whole

† E-mail addresses: rohmer@quantix.u-strasbg.fr; benard@quantix.u-strasbg.fr; poblet@argo.urv.es.

10.1021/cr9803885 CCC: $35.00
Published on Web 01/22/2000

Marie-Madeleine Rohmer was born in 1946 in Arras, France. After graduating from the Ecole Nationale Supérieure de Chimie de Strasbourg, she received her Doctorat d'Etat in 1975 from the Université Louis Pasteur, Strasbourg, France, studying under the direction of A. Veillard. After one year of postdoctoral experience at Stanford University working on heme models with Dr. G.-H. Loew, she returned to the Université Louis Pasteur, where she is now Directeur de Recherche in Centre National de la Recherche Scientifique (CNRS). Her major research field is ab initio quantum chemistry, with special interest for large transition-metal systems and related computational problems. During the last years, she has focused on the electronic structure and topology of polymetallic nanostructures.

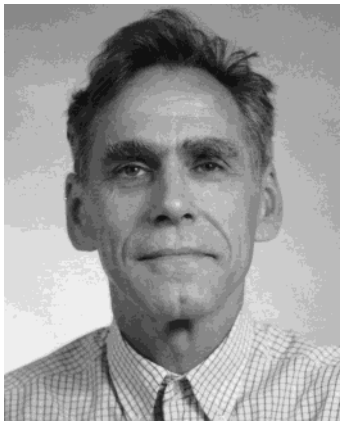

Marc Bénard was born in 1945 in Le Havre, France. He soon moved to Marseilles, started there studies in chemistry, and graduated in 1969 at the Université de Provence, after a thesis supervised by Professor André Julg and devoted to semiempirical calculations on aromatic hydrocarbons. In 1966, he entered the CNRS, the French State Agency for Research, where he is presently Director of Research 2. During a postdoctoral stay at the Max Planck Institut für Astrophysik, Munich, Germany, as a Humboldt Fellow (1972–1974), he became familiar with the various aspects of ab initio methodology. He then joined the Laboratoire de Chimie Quantique at the Université Louis Pasteur (Strasbourg, France) created in the late sixties by Alain Veillard. He became interested in the computational problems occurring in the ab initio calculation of large molecules, in the nature of the chemical bond in transition metal complexes, and in the associated distributions of electron density. Those fields of interest have then slowly evolved toward the treatment of high-nuclearity complexes, cages, and clusters by means of ab initio and DFT methodologies.

scientific community and beyond illustrates the powerful appeal of those pervasive topological patterns.

The discovery of the metallocarbohedrene class of transition metal carbide clusters by Castleman and his group in 1992[3] clearly participates in the fullerene mythology. As for the buckminsterfullerene cation C_{60}^+, the first metallocarbohedrene cluster $Ti_8C_{12}^+$ was characterized by means of mass spectrometry as

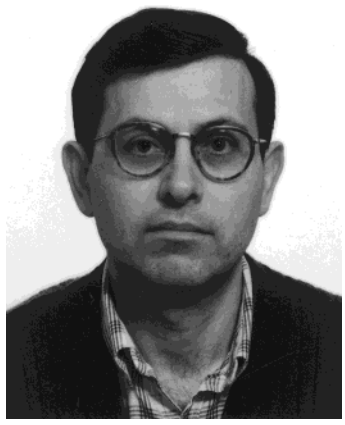

Josep-M. Poblet was born and educated in Valls, Spain, in 1956. He received his B.A. from the University of Barcelona in 1979, having done undergraduate research on theoretical studies of kinetic isotope effects in organic reactions under the supervision of Professor Enric Canadell. In 1984, he was introduced to ab initio quantum chemistry methodologies in Bénard's group. He is currently a senior lecturer in Physical Chemistry at the University Rovira i Virgili and Director of the Physical and Inorganic Chemistry Department of this university. His research field is theoretical chemistry with special interest for metallocarbohedrenes, fullerenes, polyoxoanions, and transition metal clusters.

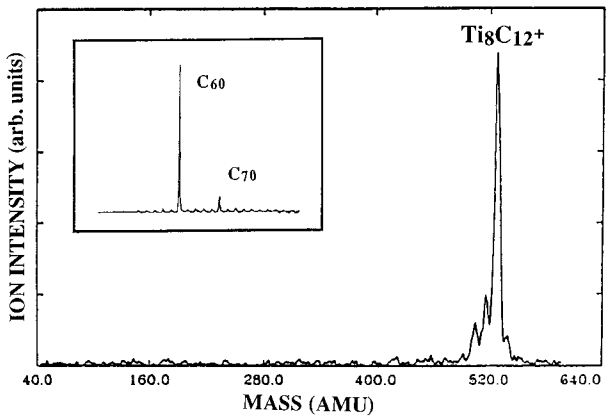

Figure 1. Mass distribution of $Ti_mC_n^+$ clusters generated from the reactions of titanium with CH_4. Reprinted with permission from ref 3. Copyright 1992 American Association for the Advancement of Science. Smaller frame: Time-of-flight spectra of carbon clusters prepared by laser vaporization of graphite, adapted from ref 2.

a "supermagic" peak totally dominant over the whole distribution of titanium carbide cluster cations (Figure 1). Then, the extraordinary abundance of $Ti_8C_{12}^+$ compared with all other $Ti_xC_y^+$ species was assigned by Guo, Kerns, and Castleman in their initial report on the possibility of achieving the smallest possible fullerene-like structure composed of 20 atoms organized along the 12 requested pentagons and containing no hexagon.[3] With its four valence electrons, neutral titanium was viewed as being "carbon-like" in the cage structure of a pentagonal dodecahedron (Figure 2) which then became isostructural, isoelectronic, and—with some restriction due to the presence of d orbitals—isolobal with the elusive C_{20} icosahedron.[4] The electronic similarity however does not hold for the M_8C_{12} clusters that were soon characterized with vanadium,[7] chromium,[8] and other metals belonging to groups 5, 6, and beyond.[8−10] Castleman soon specified that "the new met-cars are not merely a variant of the fullerenes".[11] Despite those early

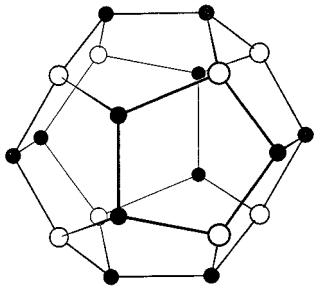

Figure 2. Structure of pentagonal dodecahedron with eight equivalent metal sites (T_h symmetry), initially proposed by Castleman's group to account for the stability of met-cars.[3]

caveats, the initial analogy with fullerenes took a large part in the success experienced by the new clusters in the chemical community. Theoretical chemistry was particularly active in designing models accounting for the stability of met-cars relative to other metal carbide clusters and predicting their chemical, physical, and spectroscopic properties. From the simple Hückel model[12] to the most elaborate ab initio and DFT treatments, more than 40 theoretical studies have been published to date.

Ironically enough, the most spectacular achievement of those theoretical studies was to evidence that the real structure of met-cars is probably not fullerene-like.[13−15] The prominent interest of many theoretical studies in the geometry and topology of the M_8C_{12} clusters should not obscure the advances that must be assigned to ab initio and DFT modeling in the prediction or interpretation of various properties of met-cars. Let us mention first the ionization potentials and electron affinities,[16−21] the effects of metal substitution leading to mixed-metal met-cars,[21] the formation of adducts with polar or nonpolar π-bonding molecules,[23] and the prediction of optical and collective electronic properties.[24] More recently, the discovery by Pilgrim and Duncan of a series of magic mass peaks assigned to metal carbide crystallites with fcc structures[25] has raised questions about the growth mechanisms leading either to met-cars or to fcc nanocrystals[10,26] and about the interconversion processes susceptible to occur between both types of clusters.[25,27] TiC_x ($x = 1-4$), Ti_2C_2, Ti_2C_3, and Nb_4C_4, considered as building blocks for either type of compound, have been the subject of theoretical investigations,[28−30] as well as small molybdenum carbide species.[31,32] Could it be that the C_2-decorated layered structures proposed by Wang and his group from DFT calculations[33] represent the "missing link" between met-cars and fcc nanocrystals?[34] The discovery, also by Wang, that the met-car peaks are far from magic and even, under certain experimental conditions, completely absent from the mass spectrum of titanium carbide *anions*[33,34] has raised the interest of theoreticians into the structures of those metal carbide clusters characterized as prominent peaks in the mass spectrum of $Ti_xC_y^-$ species.[34,35]

The recent shift of interest from M_8C_{12} alone to the wider problem of metal carbide cluster growth should not conceal that Ti_8C_{12} and to a lesser extent V_8C_{12} and the other met-cars are sharing a very special and paradoxical status: exceedingly stable, they have resisted until now all attempts of purification, either in solution or as a solid material. Production in macroscopic quantity in the soots generated in an arc between two composite Ti−C electrodes has been reported however, first, by Castleman's group[36] and, very recently, by Selvan and Pradeep.[37] In both reports, the presence of met-cars in the soots could be established either from the mass spectrum of laser desorbed soot or from the mass spectrum of thermally vaporized material from soot exposed to organic solvents. Even though the met-car abundance in some samples was estimated to ∼1%,[36] the clusters were found extremely air-sensitive and undergo complete degradation within a few minutes.[37] Theoretical modeling therefore remains one of the most powerful instruments to investigate the chemical and physical properties of this "new class of molecular clusters".[38]

II. Structure of Met-Car Cages: Suggestions, Controversies, and Computational Evidence

A. Electronic Structure of the Pentagonal Dodecahedron

Since the very first paper by Guo, Kerns, and Castleman reporting evidence for a new class of stable molecular clusters,[3] arguments relevant to the electronic structure have been used to support various topologies for the M_8C_{12} clusters. Castleman's group relied on the identical valence electron count between carbon and titanium to promote for Ti_8C_{12} the fullerenoid cage structure of Figure 2 kept rigid by 30 strong σ bonds and stabilized by a 20-electron π system delocalized over the whole cluster.[3] This representation of the electronic structure directly adapted from that of C_{20} also applies without change to the isoelectronic species Zr_8C_{12} and Hf_8C_{12} characterized soon after.[7] Lin and Hall[39] adapted this strictly covalent interpretation to the language of organometallic chemistry by describing the C_2 entities as ethylenic ligands, formally $(-C{=}C-)^{4-}$ bonded through σ donation to transition metal atoms in the 3+ oxidation state. In the test calculation carried out on the d^0 cluster Y_8C_{12}, the π system was found strongly localized on the C_2 fragments.[39] At variance with Castleman's conjecture, the extensive delocalization of the 20 π electrons in C_{20} was predicted to make the dodecahedral cluster subject to Jahn−Teller distortion and to be at least partly responsible for its instability, together with σ strain.[4,5] The alternative model proposed by Lin and Hall for dodecahedral Ti_8C_{12} and for the other met-cars explained their stability by maximizing the strength of the π bonds in the C_2 fragments and adding on the top weakly π bonding interactions between the dicarbons and the metal d electrons. The stabilizing effect of those interactions was however expected to be partly offset by the Pauli repulsion between the metal atoms and the dicarbon fragments, especially when electron-rich metals were involved.[39]

Subsequent studies carried out by Lin and Hall on Zr_8C_{12} and Nb_8C_{12},[14] and by Hay on Ti_8C_{12} and V_8C_{12},[40] confirmed the extremely localized character of the metal(III) d electrons in the dodecahedral

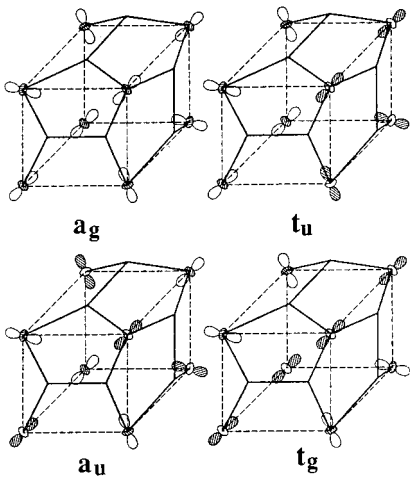

Figure 3. Molecular orbitals arising from linear combinations of localized d_{z^2}-like orbitals on each Ti oriented along the body diagonals (C_{3v} axes) of the Ti_8 cube in dodecahedral Ti_8C_{12}. Reprinted with permission from ref 40. Copyright 1993 American Chemical Society.

cages. For met-cars made of group 4 metals, the electronic state of lowest energy is a high-spin configuration (^9A_g) obtained by distributing the eight metal valence electrons (an oxidation state of +3 being assumed) into the eight combinations of radially outpointing orbitals with appropriate symmetry (Figure 3). Those orbital combinations are obtained from the coalescence of eight pyramidal $Ti(CH_3)_3$ fragments in which the remaining metal electron is accommodated in a d_{z^2} orbital collinear to the C_3 axis:

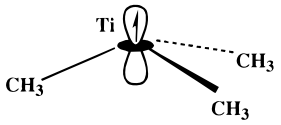

Those d_{z^2}-like combinations are nonbonding within the metal framework with respect to the C_2 π^* orbitals, which rules out any possibility of a delocalized π system. Adding eight metal electrons as in V_8C_{12} or Nb_8C_{12} yields a closed-shell configuration in which the eight orbital combinations of Figure 3 are doubly rather than singly occupied. Electronic configurations yielding delocalized π systems were characterized at much higher energies. For Ti_8C_{12}, the lowest electronic state leading to a 20-electron π-system is a ^3T_g state destabilized by 250 kcal·mol^{-1}.[40] For Zr_8C_{12}, a closed-shell configuration is found at +235.5 kcal·mol^{-1}.[14] The 28-electron π-system that could be expected for V_8C_{12} is also destabilized by more than 300 kcal·mol^{-1} with respect to the closed-shell ground state.[40]

In the two years that followed the discovery of met-cars, several implementations of the density functional theory (DFT) in its local approximation were applied to various M_8C_{12} systems, either existing or hypothetical. In most cases, the M_8C_{12} systems were assumed to adopt the structure of a pentagonal dodecahedron. Some of those reports were based upon single-point calculations performed with fixed geometries.[18,41−43] When the geometry of the dodecahedral cluster is optimized, the gradient minimization is carried out by assuming the constraints of a subset of the real point group T_h, namely D_{2h}[17,44−46] or C_{2v},[16] but the optimal structure does not significantly deviate from the T_h symmetry. One optimization process was carried out with the constraints of the icosahedral point group, assuming identical distances for C−C and Ti−C.[47] All calculations predicted large binding energies per atom (~6.6 eV) for Ti_8C_{12} as for other met-cars involving transition metals of groups 4 and 5 (Table 1). Subsequent calculations showed however that gradient corrections reduce the stabilization energies by 0.8−1.5 eV, depending on the exchange-correlation functional.[27,48,49] Grimes and Gale[17] also compared the stability of M_8C_{12} species (M = Zr, Ti, V, Fe, Si) not only with respect to individual atoms but also with respect to several forms of starting material. All dodecahedral met-cars were found stable with respect to bulk metal and graphite, except for Zr_8C_{12}, less stable by 0.77 eV. However, for the three cases where solid metal carbides are known (M = Zr, Ti, Si), all of the clusters are unstable according to the reaction

$$M_8C_{12} \rightarrow 8MC_{solid} + 4C_{graphite} \qquad (1)$$

For Ti_8C_{12}, the destabilization amounts to 9 eV, even though some energy is expected to be recovered from the condensation of macroscopic met-car into a crystalline phase.[17] Several authors also noted that the stabilization energy per atom obtained for Ti_8C_{12} (~6.6 eV) is significantly lower than that computed in the same conditions for titanium carbide (7.1−7.2 eV).[16,50]

Most reports based upon DFT calculations note that the energy levels are very densely spaced in the upper valence region with no real HOMO−LUMO gap.[17,18,41,44,45] When translated into a density of states by using a smearing function to broaden the energy levels, overlapping bands are obtained across the Fermi level, endowing the dodecahedral cluster with a typically metallic character.[16,18,24,41−43,45] This high density of states in the region of the Fermi level is in agreement with the Hartree−Fock results of Hay[40] and of Lin and Hall[14] eventually leading to a nonet ground state. However, most calculations carried out on dodecahedral Ti_8C_{12} and analyzed in terms of discrete Kohn−Sham orbitals assigned the ground state to be a triplet, due to the triply degenerate character of the HOMO occupied with either two electrons[17,41,42,44,45,47] or four electrons.[43] Rantala et al.[46] pointed out that the four orbitals arising in the region of the Fermi level of Ti_8C_{12} are separated by no more than 0.16 eV and are populated by four electrons distributed according to Fermi−Dirac statistics. Li et al.[18] proposed a closed-shell electronic structure, but the HOMO−LUMO gap does not exceed 0.07 eV. The analysis of the electronic structure in terms of a triply degenerate HOMO populated with two electrons is in agreement with the orbital sequence stemming from simple Hückel[12] and from extended Hückel[51] calculations. Several authors noted that such a configuration could favor Jahn−Teller distortion,[12,16,50] but the fractional occupation numbers assigned to the densely spaced

Table 1. Binding Energy Per Atom Computed at Various Levels of the DFT Methodology for Known or Hypothetical Met-Cars, Isostructural Boron or Nitrogen Metal Clusters, Endohedral Met-Cars $C\subset Ti_8C_{12}$, and Face-Centered Cubic Nanocrystals $Ti_{14}C_{13}$[n]

	LDF[a] (17)	LDF[b] (45,67)	DVM[c] (66,150)	LCGTO[d] (16,68)	FP-LMTO[e] (50)	LDF[f] (46)	DV-Xα (42)	DFT[g] (49)	LDA[h] (18)	LDF[a] + NL[i,j] (27)	LDF + NL[k] (21,48)
Ca_8C_{12}		5.25									
Si_8C_{12}	6.03										
Sc_8C_{12}											(5.44)/(5.95)[m]
Ti_8C_{12}	6.67	6.64	6.1	6.62	6.61	6.12	6.65	6.79 (5.95)	6.25		
Ti_8C_{12} (D_{2d})		7.35	6.66	7.1			7.38	7.47 (6.54)			
Ti_8C_{12} (T_d)		7.50								(5.92,[i] 6.19[j])	(6.56)
$(Ti_8C_{12})^+$ (T_d)										(5.69,[i] 5.95[j])	
$Ti_4Zr_4C_{12}$ (T_d)											(6.70)[l]
Zr_8C_{12}	6.90						6.48	6.60 (6.03)			
Zr_8C_{12}(D_{2d})						7.28	7.37(6.62)				
Zr_8C_{12}(T_d)											(6.81)
V_8C_{12}	6.81		5.7			6.18					(5.94)/(6.5)[m]
V_8C_{12}(D_{2d})							7.00 (5.92)				
Cr_8C_{12}											(4.6)/(5.1)[m]
Mn_8C_{12}											(4.61)/(5.0)[m]
Fe_8C_{12}	6.27		5.5								(4.98)/(5.3)[m]
Co_8C_{12}											(5.65)/(5.7)[m]
Ni_8C_{12}											(5.11)/(5.15)[m]
Cu_8C_{12}											(4.37)/(4.9)[m]
Zn_8C_{12}		4.65									(3.87)/(3.7)[m]
$C\subset Ti_8C_{12}$		6.55									
$C\subset Ti_8C_{12}$ (D_{2d})		7.40									
$C\subset Ti_8C_{12}$ (T_d)		7.51								7.39[b] (5.88[i], 6.15[j])	(6.52)
Ti_8C_{13} (exo C)											(6.41, 6.42)
$(C\subset Ti_8C_{12})^+$ (T_d)										(5.61[i], 5.90[j])	
$C\subset Zr_8C_{12}$ (T_d)											(6.79)
Zr_8C_{13} (exo C)											(6.66, 6.67)
Sc_8B_{12}	5.05										
Al_8N_{12}	4.60										
Ti_8N_{12} (D_{2d})		4.2	5.9								6.54 (5.51)
$Ti_8N_4C_8$ (D_{2d})			6.7								
Ti_6C_6 (2 × 2 × 3, fcc)		6.3									
Ti_9C_9 (2 × 3 × 3, fcc)		6.6									
$Ti_{14}C_{13}$ (3 × 3 × 3, fcc)		6.74								7.28[b] (5.70[i], 5.97[j])	
$(Ti_{14}C_{13})^+$ (fcc)										(5.54[i], 5.81[j])	

[a] Local density functional: *DMol, version 2.1*; BIOSYM Technologies: San Diego, CA, 1991. [b] Exchange-correlation functionals of Hedin and Lundqvist,[69a] parametrization by von Barth and Hedin (1972).[69b] Results are very similar to those obtained with DMOL. [c] Hamiltonian matrix elements needed in solving the Kohn−Sham equation are obtained by direct numerical integration over a diophantine mesh. [d] Same method as fnt *c*, but the numerical atomic functions are replaced by a complete set of Gaussian basis functions giving more flexibility.[16,66] [e] Full-potential linear muffin-tin orbital method. [f] Exchange-correlation functional of von Barth and Hedin (1964).[70] [g] Spin-polarized density functional using the program package DGauss.[71] Numbers in parentheses include nonlocal corrections of Becke and Perdew to the exchange-correlation energy.[72] [h] DFT/LDA equations solved by means of the discrete variational method.[73] [i] Vosko−Wilk−Nusair functional[74] for the local electron correlation, Hartree−Fock−Slater $\rho^{1/3}$ local exchange function, and Becke nonlocal correction[72a] for exchange. [j] Same as in fnt *i*), but the Lee−Yang−Parr functional[75] is used for the local and nonlocal components of correlation. [k] ADF program;[76] nonlocal corrections of Becke and Perdew to the exchange-correlation energy.[72] [l] Calculations carried out using the constraints of the C_{3v} point group. Similar binding energies were obtained for the two isomers where the four zirconium atoms occupy either the sites of the *inner* tetrahedron (133.999 eV) or those of the *capping* tetrahedron (133.977 eV). [m] Left hand-side, value computed for the T_h conformation; right hand-side, value computed for the T_d conformation. [n] Unless explicitly indicated, calculations assume for met-cars the pentagonal dodecahedral structure (T_h symmetry). Most results are obtained by means of the Local Density Approximation. When available, computed binding energies accounting for nonlocal corrections are given in parentheses.

eigenstates precluded any significant deviation from the T_h symmetry.[50] The nature of the DFT formalism which accounts for the nondynamic correlation effects certainly precludes any similarity between the low-spin states reported in the latter investigations and the delocalized π states with very high energy obtained from ab initio SCF calculations, since single determinant Hartree−Fock wave functions are unable to properly describe the delocalization of transition metal d electrons. In that context, it would have been of interest to characterize within the DFT formalism the high-spin state advocated from the ab initio calculations. The only attempt to compare states with different spin multiplicities for the T_h form of Ti_8C_{12} is reported by Chen et al.,[49] who found the singlet state to have the lowest energy.

B. Alternative Structures for Met-Cars

The burst of early studies on dodecahedral met-cars eventually left unanswered the problem raised by the mass spectrum of Figure 1: why are $Ti_8C_{12}^+$ and related clusters so stable? DFT calculations agree on the lack of any HOMO−LUMO gap, which means that the titanium carbide dodecahedron, either neutral or cationic, is not electron precise in the sense of Mingos.[52] Extended Hückel calculations reported

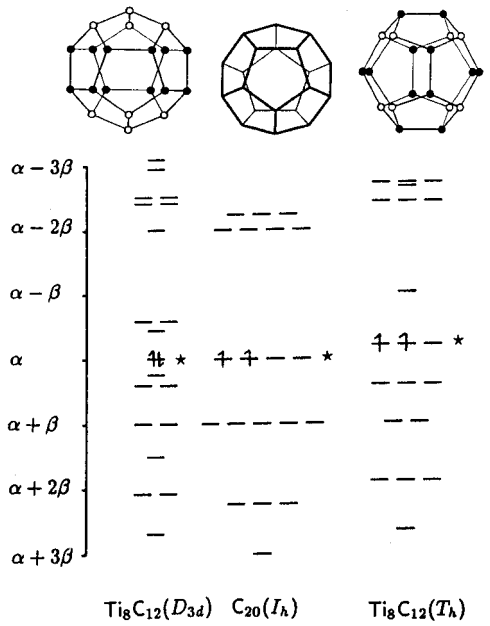

Figure 4. Hückel energy levels for 20-atom, 20 π electron cagelike molecules. Left: Ti_8C_{12} (D_{3d}, model proposed by Ceulemans and Fowler[64]). Center: icosahedral C_{20}. Right: Ti_8C_{12} (pentagonal dodecahedron, model proposed by Castleman et al.[3]). The star marks the HOMO and arrows indicate its occupation. Reprinted with permission from ref 12. Copyright 1993 The Royal Society of Chemistry.

by Srinivas et al.[51] confirm the high density of the upper valence levels. The nonet ground state of Ti_8C_{12} found from Hartree−Fock calculations accommodates the eight metal electrons in localized orbitals which are nonbonding with respect to either metal−metal or metal−dicarbon interactions.[53] Both the DFT and the HF descriptions are therefore strongly at variance with the expected fullerene model characterized, at least for C_{60}, by a relatively large HOMO−LUMO gap[56] (1.7 eV from local density functional calculations;[57] 7.3 eV at the Hartree−Fock level with TZP basis set[58]) and by an important stabilization of the highest occupied orbitals by means of a π system delocalized over the whole molecule. Furthermore, the population of the radially oriented d_{z^2}-like metal orbitals occupied with either one electron in Ti_8C_{12} or two electrons in V_8C_{12} seems difficult to reconcile with the observation of association products between met-car cations and polar, σ-donor molecules (NH_3,[3,7a,59,60] H_2O,[59,60] methanol,[59−61] acetone,[62,63]...).

Pursuing the analogy with fullerenes and C_{20}, Ceulemans and Fowler[64] reminded that the $(4k + 2)$ Hückel numbers which give the optimal dimension of the π system for cyclic molecules can be extended to the case of three-dimensional clusters, eventually defining closed shells of delocalized electrons which follow a $2(k + 1)^2$ counting rule.[65] Icosahedral C_{20} or fullerenoid Ti_8C_{12}, with 20 π bonding electrons, are therefore expected to have two electrons beyond the 18 needed to fill the shell corresponding to $k = 2$. A triplet state, giving rise to a Jahn−Teller instability, was therefore predicted for neutral Ti_8C_{12}, as it had been for C_{20},[5] in agreement with the orbital ordering deduced from a simple Hückel treatment (Figure 4).

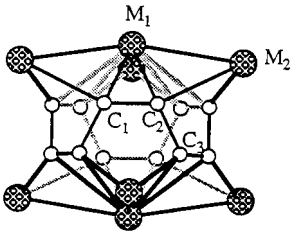

Figure 5. The C_{3v} structure of M_8C_{12} proposed by Ceulemans and Fowler[64] and optimized by Lin and Hall with M = Y and Nb. Reprinted with permission from ref 14. Copyright 1993 American Chemical Society.

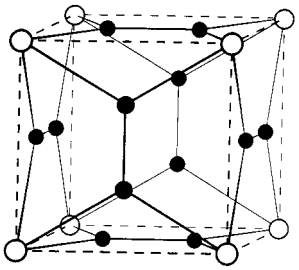

Figure 6. "Cubic" structure proposed for Ti_8C_{12} by Pauling from qualitative valence bond considerations. Reprinted from ref 78. Copyright 1992 National Academy of Sciences of the USA.

In application of the epikernel principle which requires that Jahn−Teller distortions preserve as many symmetry elements as possible,[64,77] the configurational instability of Ti_8C_{12} was predicted to be removed most effectively by lowering the symmetry from T_h to D_{3d}. Rather than considering a limited distortion of the dodecahedral cage, Ceulemans and Fowler proposed an alternative structure composed of a fully conjugated ring of 12 carbons atoms capped by two Ti_4 tetrahedra.[64] The sequence of Hückel levels (Figure 4) shows that the model proves successful in removing the ground-state degeneracy. Lin and Hall[14] optimized the geometries of Y_8C_{12} and Nb_8C_{12} by assuming the D_{3d} structure. With capping M_4 units close to planarity, the optimal D_{3d} clusters significantly deviate from the quasi-spherical shape implicitely postulated by Ceulemans and Fowler (Figures 4 and 5). As far as energy is concerned, the performance of the D_{3d} form with respect to the dodecahedral topology is surprisingly good: at the Hartree−Fock level of calculation, the trigonal conformation of Y_8C_{12} is more stable than the dodecahedral one by 20.1 kcal·mol^{-1} and the two forms of Nb_8C_{12} have similar energies.[14] The trigonal shape was however not investigated further since the isomer with T_d symmetry, whose calculated stability outperforms all other structures, had been proposed in the meantime by Dance[13] and by others.[15]

More exotic structures were advocated on the basis of qualitative considerations, or semiempirical calculations. In the very first theoretical report on the structure of Ti_8C_{12}, Pauling relied on valence bond and orbital hybridization arguments to suggest that the six C_2 groups are not protruding outside the cubic metal framework.[78] Let us note that Pauling's "cubic" architecture (Figure 6) is not topologically distinct from Castleman's pentagonal dodecahedron and was never singled out as an energy minimum associated

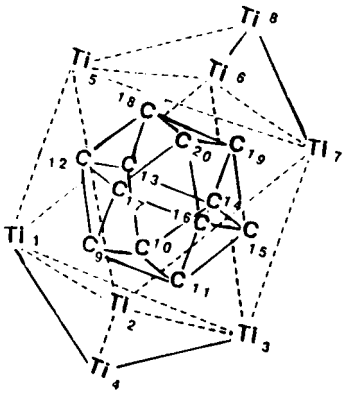

Figure 7. Bicapped antiprism structure advocated by Khan for Ti_8C_{12} from semiempirical calculations. Reprinted with permission from ref 80. Copyright 1995 American Chemical Society.

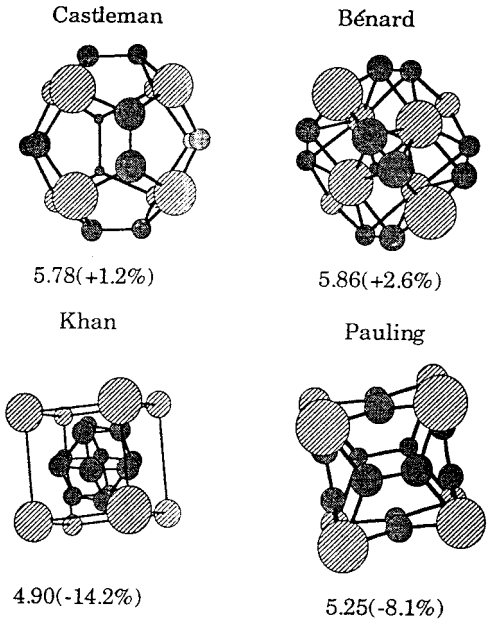

Figure 8. Prediction of the ion mobility of the $Ti_8C_{12}^+$ ion (in $cm^2\ V^{-1}\ s^{-1}$) as a function of the structure, by means of a Monte Carlo technique. Also shown is the percent deviation from the experimental mobility ($5.71 \pm 0.05\ cm^2\ V^{-1}\ s^{-1}$). Reprinted with permission from ref 84. Copyright 1994 American Chemical Society.

with that topology. Reddy and Khanna[66] optimized the geometry of the cubic structure by constraining the C_2 units to remain coplanar with the faces of the metal framework. They ended up with a conformation destabilized by 17 eV with respect to a "standard" pentagonal dodecahedron.[66]

Khan relied on Zerner's ZINDO UHF method[79] to optimize for Ti_8C_{12} a series of structures ("metal-decorated cages" or MDC) based upon the encapsulation of an icosahedral C_{12} cluster in a metal cage shaped either as a distorted cube or as a bicapped trigonal antiprism (Figure 7).[80] According to Khan, the relatively low stabilization energy per carbon atom obtained for the C_{12} cluster[81] is overcompensated by the large number of stabilizing metal−carbon interactions. The very large stabilization energy reported for the antiprism MDC (6.95 eV/atom) is estimated by summing up stabilizing contributions assigned to all Ti−C and Ti−Ti contacts less than a given threshold.[80] Despite the author's claim, such a simplistic estimate cannot be compared to the values obtained from a quantum chemical treatment of the whole system. The mechanism proposed by Khan to explain the formation of the MDC, namely the attachment of metal atoms to a preexisting C_{12} core, was ruled out by Cartier et al. on the basis of experimental evidence.[82] Despite the characterization of a metal-decorated structure very close to Khan's MDC for the bcc crystal of KAl_{13},[83] the comparison between various techniques used to produce single-metal and mixed-metal met-cars rather supported a single-step mechanism for the metal carbide cluster formation.[82] The MDC structures, as well as Pauling's cubic conformation, were also discarded on the basis of Monte Carlo simulations aimed at reproducing, as a function of the cluster shape, the mobility of met-car cations deduced from ion chromatography experiments (Figure 8).[84]

C. Dance's Tetracapped Tetrahedron and Related Conformations

More than 20 years before the discovery of met-cars, a problem inherently related to the topology of A_8B_{12} polyhedra had been proposed as an exercise on the symmetry groups of "nonmolecular objects" in Cotton's textbook "Chemical Applications of Group Theory".[85] The problem is composed of two questions:

1. What is the symmetry of a cube when a line is drawn across each of its faces in the manner shown in Figure 9? The figure is reminiscent of Pauling's

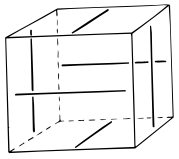

Figure 9. "Nonmolecular object" designed by Cotton to illustrate a transformation from T_h to T_d symmetry. Reprinted with permission from ref 85. Copyright 1971 Wiley-Interscience.

"cubic" interpretation of the pentagonal dodecahedron, but we have seen that this representation is equivalent to that of Figure 2 as far as topology and group theory are concerned. Then, the symmetry point group is T_h.

2. Suppose that the line on each face of the cube is rotated by θ, where $0 < \theta < 45°$ in the clockwise direction as seen from the outside. What is the point group now? *If the angle of rotation is 45°, what is the point group?* The transformation proposed in the last part of question 2 is topologically similar to the one reported by Dance in his first communication on the geometric and electronic structure of Ti_8C_{12} and summarized in Figure 10.[13] The cluster on the left represents the standard pentagonal dodecahedron in the geometry optimized by Dance within the framework of he DFT/LDA methodology and assuming the constraints of the D_{2h} point group. The optimal parameters (Ti−Ti = 3.02 Å, Ti−C = 1.99 Å, C−C = 1.40 Å) eventually agree with the T_h symmetry of the

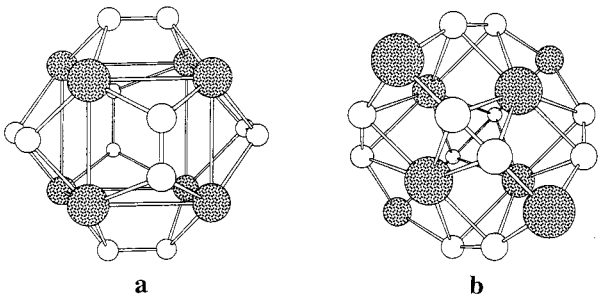

Figure 10. Ti_8C_{12}: the pentagonal dodecahedron (a, T_h symmetry) and the tetracapped tetrahedron of metal atoms (b, T_d symmetry) as optimized by Dance from DFT calculations. Reprinted with permission from ref 13. Copyright 1992 The Royal Society of Chemistry.

cluster and are in keeping with most reports on DFT and Hartree−Fock gradient optimization on Ti_8C_{12}.[40,44,45,49,50,66,86] The right side of Figure 10 presents another geometrical isomer of Ti_8C_{12} deduced from the pentagonal dodecahedron by the transformation described in Cotton's textbook, except that the six C_2 fragments have been rotated in the *counterclockwise* direction. All metal atoms, as well as all carbon atoms, were equivalent in the dodecahedral cluster. The concerted 45° rotation breaks this equivalence and discriminates two types of metal atoms, each of which occurring four times: (i) the atoms that are bonded *side-on* to three dicarbons; (ii) the atoms that are bonded *end-on* also to three dicarbons. All carbon atoms remain equivalent.

The topology of the new cluster then does not constrain anymore the eight metal atoms to form a perfect cube and authorizes a tetrahedral distortion. The four metal atoms coordinated side-on define an *inner tetrahedron* with short metal−metal distances (Ti^i-Ti^i = 2.86 Å in Dance's initial geometry obtained from gradient optimization at the LDA level).[13] There are 24 $Ti^i-C_{side-on}$ bonds with a distance of 2.19 Å. Then, the four remaining metal atoms define a second, outer tetrahedron (Ti^o-Ti^o = 4.82 Å) capping the faces of the innermost one. Each metal atom belonging to the capping tetrahedron has three nearest *carbon* neighbors defining a total of 12 Ti^o-C_{end-on} bonds (1.93 Å) and three nearest *metal* neighbors belonging to the inner tetrahedron (Ti^o-Ti^i = 2.90 Å). There is only one type of C−C bond (1.34 Å). This cluster isomer belongs to the symmetry point group T_d.[87]

The tetracapped tetrahedron (T_d) was found more stable than the pentagonal dodecahedron (T_h) by a considerable amount: 351 kcal·mol^{-1} at the LDA level,[13] slightly reduced to ∼ 300 kcal·mol^{-1} for the neutral as for the cationic cluster when the nonlocal corrections are accounted for (Table 1).[27] In a subsequent work, Dance investigated the transformation pathway from the T_h form to the T_d isomer.[88] Apart from a small energy bump (0.3 kcal·mol^{-1} at the very beginning of the distortion pathway), the transformation proceeds barrierless along a reaction path constrained with the D_2 symmetry (Figure 11).[89]

The pathway from T_h to T_d can be described as a concerted displacement of four titaniums moving inward to give the inner tetrahedron, while the four

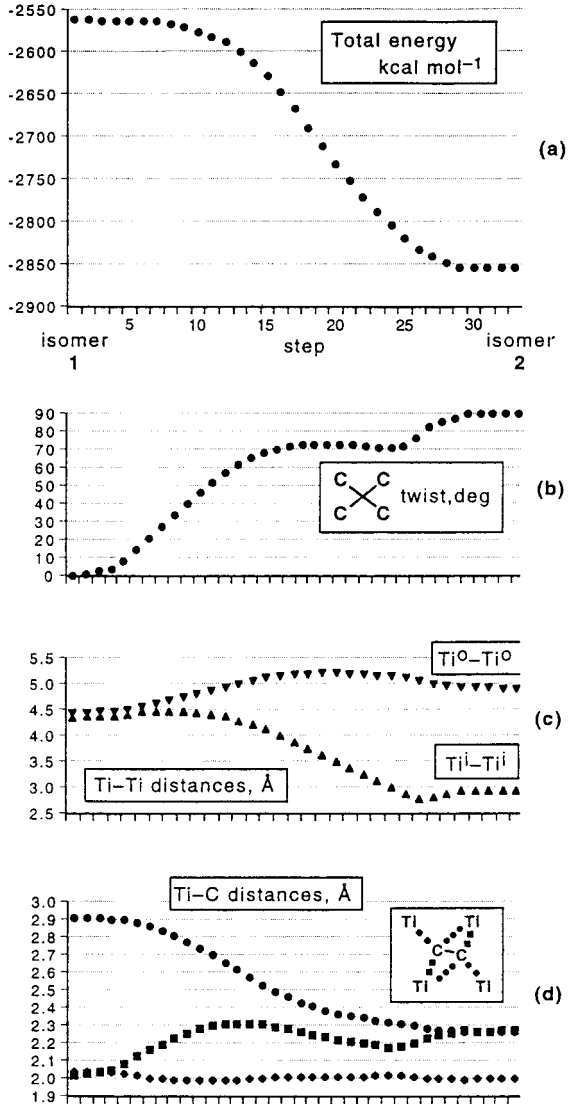

Figure 11. Energy and geometry changes during 33 steps of the transformation of the pentagonal dodecahedron (isomer 1) to the tetracapped tetrahedron (isomer 2): (a) binding energy (kcal·mol^{-1}); (b) twist of opposite C_2 groups, expressed as the C−C−C−C torsional angle; (c) the Ti^i-Ti^i and Ti^o-Ti^o distances (Å); (d) three relevant types of Ti−C distances (Å). The imposed symmetry was D_2. Reprinted with permission from ref 88. Copyright 1996 American Chemical Society.

other move outward to give the capping tetrahedron and the six (C_2) describe the 45° clockwise (or counterclockwise) rotation (Figure 11). Since the initial energy bump of 0.3 kcal·mol^{-1} is easily overstepped by the ambient thermal energy, Dance's calculations suggest that the pentagonal dodecahedron is not a local minimum and has therefore no chance to exist. Similar isomerization processes were defined for $Ti_8C_{12}^+$, Zr_8C_{12}, V_8C_{12}, and Nb_8C_{12}.[88]

Other isomers of met-cars can be thought of by removing the condition that the six C_2 fragments are rotated *in the clockwise (or counterclockwise) direction as seen from the outside*. One can imagine a third question to Cotton's exercise that could be termed as follows: "If each line of Figure 9 is rotated arbitrarily in the clockwise or in the counterclockwise direction by 45°, how many distinct figures will be obtained

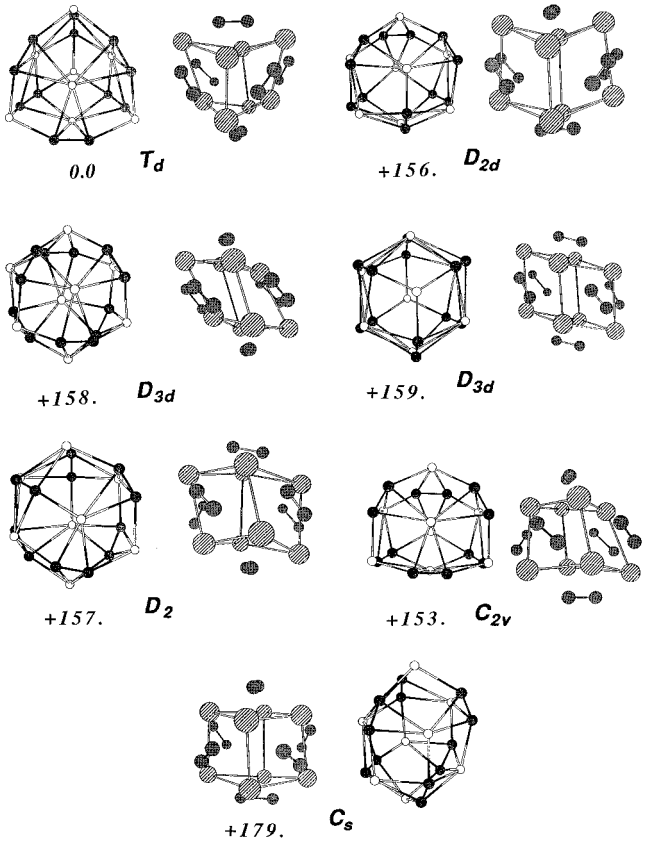

Figure 12. Optimized geometries (ab initio RHF) and relative energies (CI level, kcal·mol^{-1}) of the seven minima characterized by Rohmer et al.[90] on the potential energy surface of Ti_8C_{12}. Energy 0.0 corresponds to the $^1A_1$ ground state obtained for the T_d isomer at the multireference CI level.

and what will be their symmetry?" An easy, though tedious way of solving the problem consists of scanning all of the 2^6 possibilities: the seven isomers of Figure 12 are obtained, each one occurring a certain number of times. The solution could also be formalized as follows:

One isomer corresponds to the rotation of all lines in the same direction. It occurs twice (one for the clockwise concerted rotation, and the other for the counterclockwise rotation) and generates Dance's cluster with T_d symmetry.

A second isomer is generated by rotating five lines in one direction and the last one in the opposite direction. The symmetry is C_{2v}, and the number of occurrences is 12.

The rotation of four lines in one direction and two lines in the opposite one generates two distinct isomers depending on the location of the last two lines either on adjacent faces (C_s, 24 occurrences) or on opposite ones (D_{2d}, 6 occurrences).

Finally, an equal distribution of the lines rotated clockwise or counterclockwise should generate two isomers. When two lines rotated in the same direction are on opposite faces, an isomer with D_2 symmetry is obtained, occurring 12 times. When the three lines rotated in the same direction occupy adjacent faces, the obtained isomer has D_{3d} symmetry (8 occurrences).

We are eventually left with six isomers, and one is clearly missing when compared with Figure 12. The error should be assigned to the form with D_{3d} symmetry. In that case, and at variance with all others, inverting the rotation direction of all six lines (clockwise → counterclockwise and vice-versa) generates topologically distinct isomers, both with D_{3d} symmetry (Figure 12).

The geometries of the seven isomers of Ti_8C_{12} have been optimized at the ab initio RHF level and their energies compared at the RHF level[15] and then at the CI level[90] by Rohmer et al. The form with T_d symmetry, similar to Dance's cluster, is the most stable one at both levels of theory. At the RHF level, the relative energies are scattered between 0 (T_d) and +259 kcal·mol^{-1} (D_{3d}). The large range and the spreading of relative energies at the SCF level should be assigned to problems of nondynamic correlation generated by the delocalization of metal d electrons over several titanium atoms.[91] Single reference and—for the T_d form—multireference CI expansions were carried out in order to correlate the 20 metal electrons and then to eliminate the most severe effects of nondynamic correlation.[90] The result was a clustering of the relative energies of the six nontetrahedral isomers at 150−180 kcal·mol^{-1}, that is, 0.32−0.39 eV/atom above that of the T_d form (Figure 12).

Chen et al.[49] reported a work independent from that of Dance[13] and leading to very similar conclusions, except that the isomer found to be much more stable than the pentagonal dodecahedron was the one with D_{2d} symmetry. This may not be surprising if it is remembered that the D_{2d} form was found second lowest in energy, just after the T_d isomer, from the HF/CI calculations of Figure 12. Geometry optimization processes were carried out by Chen for the T_h and D_{2d} forms of Ti_8C_{12}, Ti_8N_{12}, Zr_8C_{12}, and V_8C_{12} using the spin-polarized density approximation as implemented in the DGauss program.[71] The cluster bonding energies are reported at the LDA level and also after introducing the nonlocal corrections of Becke and Perdew (Table 1). For Ti_8C_{12}, the energy difference between the D_{2d} and the T_h isomers is 314 kcal·mol^{-1} at the LDA level,[49] not so different from the 351 kcal·mol^{-1} stabilization claimed by Dance for the T_d form.[14] Moreover, it was proved[49] that the T_h dodecahedron structure is energetically unstable against a Jahn−Teller distortion leading to the D_{2d} form, as it is with respect to the T_d isomer.[88] It must be noted that the enhanced stability of the T_d or the D_{2d} form of Ti_8C_{12} makes the formation of those isomers exothermic with respect to metal carbide and graphite.

The D_{2d} isomer of Chen et al. has been reinvestigated in subsequent DFT studies and compared to the T_h form with similar conclusions.[42,45,49,67] The report by Lou and Nordlander[67] is particularly interesting since it is the only one to compare the three isomers T_h, T_d, and D_{2d} with the same DFT formalism (LDA using von Barth−Hedin exchange-correlation potential[70]). The metal−metal distances in the D_{2d} form (2.79 and 2.84 Å) are found shorter by ∼ 0.10 Å than in the T_d isomer and by ∼0.20 Å with respect to the dodecahedral form, which raises the question

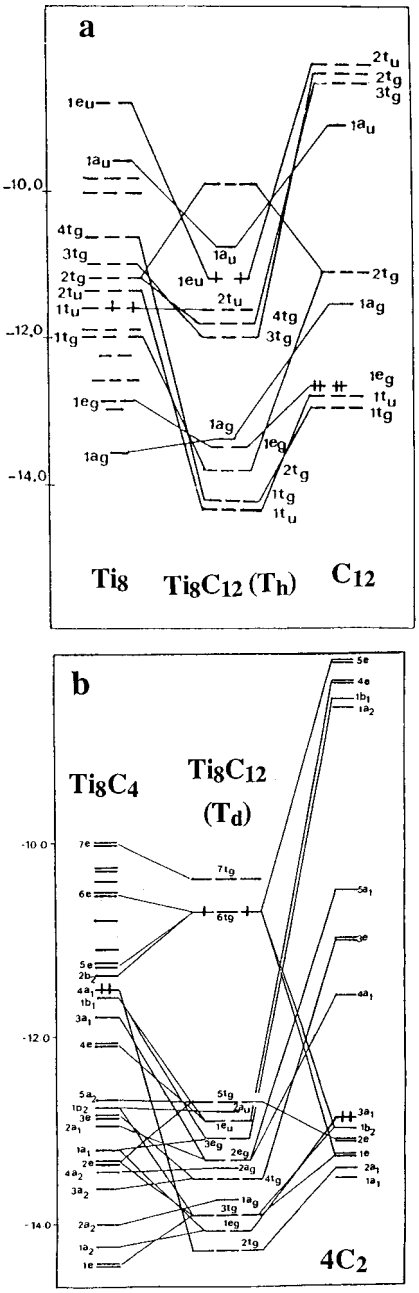

Figure 13. (a) Left-hand side: interaction diagram between cubic Ti_8 and six C_2 to give the dodecahedral conformer. (b) Right-hand-side: energy levels of the tetracapped tetrahedron conformer for Ti_8C_{12} and $4C_2$ units. From extended Hückel calculations by Srinivas et al. Reprinted with permission from ref 51. Copyright 1994 Indian Academy of Sciences.

of the existence of metal−metal bonds.[92] However, the T_d form is found more stable than the D_{2d} one by $\sim$ 70 kcal·mol^{-1} (0.15 eV/atom, Table 1).[67] The HOMO−LUMO gap in the T_d structure remains practically inexistant (0.23 eV), and close-lying states with different spin multiplicities are expected at low temperature for the neutral cluster. By contrast, the gap between the HOMO and HOMO-1 appears quite large (1.62 eV) in agreement with the extended Hückel diagram of Srinivas et al. (Figure 13).[51] Those orbital diagrams suggest a still enhanced stability for the cation or for the dication of tetrahedral Ti_8C_{12}.

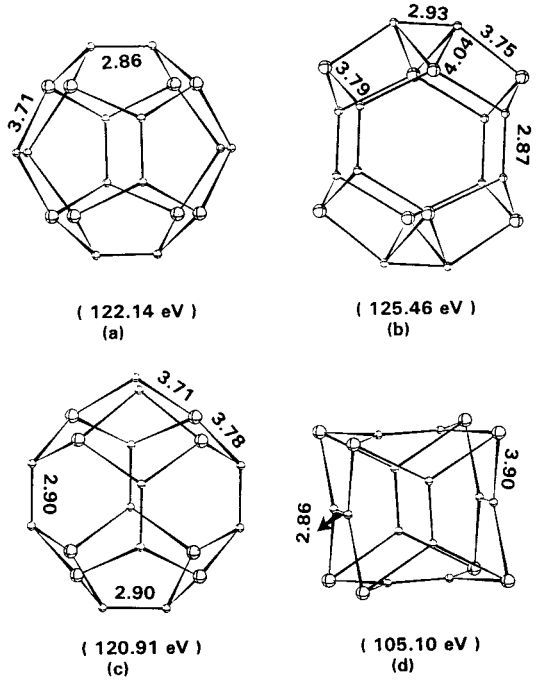

Figure 14. Some geometrical structures of Ti_8C_{12} optimized within the DFT formalism and associated binding energies with respect to free atoms. The bond lengths are in atomic units. Form (d) corresponding to Pauling's structure was not found to be a local minimum; the C_2 dimers were constrained to stay in the cubic faces. Reprinted with permission from ref 66. Copyright 1993 Elsevier.

For the D_{2d} conformation, a slightly enhanced HOMO−LUMO gap (0.5 eV) suggests that the ground state of that isomer could be a closed-shell singlet, as calculated by Chen et al.[49]

The work of Lou and Nordlander confirms that the T_d and the D_{2d} structures are both local minima in the potential energy hypersurface. It is not excluded that they could coexist in the cluster source, even though all calculations agree that the thermodynamic balance will eventually favor the T_d form. The low energy found for both isomers with respect to the T_h form suggests that the acetylenic coordination of the C_2 units, which combines σ and π donation and provides opportunities for back-donation, is systematically favored with respect to the ethylenic coordination characteristic of the dodecahedral form. In that respect, it is interesting to note that a "hybrid" Ti_8C_{12} cluster, combining two acetylenic with four ethylenic C_2 fragments, has been investigated by Reddy and Khanna (Figure 14), and its binding energy, computed at the DFT level, is intermediate between that of the dodecahedron and those of the T_d and of the D_{2d} isomers.[66] It would therefore be of interest to carry out an extensive comparison at the DFT level, of the seven isomers of Figure 12 and of the transformation pathway leading from one form to another. As a matter of fact, each form is connected to one or two other isomers through a 90° rotation of *one* C_2 ligand only (Figure 15), a process expected to be less demanding than the concerted 45° rotation of *all* C_2 units leading to the hypothetical pentagonal dodecahedron.

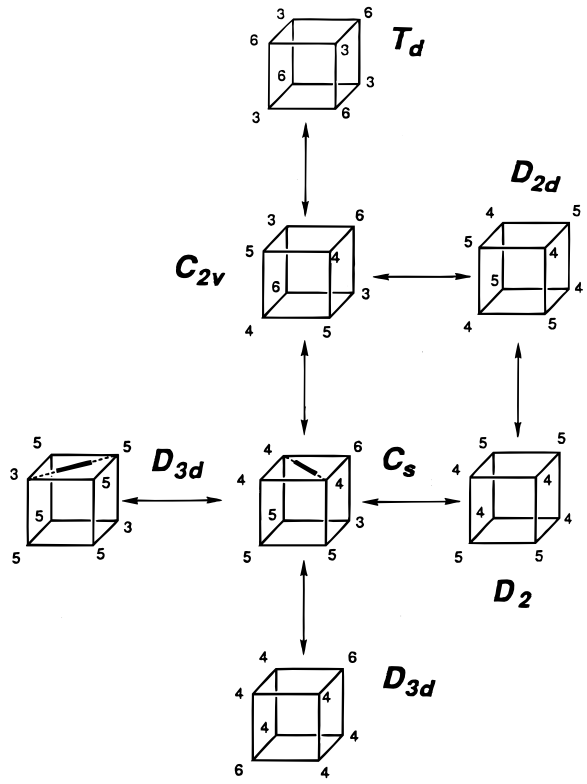

Figure 15. Schematic representation of the seven distinct topological structures of M_8C_{12} composed of six acetylenic C_2 fragments coordinated to the metal framework symbolized by a cube (see Figure 12). The numbers associated with each apex represent the number of carbon atoms at bonding distance. The transition from one structure to another is represented by arrows assuming that the topological change results from the 90° rotation of only one C_2 fragment.

III. Electronic Structure of Tetrahedral Met-Cars

A. The Orbital Diagram of Lin and Hall[14]

Several schemes have been proposed to understand the electronic structure of Ti_8C_{12} and other met-cars on a molecular orbital basis. The orbital sequence of Srinivas et al.[51] based on extended Hückel calculations clearly shows the formation of a large energy gap between the HOMO-1 and the triply degenerate, partly occupied HOMO (Figure 13). Unfortunately, the interaction diagram between a preformed Ti_8C_4 cluster and the four remaining C_2 units does not provide a clear vision of the donation and back-donation interactions between dicarbons and the metal framework.

Lin and Hall[14] describe the structure and bonding of the T_d cluster as six acetylene-like $(C_2)^{2-}$ units bonded to the four outer capping metal atoms through 12 σ bonds and to the inner tetrahedral metal atoms through the side-on (η^2-C_2) π bonding electrons, illustrated as the following:

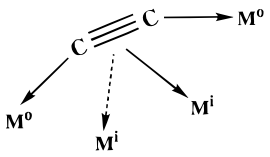

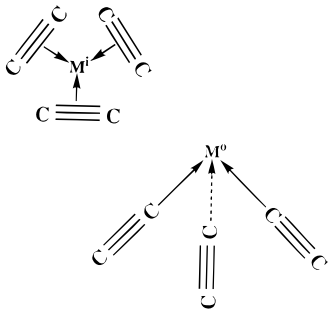

Figure 16. M_8C_{12} (tetracapped tetrahedron, T_d symmetry): the environment of the metal atoms M^i belonging to the inner tetrahdron and of the metal atoms M^o belonging to the outer (capping) tetrahedron.

Each metal of the inner tetrahedron is coordinated to three C_2 ligands in a quasiplanar, pseudotriangular arrangement, whereas each metal of the capping tetrahedron represents the apex of trigonal pyramid with three C_2 units coordinated end-on (Figure 16). In each planar $M^i(C_2)_3$ fragment, the in-plane metal orbitals $d_{x^2-y^2}$ and d_{xy} will be used to form the σ bonds with the acetylenic π orbitals, leaving the out-of-plane orbitals (d_{z^2}, d_{xz} and d_{yz}) available for other interactions. For each outer metal atom engaged in a pyramidal ML_3 fragment, another set of three orbitals (the "t_{2g}" set) is also available for extra bonding. After accounting for the donation interactions, we are then left with 12 metal orbitals in each tetrahedron. According to Lin and Hall, the degeneracy of those metal levels is split according to the metal−metal interactions that develop inside each tetrahedron (Figure 17, left-hand side for T^i, right-hand side for T^o) and between the two tetrahedra (Figure 17, center). Due to the large intermetallic distances in the capping tetrahedron, the metal−metal interactions inside T^o are negligible and the 12 metal levels on the right-hand side remain nearly degenerate. On the contrary, the short distances inside T^i induce an important splitting of the metal orbitals (Figure 17, left). The interactions between T^i and T^o reorganize the 24 lowest metal orbitals into three clusters of levels: (i) a set of nine bonding levels labeled $a_1 + t_2 + e + t_1$ according to the irreducible representation of the T_d point group; (ii) a set of nine nonbonding, or slightly antibonding, orbitals ($a_1 + t_2 + t_2 + e$); (iii) a set of six antibonding orbitals ($t_1 + t_2$).

According to that orbital sequence, electron-precise clusters with maximal stability should correspond to the complete population of either the set of bonding orbitals (18 electrons) or of the two sets of bonding and nonbonding orbitals (36 electrons). Assuming a formal charge of 2− for each acetylenic C_2 unit, the number of metal electrons assigned to the tetrahedral M_8C_{12} cluster should be calculated to be $8n - 12$, where n is the number of valence electrons of metal M. Let us note that the "magic number" of 18 electrons exactly fits the predictions of the simple Hückel method (Figure 4) and reproduces for Ti_8C_{12} (20 electrons) the significant energy gap between HOMO and HOMO-1 obtained from EHT and from DFT calculations.

This orbital sequence could explain why M_8C_{12} clusters are not characterized as magic peaks when

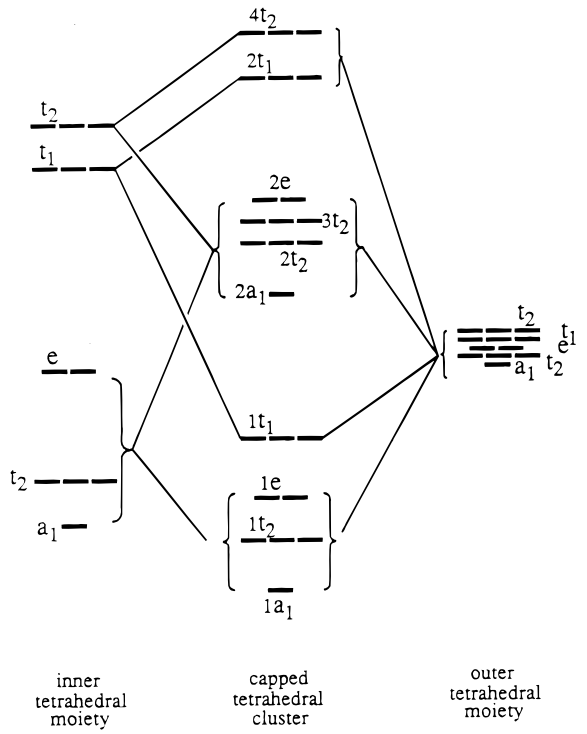

Figure 17. Schematic interaction diagram for a tetracapped tetrahedral metal cluster. The orbital ordering in the center column is based on the result of ab initio RHF calculations on the T_d form of Mo_8C_{12}. Reprinted with permission from ref 14. Copyright 1993 American Chemical Society.

M is a transition metal of group 3, like scandium or yttrium. The formal number of metal electrons, 12, is not sufficient to fill the set of bonding orbitals. In that respect, the formation of electron-precise clusters containing one metal atom of group 3, such as the $(Ti_7YC_{12})^+$ ion, should represent a facile process. Indeed, $(Ti_7YC_{12})^+$ and also probably $(Ti_6Y_2C_{12})^+$ have been characterized, but it was observed that the inclusion of yttrium atoms into a titanium-based binary met-car is not highly favored.[55] On the opposite side, met-cars with transition metals belonging to group 6 have an electron count of 36 which corresponds to the complete filling of the weakly antibonding set of metal orbitals. Those clusters are present in the mass spectrum, but they seem to be somewhat less stable than their titanium or zirconium counterparts, possibly due to the accumulation of small antibonding interactions or to an increased Pauli repulsion between electron-rich metal atoms.

The model proposed by Lin and Hall to explain the electronic structure of met-cars however raises some questions. First, it does not easily account for the stability of met-cars made with group 5 transition metals, and especially of V_8C_{12}. The orbital scheme of Figure 17 should assign to this 28-electron cluster a high-spin electronic structure with 10 electrons accommodated in the set of nonbonding orbitals.[14] Moreover, applying this orbital diagram to the Fe_8C_{12} cluster characterized by Pilgrim and Duncan[8] leads to accommodate as much as 16 metal electrons into strongly antibonding orbitals, unless Fe_8C_{12} adopts a structure different from that of the other met-cars. Another objection that could be addressed to the model of Figure 17 is the neglect of back-bonding interactions, unless it is implicitely assumed that back-donation to the acetylenic π^* orbitals leads in the first approximation to an uniform downward shift of all metal levels.

B. Metal–Dicarbon Back-Donation: Key to the Stability of Met-Cars

The importance of back-donation in stabilizing the T_d form of Ti_8C_{12} is emphasized in the work of Poblet et al. focused on the comparison between titanium carbide and copper chalcogenide clusters.[93] The comparative study between both families of compounds was inspired by the synthesis by the group of Kanatzidis of two- and three-dimensional copper polytelluride compounds with formulas $K_4Cu_8Te_{11}$, $A_3Cu_8Te_{10}$ (A = Rb, Cs), $AA'_2Cu_8Te_{10}$ (A, A′ = K, Rb, Cs), and $A_2BaCu_8Te_{10}$ (A = K, Rb, Cs).[94] Although no discrete complexes could be isolated, it appears that the building blocks of those ternary structures are pentagonal dodecahedral $Cu_8(Te_2)_6$ clusters sharing Te−Te edges and encapsulating an alkali metal or a Ba^{2+} ion (Figure 18). The similarity with Castle-

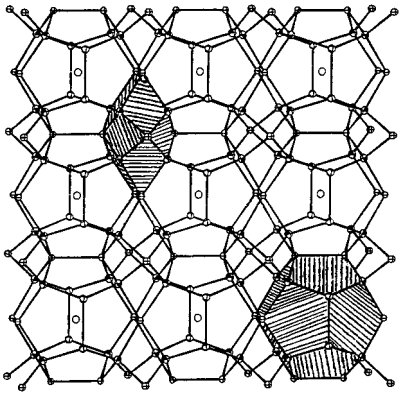

Figure 18. Layer of the $[RbCu_8Te_{10}]_n^{2n-}$ compound obtained in the group of Kanatzidis. Note the structure of pentagonal dodecahedron of the edge-sharing $Cu_8(Te_2)_6$ clusters. Reprinted with permission from ref 94b. Copyright 1995 American Chemical Society.

man's cage (Figure 2) appears obvious even though Zhang et al. warned that the characterization of a dodecahedral structure for copper chalcogenates could not be taken a priori as an argument in favor of the same topology for met-cars.[94b] One could also argue that the $[Cu_8(Te_2)_6]^{4-}$ clusters are embedded in an infinite system susceptible to influence their structure. More than 20 years earlier, however, Hollander and Coucouvanis reported the structure of the "metallocubane" clusters $[(C_6H_5)P]_4[Cu_8(S_2C_4O_2)_6]$ and $[(C_4H_9)N]_4[Cu_8(S_2CC(COOC_2H_5)_2)_6]$,[95] in which the dithiolate ligands are clearly oriented parallel to the edges of the cubic metal framework (Figure 19).

Poblet et al. carried out extended Hückel and ab initio RHF calculations on the copper telluride ions $(Cu_8Te_{12})^{4-}$, $K^+@(Cu_8Te_{12})^{4-}$, and $Ca^{2+}@(Cu_8Te_{12})^{4-}$, assumed isolated.[93] The model ions were considered either with the structure of a pentagonal dodecahedron or with that of a tetracapped tetrahedron, and the geometries were optimized for both isomers. At variance with the case of met-cars, the model with

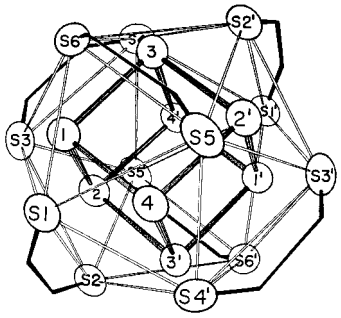

Figure 19. Structure of the Cu_8S_{12} core of the $Cu_8DTS_6^{4-}$ cluster (DTS = 1,2-dithiosquarate) characterized by Hollander and Coucouvanis. In that structure and in similar ones, the DTS ligands are oriented parallel to two edges of the underlying face of the cubic metal framework, a conformation reminiscent of the pentagonal dodecahedron. Reprinted with permission from ref 95. Copyright 1974 American Chemical Society.

T_h symmetry was found most stable for the three considered ions with large energy gaps, comprised between 181 and 280 kcal·mol^{-1}. The structural change between both families of clusters was assigned to the markedly different effect of back-donation interactions in carbides and in chalcogenides. Back-donation clearly results in four-electron destabilizing interactions when dichalcogen $[X_2]^{2-}$ ligands with doubly occupied π^* orbitals are involved. The optimal stability will therefore be obtained by maximizing the number of σ bonds and minimizing the number of ligand π^* orbitals susceptible to acquire antibonding character with respect to the metal framework. Those conditions are clearly satisfied when the $[X_2]^{2-}$ units are sp^3-hybridized, which implies the dodecahedral structure. On the opposite way, the met-cars should maximize back-bonding interactions with the empty π^* orbitals of the dicarbons. From this point of view, the dodecahedral structure is particularly counterproductive, since (i) there are only 6 π^* orbitals available, instead of 12 in the acetylenic coordination, and (ii) no advantage is taken from those orbitals since the metal electrons are accommodated in d_{z^2}-like orbitals with little interaction if any with the dicarbons. As a consequence, the equilibrium C−C distance remains approximately constant for the hypothetical Sc_8C_{12} met-car (no d electrons, d_{C-C} = 1.346 Å), for Ti_8C_{12} (8 d electrons, d_{C-C} = 1.346 Å), and for V_8C_{12} (16 d electrons, d_{C-C} = 1.336 Å).[40] For the structure of tetracapped tetrahedron, the shift from ethylenic to acetylenic coordination does not reduce the number of donation interactions; 12 σ donations have just been replaced by the same number of π donations to the atoms of the inner tetrahedron. However, the formal number of metal electrons has been increased by 12 and those electrons—or at least a large part of them, see III.C—are now expected to take part in back-donation interactions with the 12 π^* orbitals of the acetylenic dicarbons.

C. Hartree–Fock and CI Description of Ti_8C_{12} and V_8C_{12} (T_d Form)[90,96]

The orbital diagram displayed in Figure 17 is based on the result of ab initio RHF calculations carried out by Lin and Hall on the 36-electron Mo_8C_{12} cluster.[14] However, RHF calculations carried out on isostructural systems with a different electron count are not expected to display the same orbital sequence, because of the well-documented tendency of Hartree−Fock calculations to avoid the symmetry-imposed delocalization of core electrons and—to some extent—of d valence electrons.[91] As a matter of fact, the electronic configuration of lowest energy found for Ti_8C_{12} is not the closed-shell singlet $1a_1^2\ 1t_2^6\ 1e^4\ 1t_1^6\ 2a_1^2$ as expected from Figure 17 but a high-spin state, the $^5A_2$ configuration associated with the electron distribution $1t_2^6\ 1e^4\ 1t_1^6\ 1a_1^1\ 2t_2^3$. The four open-shell electrons are accommodated in four combinations of d_{z^2}-like orbitals centered on the apexes of the inner tetrahedron of metal atoms (Figure 20). Those orbitals display an almost exclusive metal character whereas the other 8 orbitals with important metal weight are heavily involved in back-donation interactions.

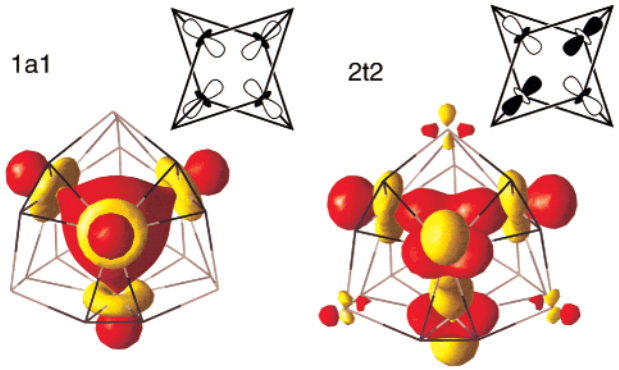

Figure 20. M_8C_{12}, conformation of tetracapped tetrahedron with T_d symmetry. Orbital combinations with a_1 and t_2 symmetry (one component) of d_{z^2}-like orbitals centered on the apexes of the *inner* tetrahedron of metal atoms. Color representations of the corresponding orbitals are taken from DFT calculations.

The four open-shell electrons of that configuration are reminiscent of the high-spin ground state assigned to the dodecahedral isomer, where the eight metal electrons were also accommodated in pure d-orbital combinations oriented perpendicular to the cluster surface. At variance with the T_h structure, however, the Ti^i−Ti^i distances in the T_d form are short enough to induce a strong antiferromagnetic coupling between the four electrons through the in-phase combination, $1a_1$, of the pseudo-d_{z^2} orbitals. The origin of that antiferromagnetic coupling is easily traced to the strong overlap of the four d_{z^2} lobes occurring at the center of the cluster (Figure 20). This antiferromagnetic coupling can be accounted for through a full CI or a CASSCF treatment with an active space incorporating the four orbitals of Figure 20 populated with four electrons ("coupling" CI). Then, the configurations with an important weight in the coupling CI can be taken as references in a multireference, singles-and-doubles expansion (MR-SDCI) involving the other metal electrons. Both treatments give rise to a *singlet ground state* ($^1A_1$) and to a low-lying triplet state ($^3T_1$), both characterized by a significant contraction of the optimal Ti^i−Ti^i distance with respect to the uncoupled $^5A_2$ state (3.05 Å vs 3.11 Å) At the optimal geometry of the

Table 2. (Left-Hand-Side) States of Lowest Energy (Singlet, Triplet, Quintet) Defined from ab Initio Calculations at the CI Level Carried out from the Molecular Orbitals of the Hartree−Fock Configuration of Lowest Energy ($^5A_2$) for Ti_8C_{12}, Zr_8C_{12}, V_8C_{12}, and Nb_8C_{12} and (Right-Hand-Side) Higher Energy States Defined at Similar Levels of Calculation from the Transfer of Four Metal Electrons from the Inner Tetrahedron of Metal Atoms (*thn*) to the Capping Tetrahedron (THN)[e]

State	low-energy states		higher energy states	
	coupling[a]	MR-SDCI[b]	coupling[a]	MR-SDCI
	Ti_8C_{12} $(thn)^4(\mathbf{THN})^0$ [c]		Ti_8C_{12} $(thn)^0(\mathbf{THN})^4$ [d]	
$^1A_1$	0.	0.	88.4	90.8
$^3T_1$	2.4	2.9	88.4	90.0
$^5A_2$	8.0	12.4	88.2	90.7
	Zr_8C_{12} $(thn)^4(\mathbf{THN})^0$ [c]			
$^1A_1$	0.	0.		
$^5A_2$	21.1	31.4	Not characterized from RHF	
	V_8C_{12} $(thn)^8(\mathbf{THN})^4$ [d]		V_8C_{12} $(thn)^4(\mathbf{THN})^8$ [c]	
$^1A_1$	0.6	0.1	3.3	14.0
$^3T_1$	0.5	0.	4.2	15.4
$^5A_2$	0.	3.3	6.2	22.1
	Nb_8C_{12} $(thn)^8(\mathbf{THN})^4$ [d]		Nb_8C_{12} $(thn)^4(\mathbf{THN})^8$ [c]	
$^1A_1$	0.1	0.5	86.0	97.6
$^3T_1$	0.04	0.		
$^5A_2$	0.	0.8	103.1	

[a] Full CI on a basis of four orbitals populated with four electrons. [b] Multireference singles and doubles CI. The references are the configuration of significant weight obtained from the coupling treatment. [c] Unpaired electrons localized on *thn*; geometry optimized for state $^1A_1$. [d] Unpaired electrons localized on **THN**; geometry optimized for state $^5A_2$. [e] Relative energies are given in kcal·mol^{-1}. Details of the calculation and total energies are given in ref 96.

singlet ground state, the MRSD-CI gives the triplet state at a relative energy of +2.86 kcal·mol^{-1} and the quintet at +12.4 kcal·mol^{-1} (+2.44 and +8.02 kcal·mol^{-1}, respectively, at the "coupling" stage) (Table 2).[97] Those values are in reasonably good agreement with the Heisenberg model[98] which assumes that the antiferromagnetic coupling can be described by a single coupling constant J such as

$$E(^3T_1) - E(^1A_1) = {}^1/_2[E(^5A_2) - E(^3T_1)] = -2J \quad (2)$$

The natural orbital (NO) analysis of the singlet-coupled ground state reflects the relative stability of the $1a_1$ orbital (NO population 1.86 e) with respect to the triply degenerate metal−metal nonbonding orbital (NO population: 2.14 e).

Interestingly, the RHF procedure characterizes for Ti_8C_{12} an *excited* quintet configuration corresponding to the transfer of the four open-shell electrons to a combination of four d_{z^2}-like orbitals centered on the metal atoms of the *capping* tetrahedron (Figure 21). According to the orbital labeling of Lin and Hall, this excitation process could be written as

$$1t_2^6\ 1e^4\ 1t_1^6\ 1a_1^1\ 2t_2^3 \rightarrow 1t_2^6\ 1e^4\ 1t_1^6\ 2a_1^1\ 3t_2^3 \quad (3)$$

If the two sets of metal atoms are symbolized by *thn* and **THN** representing the inner and the capping tetrahedra, respectively, then the electron transfer could be represented as

$$(thn)^4 \rightarrow (\mathbf{THN})^4 \quad (4)$$

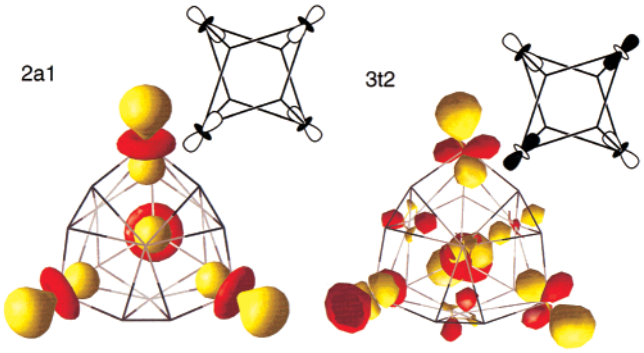

Figure 21. M_8C_{12}, conformation of tetracapped tetrahedron with T_d symmetry. Orbital combinations with a_1 and t_2 symmetry (one component) of orbitals centered on the apexes of the *capping* tetrahedron of metal atoms. Color representations are taken from DFT calculations.

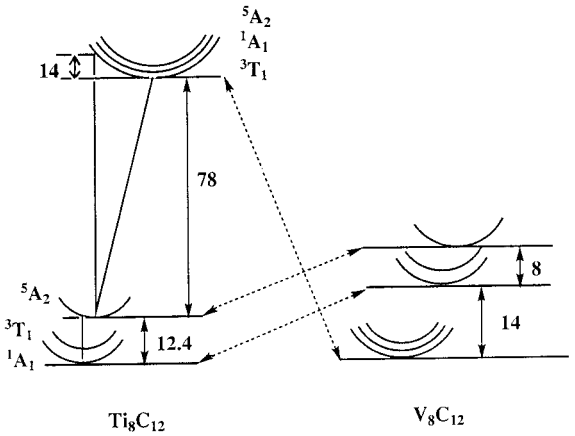

Figure 22. M_8C_{12} (M = Ti, V), T_d symmetry: Excitation energies (kcal·mol^{-1}) computed at the ab initio/CI level and corresponding to the transfer of four electrons from orbitals localized on one set of four equivalent metal atoms (inner tetrahedron for M = Ti; capping tetrahedron for M = V) to the other.

At variance with $1a_1$, the in-phase combination $2a_1$ is practically nonbonding due to the large metal−metal distances in the capping tetrahedron (Figure 21). This explains, first, the high energy of the excited electronic configuration for group 4 met-cars (+78 kcal·mol^{-1} for Ti_8C_{12},[99] Figure 22) and, then, the lack of any through-space antiferromagnetic coupling associated with that configuration (Table 2; Figure 22).

The characterization of this excited state and the requirement for d-electron localization implied by ab initio formalism explain the electronic structure of V_8C_{12} and other group 5 met-cars by assigning the eight extra electrons first to the half-filled shell of d_{z^2} orbitals of the *inner* tetrahedron and then to the empty shell of d_{z^2} orbitals of the *capping* tetrahedron. Then, the RHF configuration of lowest energy obtained for V_8C_{12} and Nb_8C_{12} is once again a $^5A_2$ state that can be symbolized as

$$1t_2^6\ 1e^4\ 1t_1^6\ 1a_1^2\ 2t_2^6\ 2a_1^1\ 3t_2^3 \quad (5)$$

or

$$(thn)^8(\mathbf{THN})^4 \quad (6)$$

The consequences of this electron distribution for V_8C_{12} are as follows: (i) contraction of the metal framework and especially of the M^i-M^i distances ($V^i-V^i = 2.941$ Å compared to $Ti^i-Ti^i = 3.11$ Å) due in part, to the full occupancy of the $1a_1$ orbital; (ii) lack of any significant antiferromagnetic interaction between the d electrons localized on the capping tetrahedron, which yields a quasi-degeneracy between the three states of lowest energy, $^1A_1$, $^3T_1$, and $^5A_2$ (Figure 22, Table 2); (iii) existence of a set of three excited states characterized by the promotion of four electrons from *thn* to **THN** and therefore corresponding to the distribution $(thn)^4(\mathbf{THN})^8$. The excited quintet obtained at the RHF level is reminiscent of the ground-state configuration of Ti_8C_{12}, subject to antiferromagnetic coupling. In the vanadium cluster, both the set of low-lying states and the set of excited states have the $1a_1$ orbital either partly or fully occupied. This explains why the energy gap between both series of states is much more narrow than for Ti_8C_{12} (Figure 22).

D. Sequence of Kohn–Sham Orbitals

This analysis of the electronic structure of Ti_8C_{12} at the ab initio CI level is basically in agreement with the sequence of DFT orbitals (Table 3) predicting a low-energy, doubly occupied $1a_1$ level and a triply degenerate HOMO populated with two electrons. In DFT calculations, however, the $2t_2$ orbital represented in Figure 20 is practically degenerate with—and in fact slightly lower than—a $2t_1$ orbital localized on the capping tetrahedron (Table 3). As a consequence, the density associated with the DFT frontier orbitals of the neutral Ti_8C_{12} met-car appears much more delocalized over the whole complex. Adding eight electrons to form V_8C_{12} yields, as in the ab initio scheme, a full population of the d_{z^2}-like orbitals ($1a_1$ and $2t_2$) and a population with four electrons of orbitals localized on the capping tetrahedron.

Table 3. Sequence of Kohn–Sham Orbitals Obtained from Gradient-Corrected DFT Calculations Carried Out on Ti_8C_{12} and V_8C_{12}[a]

Ti_8C_{12}

Metal Orbital		Main Metal Contribution	Energy (eV)
2a1	—	**THN**	-2.438
2e	— —	*thn*	-2.736
$2t_2$	— — —	*thn*	-3.163
$2t_1$	↿⇂ ↿⇂ —	**THN**	-3.186
$1t_1$	↿⇂ ↿⇂ ↿⇂	**THN**	-4.829
1e	↿⇂ ↿⇂	**THN**	-5.043
$1t_2$	↿⇂ ↿⇂ ↿⇂		-5.077
$1a_1$	↿⇂	*thn*	-5.486

V_8C_{12}

Metal Orbital		Main Metal Contribution	Energy (eV)
$3t_2$	— — —	**THN**	-3.304
$2a_1$	—	**THN**	-3.431
2e	— —	*thn*	-3.373
$2t_1$	↿⇂ ↿⇂ ↿⇂	**THN**	-4.011
$2t_2$	↿⇂ ↿⇂ ↿⇂	*thn*	-4.024
$1t_1$	↿⇂ ↿⇂ ↿⇂	**THN**	-5 703
1e	↿⇂ ↿⇂	**THN**	-5.953
$1t_2$	↿⇂ ↿⇂ ↿⇂	**THN**-*thn*	-6.227
$1a_1$	↿⇂	*thn*	-6.270

[a] ADF program;[74] nonlocal corrections of Becke and Perdew to the exchange-correlation energy[70] and triple-ζ Slater basis sets for valence electrons plus polarization on carbon atoms.

E. Laplacian Distribution of the Charge Density

Figure 23 reproduces the Laplacian distribution of the charge density[100] associated with the $^1A_1$ ground state assigned to the T_d isomer of Ti_8C_{12} and obtained from the MR-SDCI wave function.[90] The plane of Figure 23a contains one C_2 unit σ-bonded to two metal atoms of the outer tetrahedron, whereas Figure 23b illustrates the π interaction between a C_2 group and a metal atom belonging to *thn*. Broken lines are characteristic of a local charge concentration of the charge density. Both figures display a cylindrical shape for the electron distribution in the vicinity of the carbon atoms, characteristic of the acetylenic

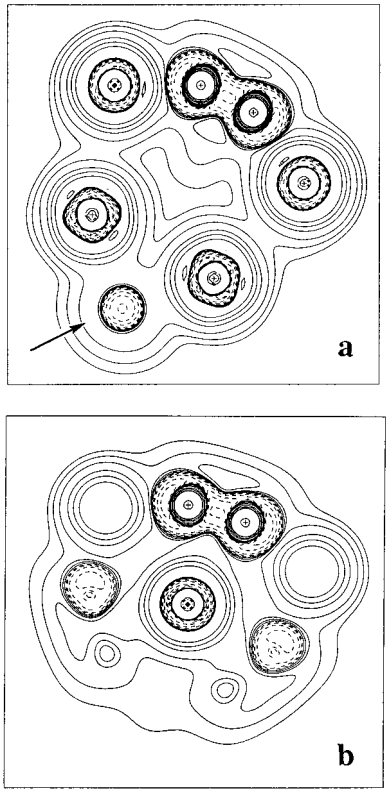

Figure 23. Plots of $\nabla^2\rho$ for Ti_8C_{12} in the conformation with T_d symmetry (from ab initio calculations, geometry optimized at the RHF level, density distribution obtained at the MRCI level for the singlet-coupled $^1A_1$ ground state): (a) plane containing one C_2 unit and two σ-bonded Ti atoms belonging to the capping tetrahedron; (b) plane containing one C_2 dimer and one Ti atom belonging to the inner tetrahedron. Solid lines are for $\nabla^2\rho > 0$ (regions of charge depletion); broken lines are for $\nabla^2\rho < 0$ (regions of charge concentration.

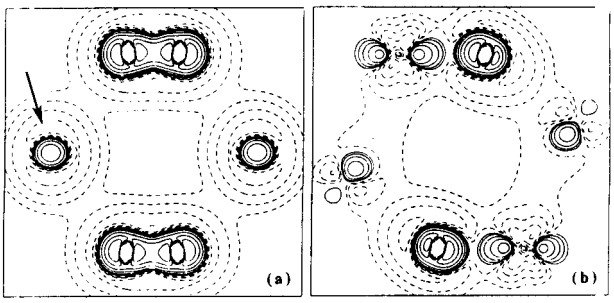

Figure 24. Plots of $-\nabla^2\rho$ in the dodecahedral Y_8C_{12} from ab initio RHF calculations by Lin and Hall: (a) plane containing two parallel C═C units and bisecting another two parallel C═C units; (b) plane containing two Y−C bonds, which are related by a center of inversion, and crossing another two Y−C bonds. Reprinted with permission from ref 39. Copyright 1992 American Chemical Society.

character of the C_2 fragment.[101] The nonelliptical character of the Laplacian distribution along the dicarbon fragments is confirmed by the circular shape of the section across the C−C bond displayed in Figure 23a.

Each carbon atom displays a local maximum in charge concentration (maximum in $-\nabla^2\rho$, referred to as a (3, −3) critical point in the topological analysis of the Laplacian distribution)[100] located along the Ti−C σ bond (Figure 23a). Along the same Ti−C bond axis, but on the metal side, is found a local *minimum* in $-\nabla^2\rho$, or a (3, +3) critical point corresponding to a depletion of charge concentration. The distribution of $-\nabla^2\rho$, with a (3, −3) critical point on the ligand side and a (3, +3) critical point on the metal side, is characteristic of σ donation.[102]

In Figure 23b, the charge distributions in the carbon atoms are governed by the donation interactions with Ti^i atoms. The π character of those donations is illustrated by the deformation of the charge density along C_2 toward the metal center. The integration of the electron density over the domain defined by the surfaces of zero gradient flux[103] provides for the C_2 units a net charge of −2.05 e, larger than the Mulliken charge (−1.33 e) and very close to the formal charge of −2 e assumed for the acetylenic C_2.

Analyses of the Laplacian function of the density have also been reported for the T_h isomers of Y_8C_{12}[39] (Figure 24) and Ti_8C_{12}.[90] At variance with the C_2 units of the T_d isomer, the sections across the C−C bonds are now clearly elliptical (Figures 23 and 24; see arrows), which gives strong evidence in that case of C−C double bond character. This ethylenic character is confirmed by the appearance of two (3, −3) critical points around each carbon, approximately oriented toward the nearest metal neighbors.[90]

F. Pentagonal Dodecahedron vs Tetracapped Tetrahedron: Quest for a Discriminating Property

Met-cars are relatively large molecules which are beyond the domain of applicability of the most accurate quantum chemical treatments. It can be easily shown from calculations carried out on diatomic models such as Ti−C or the titanium dimer at various levels of theory that the properties computed without properly accounting for electron correlation and for basis set truncation may be far from their exact values.[104] However, from the computational chemist's viewpoint, it was clear since the early DFT and ab initio calculations on the T_d and D_{2d} forms of Ti_8C_{12} and related molecules that the pentagonal dodecahedral conformation was not competitive against the isomers displaying an acetylenic coordination of the dicarbons. This conviction was based (i) on the order of magnitude of the energy difference, too large to be reversed by an improvement of the level of theory, and (ii) by the agreement obtained from a large range of methodological approaches such as ab initio SCF and MR-SDCI, DFT/LDA, and DFT with gradient corrections. It was even proved that the form with T_h symmetry cannot be considered as a local energy minimum since (i) no less than 12 imaginary frequencies were obtained from the dynamic matrix of dodecahedral Zr_8C_{12}[49] and (ii) the pathway from the fullerenoid conformation of M_8C_{12} (M = Ti, Zr) to either the T_d or the D_{2d} form is practically barrierless.[49,88] This computational evidence was slow to spread through the community specialized in the production and experimental investigation of met-cars. This should be attributed to the difficulty of finding a property amenable to experiment and susceptible to unambiguously assess the structure of the cluster. Despite an intensive exploration of the physical and spectroscopic properties of met-cars and of a systematic investigation of their chemical reactivity, it is not until the very accurate determination of the ionization potentials of Ti_8C_{12} and Zr_8C_{12} by Sakurai and Castleman[105] that a really discriminating criterion could be found in favor of the T_d form. The problem of the structure assessment was certainly an incentive to carry out a systematic scanning of the properties of single-metal and mixed-metal met-cars by means of various experimental techniques. Quantum chemical treatments, and more specifically the DFT approach, were required in most cases to test the behavior of both the dodecahedral and the tetrahedral conformations with respect to the considered property.

G. Met-Cars with Transition Metals beyond Group 5

Most experimental and theoretical investigations on M_8C_{12} clusters have been carried out to date on met-cars involving early transition metals, namely Ti, Zr, Hf, V, and Nb. However, magic peaks corresponding to the same M_8C_{12} stoichiometry were also observed with more electron rich transition metals, especially with Cr and Mo.[8] In the case of Fe, no single magic peak exists, but 8/12 stoichiometry is prominent and followed by a truncation in the spectrum.[8] However, metals of the third transition row show little propensity to form met-cars, hafnium being the exception.[9a] Concerning the metals of the first transition row, it seems that no M_8C_{12} cluster has been observed either with M = Co[9a] or with M = Cu.[202] Moreover, theoretical information concerning the structure and the stability of met-cars with transition metals beyond group 5 is rather scattered.

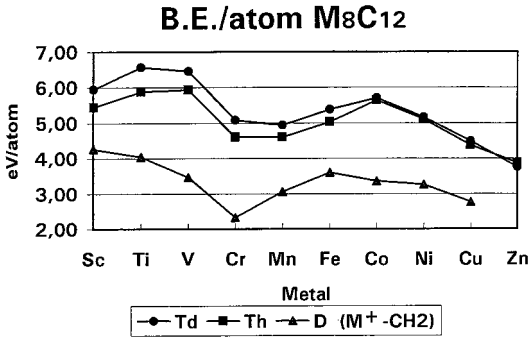

Figure 25. Calculated bonding energies (eV/atom) for the tetrahedral (●, T_d symmetry) and for the dodecahedral (■, T_h symmetry) conformations of M_8C_{12} clusters involving metals of the first transition series (M = Sc to Zn). Those values are compared with the experimental M−C bond energies reported for the $(M^+)-CH_2$ molecules (▲), from ref 106.

Local density calculations by Grimes and Gale[17] suggest that the stability of dodecahedral (T_h) Fe_8C_{12} (6.27 eV/atom) is somewhat decreased with respect to that of Ti_8C_{12} (6.7 eV/atom) and of V_8C_{12} (6.81 eV/atom). The DVM/Xα calculations by Reddy and Khanna,[66,150] still carried out on the T_h structure of M_8C_{12} (M = Ti, V, Fe, Co), also agree with a slight and continuous decrease of the bonding energy as the number of the metal valence electrons increases (Table 1). Those results are easily interpretable in terms of the population of molecular orbitals with an increasing metal−metal antibonding character.[14]

A recent DFT study by Muñoz and Poblet[48] provides a systematic overview of the bonding energies of met-cars for the whole series of first-row transition metals (Sc to Zn) for both the T_h and the T_d structures (Figure 25). The computed bond energies displayed in Figure 25 confirm some experimental trends but also provide new and unexpected features that will deserve further investigation. First, the highest stability for the M_8C_{12} clusters is obtained with M = Ti and V, in complete agreement with the interpretation of the photofragmentation experiments.[8] The increase in stability from scandium to titanium is 50% higher in the tetrahedral form than in the T_h conformation as a consequence of the better ability of the T_d form to take advantage of back-donation. The loss of bond energy between vanadium and chromium (∼1.4 eV/atom in both conformations) is much larger than expected from the previous reports. The drop of the stability computed for chromium, as well as the rise of the bond energy obtained for Fe and the secondary peak of stability displayed for Co (Figure 25), could appear at first sight in contradiction with the orbital scheme of Figure 17. As noted by Lin and Hall, a relative peak of stability was rather expected for Mo_8C_{12} and for the isoelectronic cluster Cr_8C_{12} corresponding to the complete filling of the shell of the metal−metal nonbonding orbitals.[14] In fact, the profile of the bonding energies computed for the M_8C_{12} clusters when M evolves from Sc to Cu is quite similar to the curves of the metal cation−methylene bond energies reported either from experiment[106] or from calculations[107] (Figure 25). Therefore, this profile should not be correlated with the sequence of increasingly antibonding metal orbitals but rather assigned to general trends that affect the metal−ligand bond energies across the periodic table. Those trends have been analyzed by Siegbahn in terms of a competition between the loss of exchange energy on one hand and the metal−ligand electron repulsion on the other hand.[108] The loss of exchange energy when the M−C bond is formed is largest in the middle of the row where the number of singly occupied d-orbitals culminates, and the bond strengths therefore go through a minimum for chromium (Figure 25). Promotion of the metal atom into an excited state more favorable to bonding may also in some cases decrease the bond energy. When the effect of exchange and promotion is removed, one is left with a trend of decreasing bond energies from the left to the right due to the rise of the repulsion between the electrons on carbon and the increasingly populated metal d shell. Those trends are obviously quite general, and similar profiles have been calculated for the bond energies between the metal atoms of the second transition row and various ligands.[108] If it is admitted that the relative stabilities of the various met-cars are primarily related to the intrinsic electronic properties of the metal atom, then the "magic", or the "nonmagic", character of the mass peak corresponding to a given M_8C_{12} cluster should not be correlated with the calculated bond energy per atom but will only depend on the relative stabilities of M_8C_{12} and other M_xC_y clusters, for the considered metal M. A striking illustration is provided by a comparison between Sc_8C_{12} and Cr_8C_{12}: the early transition metal met-car does not show up on the mass spectrum despite a high stabilization energy (5.95 eV/atom) whereas the spectrum of chromium carbide clusters exhibits a magic peak for the much less stable Cr_8C_{12} cluster (5.1 eV/atom).

Another unexpected result concerns the competition between the dodecahedral and the tetrahedral conformations of met-cars. As discussed above, the much higher stability of the T_d form has been widely documented with metals of groups 3−5. The results displayed in Figure 25 show that the situation is not so clear-cut for the late transition metals and, especially, for cobalt and nickel. For Co_8C_{12} and Ni_8C_{12}, the overall energy gap in favor of the tetrahedral form does not exceed 1 eV, compared to more than 10 eV for Sc, Ti, and V. Both conformations could then compete or coexist, unless clusters with a distinct stoichiometry—or with the same stoichiometry and a distinct conformation—are definitely more stable. Finally, zinc is the only metal of the first row for which the dodecahedral conformation of M_8C_{12} becomes lowest in energy (Figure 25).

IV. Physical Properties

A. Relative Stabilities of Binary Metal Met-Cars: The $Ti_{8-x}Zr_xC_{12}$ Series

The most straightforward difference between the two competing conformations consists of the equivalence of the eight metal sites in the T_h form, opposed to their separation in two groups of four in the T_d or in the D_{2d} forms. Since the laser vaporization of mixtures of metal and carbide powders easily pro-

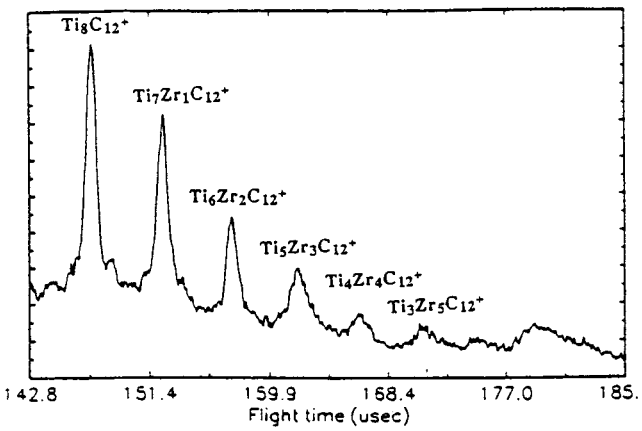

Figure 26. Mass spectrum of $Ti_8C_{12}^+$ and zirconium-substituted metallocarbohedrenes produced from the direct laser vaporization of a 4:1 molar mixture of TiC and Zr powders. Reprinted with permission from ref 110. Copyright 1994 American Institute of Physics.

duces binary metal metallocarbohedrenes,[55,110,111] in particular met-cars of the group 4 transition metals,[110] this technique was used to produce a series of Zr-substituted clusters with stoichiometries $Ti_{8-x}Zr_xC_{12}$. Those clusters could be characterized by a mass spectrometer as a series of peaks with a regular evolution of the peak intensities from $x = 0$ to $x = 5$. This regularity, particularly visible under 4:1 Ti:Zr molar ratio conditions (Figure 26),[111] has been interpreted as arising from a purely statistical substitution of Ti by Zr.[110,111] This represents a strong argument in favor of a structure with equivalent metal sites. As a matter of fact, one could reasonably expect that, in the tetracapped tetrahedron structure, zirconium has a higher affinity for a specific metal site, thus endowing the stoichiometry $Ti_4Zr_4C_{12}$ with a particular stability. The peaks of Figure 26, which do not support this conjecture, have probably delayed by several years the recognition of the T_d form as the most probable conformational isomer for met-cars.[110,111]

The problem of zirconium substitution in the tetrahedral isomers was eventually considered at the DFT level (local spin density approximation with Vosko−Wilk−Nusair parametrization for correlation,[74] Becke's nonlocal corrections to exchange, and Perdew's nonlocal corrections to correlation;[72] use of Slater-type functions to describe the frozen core and the valence shell electrons[76]) by Muñoz et al.[21] They reached the unexpected conclusion that the substitution site, inner tetrahedron (*thn*) or capping tetrahedron (**THN**) has, probably by chance, a negligible influence on the global stability of the molecule. The substitution of 1, 3, and 4 Zr atoms was considered either on *thn* or on **THN**. For $Ti_3Zr_5C_{12}$, two isomers were also considered, with 4 and 1 Zr atom(s) on *thn*, respectively. After reoptimization of all geometries, the bond energy per atom was shown to regularly increase from Ti_8C_{12} (6.56 eV) to $Ti_4Zr_4C_{12}$ (6.70 eV) and then to Zr_8C_{12} (6.81 eV). For all investigated values of x ($x \neq 0, 8$), the total bond energy difference between the two considered isomers never exceeded 1.2 kcal·mol^{-1} (Table 4). For the specific case of $Ti_4Zr_4C_{12}$, localizing the four zirconium atoms on *thn* rather than on **THN** resulted in a global energy change of 0.5 kcal·mol^{-1}, which explains why the distribution of the substitution sites for that stoichiometry does not appreciably deviate from the statistical one.

Table 4. Total Bond Energies, Bond Energies Per Atom (eV), Stabilization Energies with Respect to Ti_8C_{12} ($-\Delta E$, eV), and Stabilization Energies Per Substituted Atom ($-\Delta E/x$, eV) for Ti_8C_{12} and for Zr-Substituted Met-Cars $Ti_{8-x}Zr_xC_{12}$ ($x = 1, 3, 4, 5, 8$)[a]

met-car	posn of Zr atoms	sym	tot. bond energy	bond energy/ atom	$-\Delta E$	$-\Delta E/x$
Ti_8C_{12}		T_d	−131.227	6.561	0.0	0.0
Ti_7ZrC_{12}	*thn*	C_{3v}	−131.943	6.597	0.716	0.716
Ti_7ZrC_{12}	**THN**	C_{3v}	−131.904	6.595	0.677	0.677
$Ti_5Zr_3C_{12}$	*thn*	C_{3v}	−133.338	6.667	2.111	0.704
$Ti_5Zr_3C_{12}$	**THN**	C_{3v}	−133.383	6.669	2.156	0.719
$Ti_4Zr_4C_{12}$	*thn*	C_{3v}	−133.999	6.700	2.772	0.693
$Ti_4Zr_4C_{12}$	**THN**	C_{3v}	−133.977	6.699	2.750	0.687
$Ti_3Zr_5C_{12}$	*thn*(4)**THN**(1)	C_{3v}	−134.546	6.727	3.319	0.664
$Ti_3Zr_5C_{12}$	**THN**(4)*thn*(1)	C_{3v}	−134.501	6.725	3.27	0.655
Zr_8C_{12}		T_d	−136.294	6.815	5.067	0.633

[a] Two conformers, characterized by the atomic sites of metal substitution *thn* (inner tetrahedron) or **THN** (capping tetrahedron), have been considered for all binary metal species.

B. Collective Electronic Properties

The existence of giant dipole resonances associated with surface plasma excitation energies higher than the ionization potential value, and therefore lying in the continuum of states, was predicted from DFT calculations carried out by Rubio et al. within the LDA approximation.[24] Those authors estimated the dynamical polarizability $\alpha(\omega)$ as a response of the cluster to the application of a time-dependent dipolar external field:

$$V_{\text{ext}}(\vec{r}, w) = \vec{r}\, Y_{10} e^{-iwt} \tag{7}$$

The time-dependent DFT equations were solved by assuming a spherical averaging $V_{\text{ion}}^{\text{SAPS}}$ for the total potential of the ionic skeleton

$$V_{\text{ion}}(\vec{r}) = \sum_{j=1}^{20} V_{\text{ps}}(|\vec{r} - \vec{R}_j|) \tag{8}$$

where V_{ps} represents the electron−ion pseudopotential.[112] Let us remark that $V_{\text{ion}}(r)$ was calculated as the total potential generated by C^{4+} and Ti^{4+} ions *arranged in the pentagonal dodecahedral geometry*. The authors noted however that the consideration of another type of cage structure with C_2 dimers opposite to the faces of a distorted cube would affect the results in a minor way.[24]

Ti_8C_{12} was therefore considered as a metallic sphere with 80 delocalized valence electrons, subject to the spherically averaged potential created by the tetravalent cores of titanium and carbon atoms. With this approximation, the static polarizability, obtained for $\omega = 0$, was computed to be of the same order of magnitude as for C_{60}, with a dominant contribution coming from the 20 π electrons. The results obtained by Rubio et al. for the *dynamical* polarizability with the 80 valence electron model are reproduced in

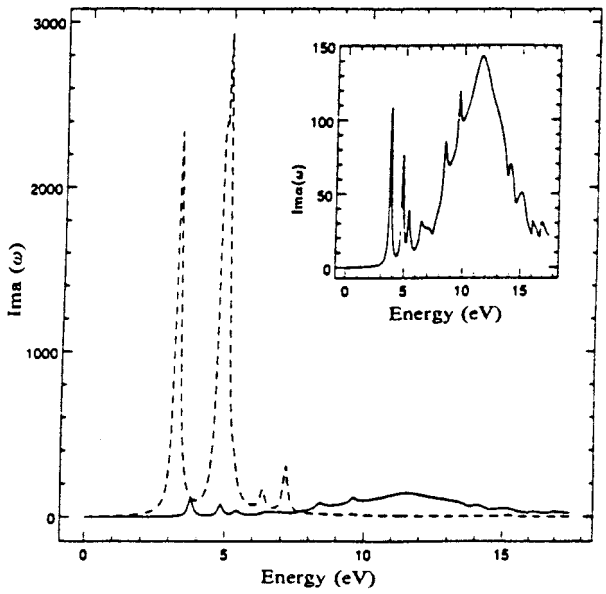

Figure 27. Imaginary part of the dynamical dipole polarizability for Ti_8C_{12} (arbitrary units). The dashed line corresponds to the independent response function, and the solid line, to the interacting one. Both C and Ti are described as tetravalent atoms. The inset shows an expanded view of the interacting response function. Reprinted with permission from ref 24. Copyright 1993 Real Sociedad Española de Física.

Figure 27.[24] The independent response function (dashed line) and the interacting one (solid line) have been represented. The particle−hole transition region is located below 6 eV, and the interacting polarizability displays a broad collective resonance at ∼12 eV. Because of the high value (>6 eV) of the two calculated surface-plasma excitations, it is concluded that, in contrast to metallic clusters, the collective resonance lies in the continuum of states and could be detected by a photoionization technique similar to that used to study the collective excitation in fullerenes.[113]

The existence of collective properties occurring in the energy range of the dipole resonance predicted by Rubio et al. was confirmed in 1995 by Castleman's group.[114] Photoionization of neutral clusters that had been conducted at various wavelengths was expected to result at least partly in multiphoton absorption. By extracting and removing "prompt" ions generated by the direct multiphoton ionization of the species present in the cluster beam, it was possible to detect the process of delayed ionization for single-metal metcars (Ti_8C_{12}, V_8C_{12}, Nb_8C_{12}, Zr_8C_{12})[114,115] as well as for binary metal clusters $Ti_xM_yC_{12}$ (M = Zr, Nb, Ta; $0 \leq y \leq 4$, $x + y = 8$).[115,116] Delayed ionization, attributed to a thermionic emission process, had been previously observed for transition metal,[117] metal oxide,[118,119] and metal carbide[119] clusters and also, possibly, in the case of fullerenes.[120] Thermionic emission results from a competition between ionization and dissociation leading to delayed electron emission.[121] It implies the presence of a high density of states between the ionization potential IP and the dissociation energy E_{diss} of the cluster, assumed to be higher than IP. If the multiphoton absorption provides the cluster with an energy comprised between those two limits, the

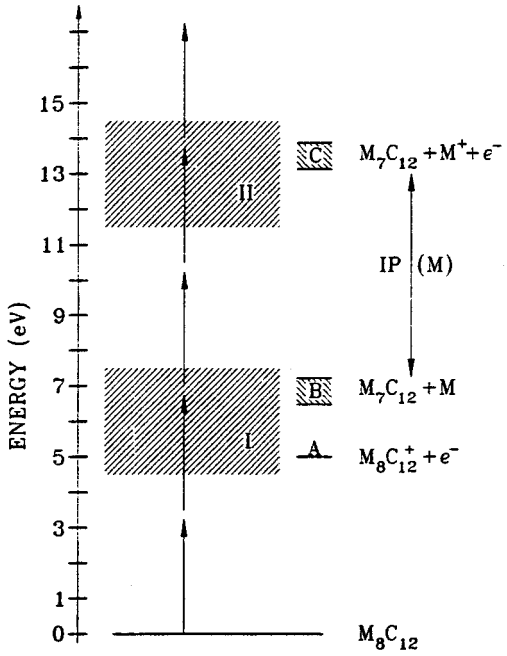

Figure 28. Energy schematic representing the two delayed ionization processes observed by May et al. Shaded region I represents the band of states populated by the initial absorption of several photons, represented by the two arrows, and subsequent relaxation processes. Shaded region II represents the band of states at higher energy populated by further absorption of succeeding photons. This band lies in the region of collective resonance theoretically predicted by Rubio et al.[24] The values given for A and B should be slightly modified to account for the most recent determinations of the ionization potential of Ti_8C_{12} (A = 4.40 eV)[105] and of the theoretically estimated value for the energy of the dissociation process $Ti_8C_{12} \rightarrow Ti_7C_{12} + Ti$ (B ∼ 8.26 eV).[21,121] C denotes the addition of the ionization potential of a free metal atom to the energy range B. Reprinted with permission from ref 114. Copyright 1995 Elsevier.

electronically excited cluster may nonradiatively decay and populate closely spaced states, both electronically and vibrationally excited. Delayed ionization then results from a slow coupling of those excited states.[114] Even though Ti_8C_{12} was a good candidate for delayed ionization due to its low IP (experimental, 4.40 eV;[105] computed, 4.60 eV [21]) and to the much higher estimates computed for E_{diss} (8.26 eV),[21,121] the specificity of that molecule appears from the lack of any other Ti_xC_y cluster in the delayed ionization mass spectrum.[114−116]

The delayed emission of atomic metal ions was obtained by another ionization channel implying successive multiphoton absorption. Highly excited species having energies in the region 12−15 eV, that is, in the region of the giant resonance predicted by Rubio et al.,[24] could undergo energy redistribution resulting in the delayed appearance of $Ti_8C_{12}^+$ or Ti^+. The scheme of Figure 28 summarizes, according to May et al.,[114] the two channels leading to delayed ionization. Assuming the value of 6.62 eV (probably underestimated)[121] for the dissociation energy of Ti_8C_{12} into Ti_7C_{12} + Ti and adding the ionization potential of Ti (6.82 eV)[122] leads to a minimum value of 13.44 eV for the excitation that would result in the delayed emission of Ti^+. This value is in the

energy range predicted by Rubio et al. for the collective resonance energy.[24] The existence of such a resonance would explain how the M_8C_{12} clusters could accommodate the large amount of energy provided by a high-order multiphoton absorption and not fragment prior to the time interval involved in the experiment.[114]

C. Ion Chromatography Studies

In most experiments focused on the production of met-cars or on the investigation of their properties, the separation of the metal carbide cluster ions produced either directly in the source or in the carrier gas was exclusively carried out on a mass criterion. Ion chromatography experiments carried out by Bowers and co-workers introduce another selection criterion by allowing a mass selected ion cloud to undergo collisions with a He buffer gas in a drift cell.[84,123] The drift time of a given species will depend on its collision cross section with He, and the various species present in the cloud will be separated as a function of their arrival time at the detector. Assuming definite experimental conditions, the arrival time of a given species is a specific property that can be related to the mobility K of the cluster ion as it passes through the He buffer gas. The value of K in $cm^2\ V^{-1}\ S^{-1}$ can be calculated by means of a Monte Carlo simulation technique as a function of the structure and geometry of the cluster ion.[84]

For $Ti_8C_{12}^+$, three structural isomers proposed from theoretical investigations were compared to the structure of pentagonal dodecahedron proposed by Castleman's group. The values of K obtained from Monte Carlo simulation were then compared to the experimental mobility of $5.71 \pm 0.05\ cm^2\ V^{-1}\ S^{-1}$ (Figure 8).[84] The structure of pentagonal dodecahedron displays the best fit with experiment (+1.2%), but the structure of tetracapped tetrahedron is also in reasonable agreement with the experimental value. Pauling's cubic assembly of metal atoms[78] and Khan's metal-decorated carbon cluster[80] yield mobility values sensibly below the acceptable range (Figure 8).

A similar study carried out on $Ti_8C_{13}^+$ yielded an excellent agreement between the experimental K value of $5.49\ cm^2\ V^{-1}\ S^{-1}$ and a computed value based upon a structure of pentagonal dodecahedron with an exohedral extra carbon.[123] The value of K associated with an endohedral structure deviates from experiment by as much as 7.5%. Since the thermodynamic stability of the endohedral structure seems well established from various theoretical studies,[21,27,67] the experimental conditions leading to the observed cluster ion had to be considered. Bowers' experimental K values were obtained for $Ti_8C_{13}^+$ ions directly created in the laser vaporization source, for which an exohedral growth of the cluster seems most probable. This interpretation is supported by reactivity experiments carried out on $Ti_8C_{13}^+$ and $Ti_8C_{14}^+$ ions generated in similar conditions.[63] Contrary to met-car clusters which generate only association products with polar reactants, those carbon-rich ions undergo a reactive process with acetone leading either back to the naked $Ti_8C_{12}^+$ species or to the replacement of the extra carbon(s) by an acetone molecule.[63] The $Ti_8C_{13}^+$ ions created by photon-induced loss of 6 Ti atoms from $Ti_{14}C_{13}^+$ [25] might have a different structure, possibly endohedral, and a different mobility value.[123]

D. Ionization Potentials

Brock and Duncan[22] collected in 1996 some of the values computed for the ionization potentials of the most common M_8C_{12} clusters (M = Ti, V, Zr) and issued a rather pessimistic statement about the difficulty to reconcile the trends in computed IP's with the experimental IP thresholds that were available at that time. The collection of theoretical and experimental IP values has been reproduced and completed in Table 5. It is clear that there have been a variety of calculations, especially carried out on Ti_8C_{12}, apparently leading to a widespread range (from 4.37 to 7.05 eV) for the predicted IP values (Table 5). However, a critical examination of the theoretical results shows that the calculated trends obtained *for the isomers with T_d symmetry* are in surprisingly good agreement with the most recent and accurate values obtained for Ti_8C_{12} and Zr_8C_{12} by Sakurai and Castleman.[105]

A first remark concerns the values of 6.82 and 6.74 eV reported in Table 2 of ref 22. Those values are assigned by Brock and Duncan to the IP's of Ti_8C_{12} and V_8C_{12}, respectively, as calculated by Reddy and Khanna[66] in the T_d form. This assignment clearly results from a misinterpretation since (i) Reddy and Khanna never computed met-cars in the T_d form and (ii) the values of 6.83 and 6.74 eV mentioned by Reddy and Khanna represent the ionization potentials of the Ti and V *atoms* and *not* those of met-cars incorporating those elements.

Then, it can be seen from Table 5 that the range of the IP values computed for Ti_8C_{12} and Zr_8C_{12} critically depends on the assumed conformation, whereas the case of V_8C_{12} is less clear-cut. The vertical ionization potential of dodecahedral Ti_8C_{12} is computed by Lou and Nordlander[19,22] to be 5.4 eV. Quite consistently, a value of 5.33 eV is proposed by Grimes and Gale for the *adiabatic* IP of the same conformer.[17,44] Reddy et al.[16] and Li et al.[18] are both using the discrete variational (DVM) approach, a numerical method for solving the Kohn−Sham equations,[73] and find vertical IP's shifted up by ~0.6 eV with respect to the present standards of DFT calculations. A surprisingly low value of 4.3 eV is mentioned by Reddy et al.[16] for the vertical IP of V_8C_{12}, but this value has not been confirmed in subsequent publications. The value of 5.92 eV (adiabatic) due to Grimes and Gale seems more credible, and the trend toward an increase of the IP with the number of d electrons is confirmed by the adiabatic IP of 7.49 eV calculated by the same authors for Fe_8C_{12}.[17] An opposite trend appears when replacing Ti by Zr: the computed IP value (4.89 eV) is decreased by 0.44 eV with respect to Ti_8C_{12}.[17]

The four values reported so far for the computed IP′ of Ti_8C_{12} in the tetrahedral form are clustered between 4.37[20,22] and 4.7 eV.[21] *This corresponds to a decrease of ~1 eV with respect to the lowest values*

Table 5. Ionization Potentials and Electron Affinities (Computed and Experimental) for Various Met-Cars[g]

	Ti_8C_{12}	$C\subset Ti_8C_{12}$	V_8C_{12}	Zr_8C_{12}	Nb_8C_{12}	Si_8C_{12}	Cr_8C_{12}	Fe_8C_{12}	ref
				Calculated Ionization Potentials (DFT)					
sym									
T_h	6.02[a]		4.3[a]						16
	5.33[b]		5.92[b]	4.89[a]		6.92[b]		7.49[b]	17
	5.92[a]								18
	5.4[a]	5.6[a]							19, 67
D_{2d}	5.8[a]	5.0[a]							19, 67
	7.05[a,c]			6.58[a,c]					42
T_d	4.5[a]	6.3[a]							19, 67
	4.37[a]		5.53[a]	3.99[a]					20, 27
	4.7[a]/4.6[b]		5.5[b]	4.2[a]/4.1[b]	5.4[b]				21
	4.43[b]								35
				Experimental Measurements (IP)					
method[d]									
CID	<6.82								124
CID			<6.74						125
PI	4.9 ± 0.2		>5.76	>5.76	>5.76				22
PI	4.40 ± 0.02			3.95 ± 0.02					105
				Calculated Electron Affinities (DFT)					
sym									
T_h	1.71[b]		2.18[b]	1.59[b]		3.40[b]		4.24[b]	17
	1.10[a]								18
		1.9[a]							67
D_{2d}		1.2[a]							67
T_d		0.8[a]							67
	1.26[b]			1.05[b]					21
	1.30[b]								35
				Experimental Measurements (EA)					
method[d]									
PES	1.16 ± 0.05[a]								126
	1.05 ± 0.05[b]		1.80[b,e]	1.02[b,f]	1.65[b,f]		2.28[b,e]		126, 127

[a] Vertical. [b] Adiabatic. [c] Calculations carried out using the discrete variational method (DVM). [d] CID, collision-induced dissociation; PI, photoionization spectroscopy; PES, photoelectron spectroscopy. [e] ±0.08. [f] ±0.06. [g] Calculations have been carried out with Xα or DFT-like methods assuming for the clusters the structures of pentagonal dodecahedron (T_h symmetry), of distorted cube with D_{2d} symmetry, and of tetracapped tetrahedron (T_d symmetry).

reported for the T_h form. Lou and Nordlander reported IP values for the three isomers (T_h, T_d, and D_{2d}) within the same methodological framework. The value of 4.5 eV (vertical) calculated for the T_d form is lower by 0.9 eV than that of the pentagonal dodecahedron. The trends associated with metal change are the same as for the T_h form: an increase of the computed IP (by 0.9−1.1 eV) when Ti is replaced by V and a decrease, by 0.4−0.5 eV, when going from Ti to Zr.[128]

One could have expected the T_d and D_{2d} isomers of met-cars to display a similar behavior, since the deformation of the metal framework does not appear strikingly different (Figure 12) and the global stabilization of both isomers differs by no more than 3 eV (0.15 eV/atom).[67] Surprisingly, the trends obtained from calculated IP's are quite opposite. Lou and Nordlander report an *increase* of the vertical IP of Ti_8C_{12} (D_{2d}) with respect to the T_h form. Xia et al report still higher values for the D_{2d} forms of both Ti_8C_{12} (7.05 eV) and Zr_8C_{12} (6.58 eV) (Table 5).

Since the disclosure by Brock and Duncan of the previously unpublished results of Lou and Nordlander on naked Ti_8C_{12},[22] it became clear that ionization potentials could represent the discriminating property that was looked after to assign the structure of met-cars. However, the first experimental indications concerning the ionization potentials of met-cars were obtained as a byproduct of collision-induced dissociation processes carried out on metal carbide cluster cations with various stoichiometries.[124,125] Since the single-step dissociation product of the $M_9C_{12}^+$ cluster ions (M = Ti, V) was shown to be the met-car *cation* $M_8C_{12}^+$ therefore resulting from the loss of a neutral metal atom, it was inferred that the IP's of the met-cars should be lower than that of the associated metal, namely 6.82 eV for Ti[124] and 6.74 eV for V.[125] A different method, based on photoionization spectroscopy, was used by Brock and Duncan to determine the vertical IP's.[22] A value of 4.9 ± 0.2 eV was obtained for Ti_8C_{12} (Table 5). For V_8C_{12}, Zr_8C_{12}, and Nb_8C_{12}, an indirect determination based on the dependence of signal intensities upon the power of the ionization laser employed eventually suggested that the IP's should be higher than 5.76 eV. The trend, especially when going from Ti_8C_{12} to Zr_8C_{12}, was definitely opposite to all calculated values (Table 5). Quite recently, Sakurai and Castleman conducted a photoionization spectroscopy study of the pure and mixed titanium/zirconium met-cars to determine their IP's with a more direct approach, based on the investigation of the photoionization efficiency curves (PIE) near threshold.[105] The results obtained for $Ti_{8-x}Zr_xC_{12}$ ($x = 0-4, 8$) with the corresponding error bars are reproduced in Figure 29. For pure metal met-cars, the obtained IP's are 4.40 ± 0.02 eV for Ti_8C_{12} and 3.95 ± 0.02 eV for Zr_8C_{12} (Table 5). Those values are in excellent agreement with the computed potentials reported for the T_d conformation of met-cars by Dance (4.37 eV for Ti_8C_{12}, 3.99 eV for

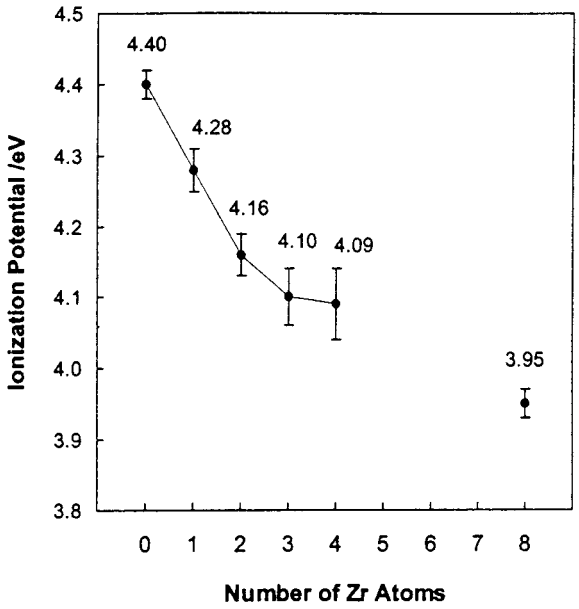

Figure 29. Ionization potentials measured by Sakurai and Castleman for the $Ti_{8-x}Zr_xC_{12}$ (x = 0−4, 8) clusters. Reprinted with permission from ref 105. Copyright 1998 American Chemical Society.

Zr_8C_{12}, vertical IP's)[20] and by Poblet et al. (4.6[21] or 4.43 eV[35,128] for Ti_8C_{12}, 4.1 eV for Zr_8C_{12}, adiabatic IP's). Sakurai and Castleman noted that agreement and discussed its consequences on the preferred conformation of met-cars, concluding that the T_d symmetry met-cars are present in considerable amounts.[105]

E. Electron Affinities

Electron affinities (EA's) represent another important property, almost readily available from DFT calculations. In contrast to ionization potentials, there is no clear-cut difference between the range of EA's computed for the T_h form and for the T_d isomer (Table 5). Grimes and Gale report an adiabatic electron affinity of 1.71 eV for dodecahedral Ti_8C_{12} and a slightly lower value (1.59 eV) for Zr_8C_{12}.[17] However, Li et al.[18] obtain a very low value of 1.10 eV for the *vertical* EA of dodecahedral Ti_8C_{12}. Poblet et al.[21,35] investigated the T_d form and report an adiabatic EA of 1.26/1.30 eV for Ti_8C_{12}. A still lower value (1.05 eV) is computed for Zr_8C_{12}.[21] Accurate experimental estimates of the electron affinities of met-cars have been obtained by Wang et al. in 1996[126] and 1997[127] from photoelectron spectroscopy experiments performed on met-car *anions*. The values reported for Ti_8C_{12} (vertical EA, 1.16 ± 0.05 eV; adiabatic EA, 1.05 ± 0.05 eV)[126] and for Zr_8C_{12} (adiabatic EA, 1.02 ± 0.05 eV)[127] are remarkably low, especially when compared to the experimental adiabatic EA's obtained for other met-cars (V_8C_{12}, 1.80 eV; Cr_8C_{12}, 2.28 eV; Nb_8C_{12}, 1.65 eV; see Table 5).[127] The agreement is good with the EA's computed assuming the T_d conformation. Wang indeed explains the low EA's of group 4 metal met-cars by referring to the orbital scheme specifically associated by Lin and Hall to the tetrahedral conformation of the M_8C_{12} clusters.[14] The other features of the photoelectron spectrum of $Ti_8C_{12}^-$ and $V_8C_{12}^-$ have also been interpreted in relation with that orbital scheme (Figure 30).

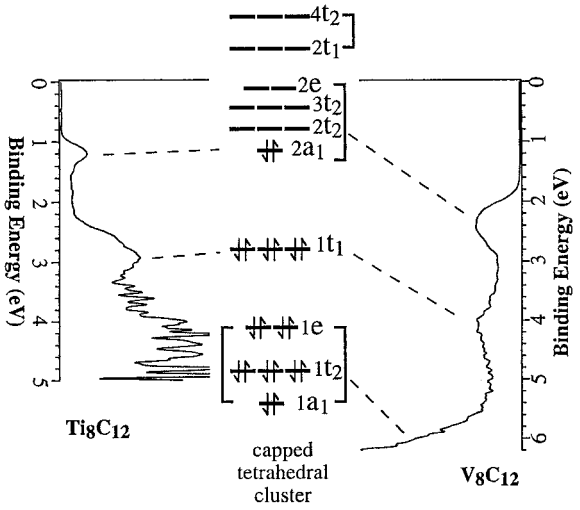

Figure 30. Photoelectron spectra of $Ti_8C_{12}^-$ and $V_8C_{12}^-$ obtained by Li et al. at 6.42 eV photon energy, compared with the valence molecular orbitals derived by Lin and Hall for the tetracapped tetrahedral met-cars (see Figure 17). The orbital occupation is for Ti_8C_{12}. Reprinted with permission from ref 127. Copyright 1997 American Chemical Society.

V. Chemical Reactivity of Met-Cars

A. Methods of Investigation

Several techniques have been tuned to investigate the reactivity of the metal carbide cluster ions formed in a laser vaporization source. The earliest investigations carried out in Castleman's group relied on a preliminary mass selection of the desired cluster. The ion beam was then injected into a drift tube where the selected cluster encounters the reactant mixed with helium as a buffer gas.[59] The FTICR (Fourier transform ion cyclotron resonance) mass spectrometer studies reported by Byun, Freiser, and coworkers[129,131] basically rely on the same principle even though the total pressure of the reaction chamber is $\sim 10^{-6}$ Torr, compared to 0.7 Torr in Castleman's experiments. A new method of forming met-car ligand complexes was then reported by Castleman et al. involving the direct interaction of the vaporized metal with mixtures of methane and selected reactant gases.[61]

The dominant features of the reactivity of $Ti_8C_{12}^+$ toward various molecules had been reported by Castleman et al. very soon after those molecules have been discovered.[59] They have been completed later and extended to other met-cars such as $Ti_7NbC_{12}^+$ and $Nb_8C_{12}^+$.[61] Byun, Freiser and co-workers have investigated the reactivity of $V_8C_{12}^+$, $Nb_8C_{12}^+$, and M−C nanocrystals.[60,129,131,162] Theoretical investigations on the association reactions of Ti_8C_{12} with halogen atoms, small polar molecules, carbon monoxide, and π-bonded hydrocarbons have been reported by Poblet et al.[23] and by Ge et al.[130] The present state of the art concerning the reactivity of met-cars is summarized in the next sections.

B. Association Reactions of $Ti_8C_{12}^+$

(i) $Ti_8C_{12}^+$ is very reactive toward polar molecules such as CH_3OH, H_2O, and NH_3 (or ND_3). The mass spectrum of the products arising from the reaction is composed of eight peaks corresponding to the association products $Ti_8C_{12}^+(P)_n$, $1 \leq n \leq 8$.[59] An increase of the reactant pressure just displaces the relative peak heights toward higher values of n. No additional peak is observed. It can be easily deduced from such a spectrum that the reaction proceeds through multistep attachment of the reactant to each metal center:

$$Ti_8C_{12}^+(P)_{n-1} + P \rightarrow Ti_8C_{12}^+(P)_n \qquad (9)$$

(ii) Stepwise association reactions are also observed between $Ti_8C_{12}^+$ and molecules which do not have permanent dipole moment but do have a π-bonding system such as benzene and ethylene. At variance with polar molecules, no more than four such π-bonded molecules can be attached to $Ti_8C_{12}^+$.[59,61] As for many observed properties of met-cars, the termination of the sequential reaction at $n = 4$ has been used, though unconclusively, as an argument in the controversy that has developed about the structure of those clusters. The truncation of some association series at $n = 4$ suggests that the reaction stops after completing the coordination sphere of a preferred type of metal atoms, occurring four times. It has been therefore interpreted in favor of a tetragonal structure with either T_d or D_{2d} symmetry and with two types of metal sites.[129,131] However, Castleman et al. objected that the truncation at $n = 4$ of the association series with π-bonded molecules is consistent with the symmetric T_h structure since those molecules can form surface complexes, with each ligand bridging two metal atoms in a pentagonal ring.[59,61] This interpretation is however reconsidered in a subsequent paper[132] (see below), in agreement with the recent move of Castleman's group toward the recognition of the T_d form as the dominant isomer of Ti_8C_{12}.[105]

(iii) Association reactions have also been observed between $Ti_8C_{12}^+$ and pyridine terminating at $Ti_8C_{12}^+(pyridine)_4$.[61] With acetone, five adducts are observed, namely $Ti_8C_{12}^+(acetone)_{1-5}$.[62,63]

(iv) Adsorption of methane molecules on neutral Ti_8C_{12} has been observed at low temperature.[132] The characterization by a mass spectrometer of those low-energy adsorbates resulting from charge induced dipole interactions rules out the hypothesis proposed by Brock and Duncan of a production of Ti_8C_{12} by fragmentation of larger neutral metal−carbon species upon photoionization.[22] The energy involved in such a fragmentation process would then yield a desorption of the methane molecules. The high stability of *neutral* Ti_8C_{12} is thus inferred from its presence in large amount in the cluster beam.[132] When sufficiently cooling the nozzle from which the cluster beam is ejected, mass peaks corresponding to $Ti_8C_{12}(CH_4)_n$ ($n = 0-5$) were observed, the most intense ones corresponding to the pure met-car ($n = 0$) and to the tetramethane adsorbate ($n = 4$).[132] Sakurai and Castleman acknowledge that the bridging model proposed earlier to explain the bonding of four π-bonded molecules to a dodecahedral met-car does not apply to methane and conclude that the truncation at four is likely to arise from different electronic and chemical characteristics of the two different groups of titanium atoms in a cluster cage with T_d structure.[132]

C. Reactions of Niobium-Containing Met-Cars and Titanium Carbon Clusters with Acetone

The partial or complete replacement of Ti by Nb strongly modifies the reactivity of the met-car cage, especially with respect to acetone. $Ti_7NbC_{12}^+$ and $Nb_8C_{12}^+$ react with acetone to give adducts with one and two oxygen atoms, thus implying that niobium-containing met-cars can induce carbon−oxygen bond-breaking.[60,61] $Ti_7NbC_{12}^+$ and $Nb_8C_{12}^+$ as well as their oxygen adducts can undergo further associations with a limited number of acetone molecules (4 for $Ti_7NbC_{12}^+$; 2 for $Nb_8C_{12}^+$, $Nb_8C_{12}^+O$, $Ti_7NbC_{12}^+O$, and $Ti_7NbC_{12}^+O_2$; 1 for $Nb_8C_{12}^+O_2$).[60,61]

The chemical stability of $Ti_8C_{12}^+$ was evidenced by comparing its reaction pattern with acetone to that of the neighboring titanium carbide clusters $Ti_8C_{11}^+$, $Ti_8C_{13}^+$, and $Ti_8C_{14}^+$.[63] At variance with $Ti_8C_{12}^+$ and other met-cars, $Ti_8C_{11}^+$ is able to break the chemical bonds of acetone to give $Ti_8C_{11}^+(COCH_3)$. Association reactions of this latter product with 1−3 acetone molecules, and of $Ti_8C_{11}^+$ itself with 1−4 acetone molecules are also observed.[63] The breaking of the stable C−C bond of acetone, which was not observed with Nb-containing met-cars is attributed to the chemical activity of a vacancy site in the uncomplete cage structure of $Ti_8C_{11}^+$. Carbon-rich clusters $Ti_8C_{13}^+$ and $Ti_8C_{14}^+$ undergo three reaction channels: (a) association with one acetone molecule; (b) abstraction of extra carbon atom(s) assumed exohedral, to give $Ti_8C_{12}^+$; and (c) replacement of the exohedral carbon(s) by an acetone molecule.[63]

D. Reaction of $Ti_8C_{12}^+$ and Other Met-Cars with Methyl Iodide

The only abstraction reaction characterized to date with $Ti_8C_{12}^+$ occurs with methyl iodide and involves the breaking of the I−C bond to give the monoadduct $Ti_8C_{12}^+I$:

$$Ti_8C_{12}^+ + CH_3I \rightarrow Ti_8C_{12}^+(I) + CH_3 \qquad (10)$$

[62]

The monoiodine adduct can further react with polar molecules such as methanol to give the distribution $Ti_8C_{12}^+(I)(CH_3OH)_{1-7}$. It should be noted however that intensity distribution of the seven peaks corresponding to methanol adducts is not regular. The two adducts $Ti_8C_{12}^+(I)(CH_3OH)_4$ and $Ti_8C_{12}^+(I)(CH_3OH)_7$ seem to display particular stability.[61] The replacement of one, two, or four Ti atoms by zirconium, which has the same electronic configuration, does not modify the reactivity of mixed metal met-cars with respect to methyl iodide.[62]

Once again, niobium-containing met-cars seem to be more reactive than $Ti_8C_{12}^+$. $Ti_7NbC_{12}^+$ and $Nb_8C_{12}^+$ are capable of taking up multiple iodine atoms to form $Ti_7NbC_{12}^+(I)_{1-4}$ and $Nb_8C_{12}^+(I)_{1-5}$.[62] Fivefold

adducts are also observed between $Nb_8C_{12}^+$ and bromine, but reaction with CH_3Cl truncates at $Nb_8C_{12}Cl_4^+$. One should therefore expect the reactivity of $V_8C_{12}^+$ toward CH_3X (X = Cl, Br, I) to resemble that of Nb_8C_{12}. A difference is observed however, since the reaction always truncates at four adducts and not at five as for niobium.[129,131]

The diversity in the response of met-cars toward halide abstraction has led to the conclusion that this reaction is monitored by the electronic configuration of the metal elements[62] and more specifically correlated to the number of weakly coupled metal electrons accommodated in the slightly antibonding set of metal orbitals. Most calculations agree that this number should be equal to 2 for neutral Ti_8C_{12}. One such electron is therefore available in the cluster cation to give a strong covalent bond with iodine. When titanium is replaced by vanadium, or niobium, eight more metal electrons become available, and according to the RHF orbital scheme of Rohmer et al.,[90,96] four of them, accommodated on orbital combinations localized on the large tetrahedron, should be weakly coupled. It is assumed that the ionization of Nb_8C_{12} makes available for bonding one more d electron, accommodated in the triply degenerate orbital $2t_2$ localized on the inner tetrahedron. Five covalent bonds are therefore possible with halogen atoms. At higher reagent pressure, $Nb_8C_{12}I_5^+$ further reacts with CH_3I to give an association product $Nb_8C_{12}I_5(CH_3I)^+$.[60] This behavior confirms that the cluster cation has no more than five unpaired electrons and cannot abstract more iodine atoms from CH_3I. The reactivity of the vanadium met-car appears more puzzling since the halogen abstraction stops at four adducts instead of five. Since the abstraction processes are expected to take place at the metal atoms of the capping tetrahedron, one could tentatively suggest that the inner metal sites become sterically unreachable to a fifth incoming halogen atom. Similar considerations could explain the long reaction time necessary to observe the attachment of a fifth atom of I or Br to $Nb_8C_{12}X_4^+$.[62] The case of $Ti_7NbC_{12}^+$ is also particularly interesting, since no more than two weakly coupled metal electrons should be present in the cation. However, the strength of the metal−halogen bonds seems sufficient to overcome the metal−metal coupling in the small tetrahedron and then to promote one d electron from the $1a_1$ bonding orbital combination to the $2t_2$ nonbonding one (Figure 20). Four covalent bonds then become possible between iodine atoms and metals belonging now to the *inner* tetrahedron.

E. Oxidation-Induced Reactions of Ti_8C_{12} and Other Metal Carbon Clusters

$Ti_8C_{12}^+$ seems to be inert with respect to molecules having neither a permanent dipole moment nor a π-bonding system, such as oxygen and methane.[59] However, neutral metal−carbon species produced in a laser vaporization source rearrange in the presence of oxygen to yield selectively and exclusively $Ti_8C_{12}^+$.[133,134] To better understand this oxygen-induced ionization reaction, a systematic investigation of the reactivity of ionic and neutral metal carbide clusters (M = Nb, Zr, V, Ta) toward dioxygen has been carried out.[134] As for Ti−C clusters, it was noted that neutral carbide clusters of Nb and Zr undergo ionization in the presence of oxygen. A structural reorganization of the clusters was also observed. With zirconium, three intense mass peaks were assigned to the cluster ions $Zr_8C_{12}^+$, $Zr_6C_6^+$, and $Zr_4C_4^+$. The oxidation of neutral niobium carbide clusters yields a more complex spectrum characterized by the dominance of cubiclike cluster ions. Reaction of *ionic* $Nb_xC_y^+$ clusters with dioxygen follows a markedly different path.[30,134] The reaction proceeds through a sequential loss of C_2 units eventually yielding either the naked metal cluster Nb_x^+ or Nb_xC^+ depending on y being even or odd. No single carbon atom loss channel is observed either from met-car or from fcc-type cluster ions including $Nb_4C_4^+$. In view of those results, it was proposed to reconsider the $2 \times 2 \times 2$ cubic structure of $Nb_4C_4^+$ [30] and to propose an alternative conformation based upon C_2 building blocks.[134] Calculations however suggest that the proposed isomer with two C=C bonds is strongly destabilized with respect to the cubic framework.[48] Moreover oxidation experiments carried out by Yeh et al. under a static pressure of oxygen at $\sim 7.2\ 10^{-8}$ Torr allowed one to detect the oxidation product $Nb_4C_3O^+$, although in a very small amount.[30] In certain experimental conditions, an abstraction reaction occurs between $Nb_4C_4^+$ and water, or methanol, forming $Nb_4C_4OH^+$ and $Nb_4C_4OCH_3^+$, respectively.[30]

F. Reactivity of $V_8C_{12}^+$ and $Nb_8C_{12}^+$

At variance with $Ti_8C_{12}^+$, $V_8C_{12}^+$ reacts with oxygen to generate first $V_8C_{10}^+$. That cluster itself reacts with oxygen to give additional metal−carbon clusters and oxidation products.[129] The difference in reactivity between $Ti_8C_{12}^+$ and $V_8C_{12}^+$ has been interpreted as arising from the larger number of metal electrons in the vanadium cluster which tend to populate near-degenerate nonbonding orbitals.[129] Investigated by Byun, Freiser, and colleagues, the reactivity of $V_8C_{12}^+$ is also characterized by association reactions with π-bonding molecules that truncate sharply at $V_8C_{12}^+L_4$ (L = C_6H_6, CH_3CN) as for $Ti_8C_{12}^+$. The vanadium met-car reacts with traces of water by association of one H_2O molecule, followed by dehydrogenation of a second water molecule to give presumably $V_8C_{12}(OH)_2^+$. Further association reactions are observed, with truncation at four attachments which eventually yields $V_8C_{12}^+(O)(H_2O)_3$.[129,131] With methyl halides, sequential abstraction reactions are observed that truncate sharply at $V_8C_{12}X_4^+$ (X = Cl, Br, I).[131]

Freiser and co-workers completed their study of the reactivity of $V_8C_{12}^+$ by a systematic investigation carried out on $Nb_8C_{12}^+$.[60] Most reactions previously observed by Castleman's group[62] were reproduced at a different pressure of the He expansion gas containing the reagents (10^{-8}−10^{-5} Torr). Stepwise association reactions with both polar and π-bonding molecules (H_2O, NH_3, alcohols, CH_3CN, C_6H_6) are observed to truncate at $Nb_8C_{12}^+L_4$. In the case of polar reagents, more ligands can be added to $Nb_8C_{12}^+L_4$, but they grow very slowly compared to the first four. Addition of water to $Nb_8C_{12}^+$ initially proceeds as for

$V_8C_{12}^+$ by an addition of H_2O, followed by the fixation of a second water with elimination of H_2. The same process is repeated once again, yielding $Nb_8C_{12}(OH)_2(H_2O)^+$ and eventually $Nb_8C_{12}(OH)_4^+$. The reaction does not proceed further. The reaction with alcools proceeds exactly the same way, leading to $Nb_8C_{12}(OR)_4^+$. Note that this second dehydrogenation is typical of $Nb_8C_{12}^+$ and is not observed for $V_8C_{12}^+$. Further association reactions eventually leading to $Nb_8C_{12}(OR)_4(ROH)_{1-4}$ can also be observed at longer reaction times. Abstraction reactions with methyl halides CH_3X have been reviewed in section V.D.

G. Theoretical Investigations on the Reactivity of Ti_8C_{12}

Two recent studies have been specifically focused on the reactivity of met-cars and have used Ti_8C_{12} as a model to investigate association reactions with chlorine atoms, polar molecules, and hydrocarbons with a π-bonding system. Ge et al.[130] considered that the observed association of eight polar molecules, with $Ti_8C_{12}^+$ [59] and the ion mobility measurements carried out by Bowers[84] are sufficiently convincing arguments in favor of the T_h conformation. Assuming the dodecahedral structure for the met-car cage, they carried out ab initio RHF calculations with minimal basis sets on Ti_8C_{12} itself and on the adducts $Ti_8C_{12}(H_2O)_8$ and $Ti_8C_{12}(C_2H_4)_4$. A closed-shell electronic configuration was found for Ti_8C_{12} assuming the constraints of the D_{2h} symmetry, but the reported HOMO−LUMO gap (2.32 eV) appears extremely low with respect to ab initio standards. No reference is given to the work of Hay on the ab initio ground state of dodecahedral Ti_8C_{12}.[40] From the calculations on the water adduct, the authors conclude that the coordination of eight H_2O molecules induces a rearrangement of the electronic configuration of Ti_8C_{12} and yields a very large binding energy of 18.735 eV for the eight water molecules. This binding energy is assigned to the charge transfer from the H_2O molecules to the cluster and associated with an important increase of the HOMO−LUMO gap (3.90 eV). The strong negative charge of the met-car in $Ti_8C_{12}(H_2O)_8$ (−1.74 e) and the large increase of the HOMO−LUMO gap suggest that the "electronic change" of Ti_8C_{12} in the water adduct partly offsets a bias in the RHF wave function of the naked cluster. A still larger increase of the HOMO−LUMO gap is reported for the tetraethylene adduct (4.49 eV), but the charge transfer (0.99 e) occurs in the opposite way, i.e., from the met-car to the ethylene ligands, and the $Ti_8C_{12}(C_2H_4)_4$ complex is computed to be unstable, with a negative binding energy of −1.03 eV.[130]

The other study is due to Poblet et al.,[23] who investigated by means of ab initio RHF and DFT calculations the addition of Cl, NH_3, CO and C_6H_6 to the tetrahedral form of neutral Ti_8C_{12}. The RHF conformation used to describe Ti_8C_{12} is the quintet state $^5A_2$ corresponding to the localization of four d electrons into four combinations of d_{z^2}-like orbitals centered on the atoms of the inner tetrahedron *thn*. When an adduct is obtained with four chlorine atoms, the cluster is formally stripped from its unpaired electrons and the configuration resulting from this oxidation process is a closed-shell singlet $^1A_1$. The Mulliken charge computed for each chlorine is −0.41 e, which corresponds to the net charge generally found for a Cl^- ligand. With chlorine as with other ligands, two conformations are possible for the tetra-adducts depending on the type of the metal sites chosen for the association process (see Figure 31 for the case of $Ti_8C_{12}(NH_3)_4$). The formation of the $Ti_8C_{12}(Cl)_4$ ligand is largely exothermic (186 kcal·mol^{-1}) with respect to the neutral fragments Ti_8C_{12} + 4Cl. Note that the nonet ground state of *dodecahedral* Ti_8C_{12} seems ideally suited to transfer electrons to eight surrounding chlorine atoms. The binding energy with respect to the neutral fragments amounts 414 kcal·mol^{-1}, not sufficient however to balance the destabilization of the cage cluster. The results obtained with Cl and with other ligands are summarized in Table 6. DFT calculations suggest that the fixation of NH_3 molecules is largely exothermic and does not strongly depend on the type of the metal site. Eight NH_3 molecules can be eventually attached to the cluster with an overall stabilization of 163 kcal·mol^{-1} (131 kcal·mol^{-1} from RHF calculations). Four CO molecules are easily fixed to the metal atoms of the large tetrahedron (binding energy, 88 kcal·mol^{-1}), but the coordination of four additional CO's on the atoms of the inner tetrahedron is more difficult according to DFT calculations (BE, 36 kcal·mol^{-1}) or even impossible according to RHF. Four molecules of benzene can also be fixed on the metal atoms of **THN** (BE, 107 kcal·mol^{-1}), but the association of more benzene ligands proves impossible, in agreement with experimental results. Recent DFT calculations focused on the addition of CO and NH_3 on the tetrahedral conformation of V_8C_{12} suggest a stronger affinity of the vanadium met-car toward

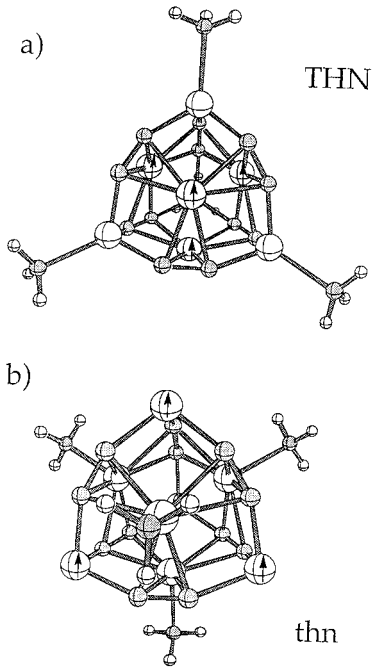

Figure 31. Optimized structures for $Ti_8C_{12}(NH_3)_4$ from DFT calculations: (a) ligands attached to the metal atoms of the outer tetrahedron of metal atoms **THN**; (b) ligands attached to the metal atoms of the inner tetrahedron of metal atoms *thn*.

Table 6. Metal−Ligand Bond Lengths (Å) and Binding Energies (BE, kcal·mol^{-1}, Corrected from BSSE for RHF) Obtained from RHF[a] (Left) and from DFT[b] (Right) Calculations and Corresponding to the Addition of *n* Molecules of L (L = CO, C_6H_6, NH_3, Cl, *n* = 4, 8) to Ti_8C_{12} and to the Addition of 4 and 8 Molecules of CO and NH_3 to V_8C_{12}

				Ti_8C_{12}, RHF		Ti_8C_{12}, DFT		V_8C_{12}, DFT	
L	n	sym	site	d_{Ti-L}	BE	d_{Ti-L}	BE	d_{V-L}	BE
CO	4	T_d	**THN**	2.41	34	2.24	88	2.08	120
			thn	2.41	−46[c]	2.13	36	2.04	80
	8					2.27/2.15	109	2.09/2.08	191
C_6H_6	4	T_d	**THN**	2.67	35	2.49	107		
			thn	dissociation		dissociation			
NH_3	4	T_d	**THN**	2.26	118	2.29	96	2.20	114
			thn	2.23	36	2.30	83	2.21	87
	8			2.26/2.52	131	2.31/2.31	163	2.21/2.23	181
Cl	4	T_d	**THN**	2.28	186				
			thn	2.31	154				
	8			2.24/2.26	340				
	8	T_h	cubic	2.25	224[d]				

[a] Calculations carried out by means of the TURBOMOLE program.[135] [b] Calculations carried out by means of the ADF program.[76] [c] Repulsive interaction energy. [d] Stabilization energy with respect to the lowest quintet state of Ti_8C_{12} (T_d) + eight Cl atoms in their ground state. The binding energy with respect to the nonet ground state of Ti_8C_{12} (T_h) is 414 kcal·mol^{-1}.

both types of ligands and an easier fixation of eight substituents (Table 6).[48]

VI. Magic Peaks and Cluster Growth: From Small M_xC_y Clusters to Metal Carbon Nanocrystals

A. Met-Cars Are Not Alone!

The prominence of the mass peak corresponding to $Ti_8C_{12}^+$ as produced in Castleman's laser-induced plasma reactor[3] appears so impressive that the mere existence of other titanium carbon clusters in detectable yields appears problematic (Figure 1). It soon appeared however that mass peaks corresponding to small M_xC_y clusters could be obtained from the photofragmentation,[136] from the metastable decay,[137,138] or from the collision-induced dissociation[124,125,139] of the M_8C_{12} cations and gave indications about the preferred dissociation pathways of pure metal[124,125,136−138] and of mixed-metal[139] met-cars. (Figure 32). The dissociation fragments observed for M_8C_{12} species depend on the nature of M. Dissociation of $Ti_8C_{12}^+$ and $V_8C_{12}^+$ proceeds through successive losses of metal atoms[125,136] whereas losses of neutral MC_2 fragments are also observed along the photodissociation process of $Zr_8C_{12}^+$.[136] The successive loss of several metal atoms should not be interpreted as an indication of the presence of a tightly bound C_{12} cluster in $Ti_8C_{12}^+$ supporting the existence of the isomers depicted in Figures 5 and 7. This different behavior only suggests that Ti and V are more loosely attached to the cluster than is zirconium, as confirmed by the computed bond energies, higher for Zr_8C_{12} than for Ti_8C_{12} (Table 4).

The exploration of other synthetic routes toward metal carbon clusters emphasized the importance of experimental conditions in the obtained distribution of mass peaks. For example, Lu et al.[140] modified the common arc discharge technique by replacing the common arc by a pulsed arc cluster ion source (PACIS) using a cathode made of metal oxide and coupled to a reflection time-of-flight mass spectrometer. The mass distribution of vanadium cluster cations obtained from PACIS experiments indeed culminates around $V_8C_{12}^+$, but the met-car itself does not appear especially stable with respect to other

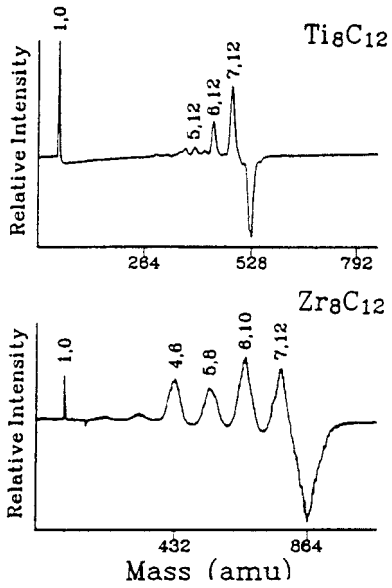

Figure 32. Photodissociation mass spectra obtained by Pilgrim and Duncan for $Ti_8C_{12}^+$ and $Zr_8C_{12}^+$ at 532 nm. The negative peaks represent depletion of the mass-selected parent ion, while the positive peaks represent the fragment ions. The titanium cluster loses a series of metal atoms, while the zirconium cluster loses $M-C_2$ units. Reprinted with permission from ref 136. Copyright 1993 American Chemical Society.

species such as $V_7C_{12}^+$, $V_7C_{11}^+$, or $V_6C_{11}^+$. The reasons this spectrum appears different from the ones obtained by means of laser vaporization are not completely understood but should be attributed either to the presence of oxygen originating in the V_2O_5 sample at the cathode or to the subsistence of unquenched plasma at the spectrometer.[140] By contrast, laser-induced photofragmentation of transition metal-coated fullerenes $C_{60}M_x$ and $C_{70}M_x$ (M = Ti, V) was shown to yield M_8C_{12} clusters as the most abundant product as soon as the laser intensity is sufficiently high to break the fullerene cage and remove the carbon surplus.[141]

In the region of high-nuclearity clusters, a first breakthrough was made by Wei et al. who explored the mass spectrum of zirconium carbon clusters and showed that magic peaks do exist beyond $Zr_8C_{12}^+$.[9,142]

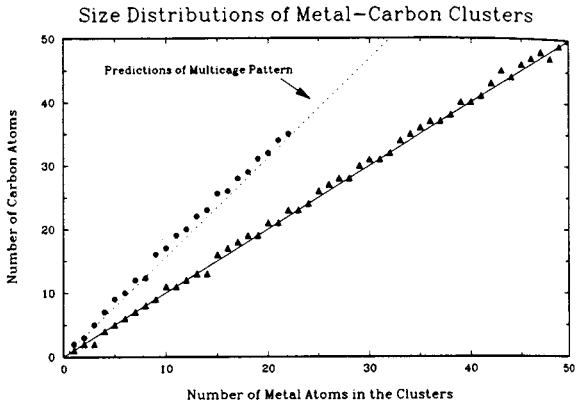

Figure 33. Plot of cluster size distribution of metal−carbon clusters: (▲) experimental values of Ta_mC_n clusters; (●) experimental values of Zr_mC_n clusters. Straight line: prediction of the fcc structural model (1:1 metal:carbon ratio). Dashed line: prediction of the multicage model proposed by Wei et al.[9,142] A similar progression should be obtained from the layered cubic model proposed by Wang and Cheng.[33] Reprinted with permission from ref 143. Copyright 1994 Elsevier.

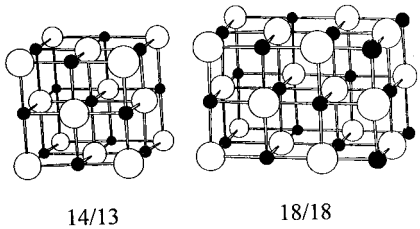

Figure 34. 3 × 3 × 3 and 3 × 3 × 4 fcc nanocrystal structures proposed for the $M_{14}C_{13}$ and $M_{18}C_{18}$ clusters. Reprinted with permission from ref 109. Copyright 1994 Plenum Press.

Those peaks were assigned the stoichiometries $Zr_{13}C_{22}$, $Zr_{14}C_{23}$, $Zr_{18}C_{29}$, and $Zr_{22}C_{35}$ and correspond all to a metal:carbon ratio close to 2:3. The abrupt and reproducible intensity drop of the mass peaks after the (8,12), (14,21/23), (18,29), and (22,35) stoichiometries were interpreted by the authors as revealing the closure of met-car-type structures with one, two, three, and four dodecahedral cages, respectively. Another structural interpretation has been recently suggested by Wang et al.[33] and will be discussed in detail below. Similar clusters were produced with niobium under certain experimental conditions.[10] By contrast, no met-car peak was observed with tantalum and all obtained Ta_xC_y clusters correspond to a 1:1 Ta:C ratio[140] (Figure 33). Those clusters were assigned a fcc structure, and the cluster sizes of Figure 34 were correlated to the various parallelepipedic fragments of a growing crystal.

A reinvestigation of the titanium carbon and vanadium carbon cluster series by Pilgrim and Duncan, using an experimental technique similar to that of Castleman, showed that the production of fcc nanocrystals with a 1:1 M:C ratio could be competitive with that of met-cars.[25,109] The mass spectrum of Figure 35 displays two magic peaks with comparable intensities, one assigned to the met-car (8,12) and the other corresponding to the (14,13) stoichiometry expected for a 3 × 3 × 3 fcc lattice fragment (Figure 34). Other peaks appear on the $Ti_nC_m^+$

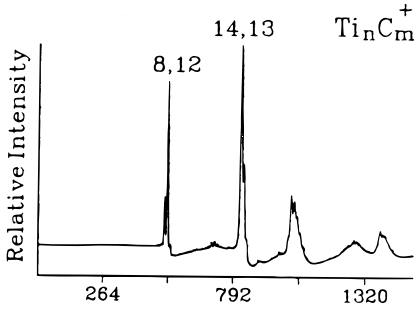

Figure 35. Mass spectrum of titanium−carbon cation clusters obtained by Pilgrim and Duncan. The $Ti_8C_{12}^+$ and $Ti_{14}C_{13}^+$ clusters are formed preferentially. A series of larger clusters is observed. Reprinted with permission from ref 25a. Copyright 1993 American Chemical Society.

spectrum that were correlated with larger parallelepipedic fcc nanocrystals.[25,109] Experiments carried out by Wei et al.[10] on the formation of niobium carbon clusters showed that the balance between met-cars—and more generally clusters with high carbon yield referred to as multicage met-cars—on one hand, and fcc nanocrystals, on the other hand was strongly dependent upon experimental conditions, suggesting that the cubic structures do not develop on top of met-cars but rather grow independently.[10]

Laser-induced photodissociation of 3 × 3 × 4 and 3 × 3 × 3 nanocrystals of titanium have been reported by Pilgrim and Duncan.[25,109] The photodissociation of $Ti_{17}C_{19}^+$ generated the mass spectrum reproduced in Figure 36a where the most intense peaks are assigned to the metallocarbohedrene $Ti_8C_{12}^+$ and to the fcc crystallite $Ti_{14}C_{13}^+$. Results obtained from the photodissociation of this latter nanocrystal are more surprising, since the most prominent dissociation peak does not correspond to the expected met-car cage but to $Ti_8C_{13}^+$ (Figure 36b).

An explanation proposed for the formation of this cluster suggests as a first step the elimination of the six metal atoms at the center of the cubic faces followed by the reorganization of the facial carbons into C_2 units. A met-car cage is formed, whereas the central carbon remains trapped inside, yielding the encapsulation complex $(C\subset Ti_8C_{12})^+$.[25] $V_{14}C_{13}^+$ has the same dissociation pattern, but $Zr_{14}C_{13}^+$ does not seem to display any endohedral structure in its dissociation spectrum. The mass spectrum obtained by Yu et al.[144] from laser-induced plasma reaction of titanium vapor with dehydrogenated CH_4 shows around the dominant peak corresponding to $Ti_8C_{12}^+$ two satellite peaks respectively assigned to the endohedral met-cars $(C\subset Ti_8C_{12})^+$ and $(C_2\subset Ti_8C_{12})^+$. The assignment of $Ti_8C_{14}^+$ as an encapsulation species is hardly compatible however with the facile loss of C_2 previously observed from metastable dissociation experiments carried out in Castleman's group.[137,138] In the same report, however, the great stability of the $Ti_8C_{13}^+$ species has been noted and related for the first time to the possible existence of endohedral met-cars. This hypothesis has been supported later by the abundance of the $V_8C_{13}^+$ species obtained from the metastable decay of $V_9C_n^+$ ($n = 14-17$).[138]

To end up this short review on non met-car M/C clusters, it appears that the relative importance of

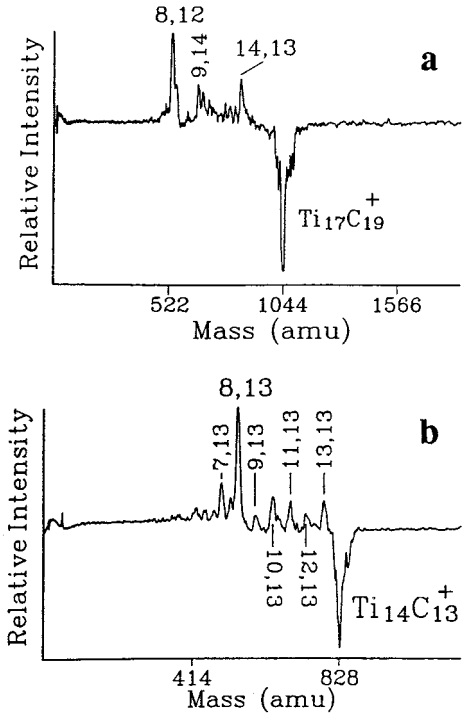

Figure 36. Photodissociation mass spectra obtained by Pilgrim and Duncan for (a) $Ti_{17}C_{19}^+$ and for (b) $Ti_{14}C_{13}^+$. For the larger nanocrystal ($3 \times 3 \times 4$ structure), the main fragments are $Ti_{14}C_{13}^+$ and Ti_8C_{12}. For $Ti_{14}C_{13}^+$ ($3 \times 3 \times 3$ structure), the fragmentation pattern indicates a sequence of metal atom losses, and the most intense fragment is $Ti_8C_{13}^+$. Reprinted with permission from ref 25a. Copyright 1993 American Chemical Society.

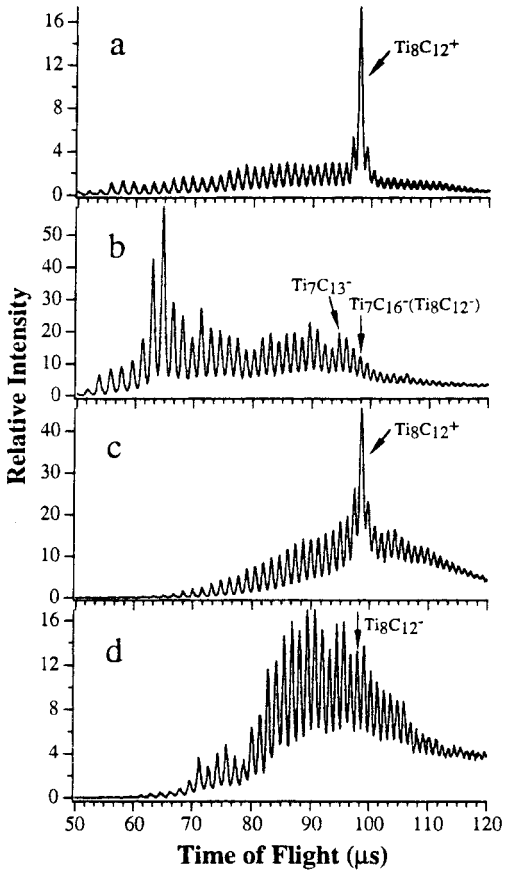

Figure 37. Mass spectra of $Ti_xC_y^+$ and $Ti_xC_y^-$ obtained by Wang, Li, and Wu in the same experimental conditions. (a) Positive ion mass spectrum of $Ti_xC_y^+$ clusters when a titanium target is vaporized with a 5% CH_4 seeded helium carrier gas, showing the "magic" $Ti_8C_{12}^+$ met-car. Laser vaporization conditions: 10 mJ/pulse at 532 nm, 7 ns pulse width. (b) Negative ion mass spectrum of $Ti_xC_y^-$ clusters under similar conditions as (a), showing that the anticipated met-car anion $Ti_8C_{12}^-$ is not produced. (c) Positive ion mass spectrum of $Ti_xC_y^+$ clusters when a solid TiC target is vaporized with neat helium carrier gas, showing the "magic" $Ti_8C_{12}^+$ met-car. (d) Negative ion mass spectrum of $Ti_xC_y^-$ clusters under similar conditions as (c) (7 mJ/pulse), showing that the met-car anion $Ti_8C_{12}^-$ is produced with significant abundance. Reprinted from ref 126. Copyright 1996 American Chemical Society.

the met-car peak with respect to other species present in the mass spectrum might drastically depend on the charge of the clusters produced in the laser vaporization source, but is also heavily influenced by the experimental conditions. The original report by Castleman's group displaying the exceptional abundance of $Ti_8C_{12}^+$ (Figure 1) was obtained by detecting only the *cationic species* that were directly produced in the source.[3] All subsequent experiments carried out on the group of cationic M/C clusters confirmed the magic, or supermagic, character of the met-car peak. Selecting the *neutral species* produced a different mass spectrum with enhanced contributions from small non-met-car clusters. The mass spectra of neutral Ti/C and V/C clusters obtained by Wei et al. at various fixed laser wavelengths show that, besides M_8C_{12}, the peaks corresponding to (1,2), (2,4), (3,6), (4,8), (5,10), (6,12), and (7,13) are local maxima for Ti_nC_m and V_nC_m.[7b] It was deduced from that progression that MC_2 is the main building unit in the formation of met-cars. Brock and Duncan later discussed this interpretation,[22] asserting that the spectra obtained by Castleman's group result from phtofragmention processes and does not correspond to the nascent distribution. The mass spectrum reported by Brock and Duncan and assumed to represent the nascent distribution of neutral Ti/C clusters also truncates at Ti_8C_{12}, but the met-car stoichiometry is not superabundant. The cluster distribution, starting at (3,2), is different from that of Wei et al. and does not clearly point out a specific building block. Sakurai and Castleman[26] recently confirmed the experiment by Brock and Duncan but showed that the relative abundance of "nascent" neutral Ti_8C_{12} is extremely dependent upon the experimental conditions and, particularly, upon the power of the vaporization laser. More recently, the same authors[132] characterized neutral methane adsorbates $Ti_8C_{12}(CH_4)_n$ ($n = 1-5$) and, assuming a low adsorption energy, concluded that the adsorbates could not resist a fragmentation process. Neutral Ti_8C_{12} is therefore expected to be present in large amount in the cluster beam (see V.B).[132]

Wang et al. applied the standard techniques described by Castleman et al. to produce and detect metal carbon cluster *anions*.[126] The mass spectra showing the distribution of the titanium carbon cluster anions obtained either from the vaporization of pure metal with a CH_4-seeded helium carrier gas or from the vaporization of a solid TiC target in pure helium are reproduced in Figure 37 and compared to the well-known mass spectra obtained in the same

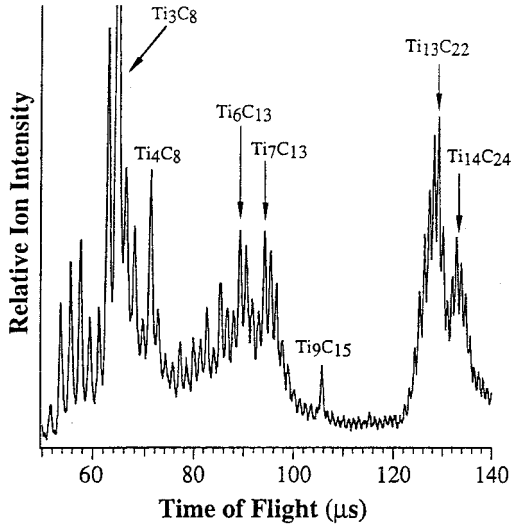

Figure 38. Mass spectra of $Ti_xC_y^-$ anions obtained by Wang et al. from laser vaporization of a pure Ti target with a He carrier gas containing 5% CH_4. The $Ti_3C_8^-$ is out of scale and is twice the full scale. Reprinted with permission from ref 34. Copyright 1998 American Chemical Society.

experimental conditions for the *cationic species*. Figure 37b shows that the expected met-car anion $Ti_8C_{12}^-$ is *not* produced in the laser vaporization source when using a pure metal sample. $Ti_8C_{12}^-$ is produced in significant amount by laser vaporization of solid TiC but appears in the spectrum as a totally nonmagic peak.[126] In a more detailed mass spectrum obtained in the same experimental conditions as for Figure 37b, Wang et al.[34] characterize the magic peaks present in the spectrum of $Ti_xC_y^-$ and occurring at $(x,y) = (3,8)$, (4,8), (6,13), (7,13), and (9,15) (Figure 38). High-nuclearity clusters anions also appear as magic peaks, such as $Ti_{13}C_{22}^-$ and $Ti_{14}C_{24}^-$. Those high-nuclearity, carbon-rich species appear for the first time in the mass spectrum of titanium carbon clusters and have stoichiometries similar to the "multicage structures" observed by Castleman et al. in the mass spectrum of Zr/C and Nb/C cluster cations. It will be seen in the discussion below that another interpretation is proposed by Wang et al.[33] We will discuss in the next subsections the various theoretical studies that have been recently devoted to the structure and properties of those metal carbon clusters, with particular emphasis on titanium, and in relation with the growth and dissociation mechanisms of met-cars and fcc nanocrystals.

B. Theoretical Studies on Small Ti/C Clusters: From TiC to Ti_2C_4

The increasing interest in the growth pattern of Ti_8C_{12} and fcc nanocrystals containing titanium or other early transition metals has triggered several systematic studies focused on the structure and stabilization energies of small-nuclearity Ti/C clusters. The TiC molecule has been studied at the CASSCF and at the MRCI levels. A comparative study has been carried out by Scuseria et al.,[104,145] who found that the calculations carried out with the hybrid density functional B3LYP are in good agreement with high level ab initio approaches such as MRCI and CCSD(T). All calculations accounting for correlation confirm that the ground state of TiC is the $^3\Sigma^+$ state with the equilibrium Ti−C distance varying from 1.66 to 1.76 Å and the binding energy comprised between 2.35 and 3.6 eV according to the type of calculation.[146] B3LYP calculations predicted a bond length of 1.679 Å and a binding energy of 3.60 eV.[104] Let us note that an experimental determination reports a somewhat higher value for the dissociation energy (4.38 eV).[151]

For clusters containing a single metal atom TiC_n ($n = 2-4$), geometry optimizations by Sumathi and Hendrickx (SH)[28,147] were performed at both the DFT B3LYP and the ab initio CASSCF levels, using for titanium the (14s11p6d3f/8s6p4d1f) basis set formed by adding diffuse 4p and 3d functions and f-type polarization functions to Wachter's (14s9p5d) basis set.[148] For carbon, the standard DZP (9s5p1d/4s2p1d) basis set was used. The CASSCF calculations were completed by single-point MRCI calculations carried out with large polarized ANO[149] basis sets. The lowest singlet, triplet, and quintet states were systematically investigated and their geometries optimized for each molecular topology associated with a local energy minimum or with a saddle point of the potential energy hypersurface. For TiC_2 in the C_{2v} conformation, the performance of different methods (MRCI, CASSCF, B3LYP, and BP86) in predicting the relative energies of the various excited states was compared, and the ordering of the four lowest states characterized at the MRCI level was found similar with the B3LYP calculations. The binding energy at the MRCI level for the global energy minimum, corresponding to the $^3B_1$ of the triangular C_{2v} conformation, was calculated to be 10.9 eV, in good agreement with the experimental dissociation energy of 11.8 eV.[151] The agreement with the binding energy obtained from the B3LYP calculations (13.5 eV) is also reasonable (Table 7). Finally, an excellent agreement between CASSCF and B3LYP was found for the calculated activation energies separating the ground-state $^3B_1$ of the C_{2v} isomer from the $^3\Sigma^-$ state optimized in the linear conformation (CASSCF, 18.95 kcal·mol^{-1}; B3LYP, 14.5kcal·mol^{-1}).

The vibrational frequencies computed by SH via numerical differentiation at the B3LYP level offer an interesting point of comparison with experiment. Those frequencies were observed by Wang, Ding, and Wang for the series of TiC_x^- ($x = 2-5$) clusters and assigned to the totally symmetric modes which are allowed in the photodetachment transition.[153] The observed values are 560, 650, 440, and 240 cm^{-1} for TiC_n, with n varying from 2 to 5. They are interpreted in terms of cyclic—or fanlike—structures. The corresponding values calculated by SH are 587, 686, and 472 cm^{-1} for TiC_2, TiC_3, and TiC_4, respectively (Table 7). The observed trend is well reproduced, including the unexpected increase of the observed frequency from TiC_2 to TiC_3. According to Wang et al., this increase is explained by the existence of two symmetric ring-breathing modes in cyclic TiC_3, one involving the C−C motion on the opposite corners and the other involving the Ti−C stretching along the 2-fold axis.[153] The observed frequency was as-

Table 7. Adiabatic Electron Affinities (eV), Vibrational Frequencies Allowed in the Photodetachment Transition of TiC_n Species (Totally Symmetric Modes, cm^{-1}), and Calculated Binding Energy Per Atom (BE/atom, eV)

	TiC	TiC_2	TiC_3	TiC_4	Ti_2C_2	Ti_2C_3	Ti_2C_4	ref
EA (exptl)		1.542	1.561	1.494				33, 34, 153
vib freq(exptl)		560	650	440				153
vib freq(B3LYP)	988	587	686	472				28, 104, 147
BE/atom								
SH(B3LYP)		4.5			3.8			147, 157
Scuseria(B3LYP)	3.60							104
Reddy(LDA)	4.5	4.1			4.0	4.9		66, 150
Ge(LDA)		4.8					5.9	152
exptl	4.38	3.93						151

	Ti_3C_8	Ti_4C_8	Ti_6C_{13}	Ti_7C_{13}	$\mathbf{Ti_8C_{12}}$	Ti_9C_{15}	$Ti_{14}C_{13}$	$Ti_{13}C_{22}$	$Ti_{22}C_{35}$	ref
EA(exptl)	2.5[a]	1.8[a]	2.2[a]	2.1[a]	**1.05 ± 0.05**	1.8[a]		3.0 ± 0.1		33, 34, 153
EA(calcd)										
Wang(form a)[b]	2.33	2.12	2.30	2.34		1.80		3.0		33, 34
Wang(form b)[b]	2.65	0.84	2.97	2.88		2.05		3.0		33, 34
Muñoz et al.	2.52	1.52	2.05	1.96	**1.30**					35
BE/Atom										
Reddy(LDA)					**6.7**[c]		6.7			66, 150
Dance					**5.92**[d]**/6.19**[e]		5.70[d]/5.97[e]			27
Wang(form a)	5.90	5.89	6.10	6.04				6.60	6.66	33, 34
Wang(form a)[f]	5.95	5.91	6.12	6.06						35
Muñoz et al.	6.07	6.10	6.38	6.50	**6.58**					35
Ge(LDA)		6.4								152

[a] ±0.2 eV. [b] Form a: conformation of lowest energy calculated by Wang et al. Form b: second lowest conformation calculated by the same authors. [c] D_{2d} conformation. [d] Vosko−Wilk−Nusair functional[74] for the local electron correlation (see Table 1). [e] Lee−Yang−Parr functional[75] for the local and nonlocal components of correlation (see Table 1). [f] Conformation characterized first by Wang[34] and reoptimized by Muñoz et al. by means of the ADF program, using the Becke−Perdew nonlocal corrections in order to be directly comparable with the new conformers proposed in ref 35.

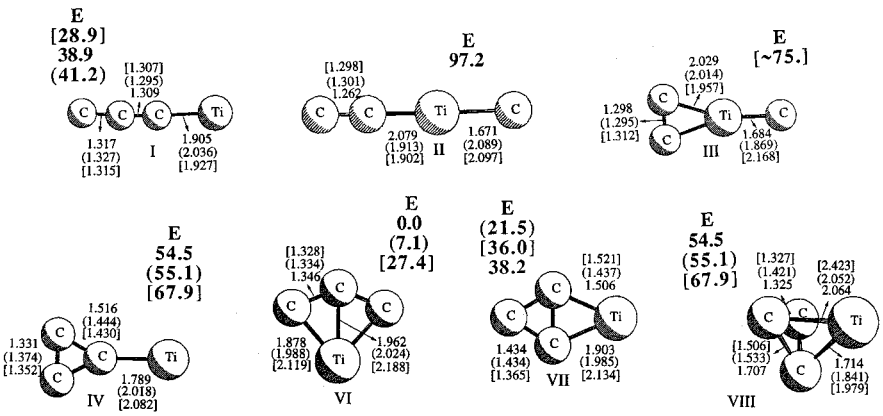

Figure 39. Optimal bond distances (Å) and relative energies (*E*, eV) obtained by Sumathi and Hendrickx for the singlet, (triplet), and [quintet] lowest energy states corresponding to various conformers of TiC_3 (from DFT/B3LYP calculations). Reprinted with permission from ref 28. Copyright 1998 American Chemical Society.

signed to the latter mode and was expected to be comparable to that of the Ti−C diatomic (704 cm^{-1} from MRCI calculations, 988 cm^{-1} from B3LYP).[104]

After those validation tests of the B3LYP calculations, SH continued their investigations on Ti_2C_2[154] and Ti_2C_3[29] clusters at the B3LYP level only. The B3LYP results are summarized in Table 7 and in Figures 39−43.

For the Ti/C clusters containing a single metal atom and up to four carbons, the ground state is associated with "fan" conformations in which the metal is directly bound to all atoms of a carbon chain. The investigation of different spin states is important: for TiC_2, the ground state is a triplet, but TiC_3 and TiC_4 have a singlet ground state. The structure corresponding to the second lowest energy minimum is a "kite" conformation for TiC_3 where Ti is bound to two atoms of a carbon triangle (triplet ground state, +21.5 kcal·mol^{-1}). For TiC_4, the second lowest conformation is linear (triplet ground state, +41.8 kcal·mol^{-1}). Nonplanar structures correspond to a saddle point for TiC_3 and to a high energy minimum (singlet, +58.8 kcal·mol^{-1}) for TiC_4.

Ti_2C_2 is isoelectronic with TiC_3, but its ground state was found not to be isostructural. The equivalent of the "fan" conformation obtained by replacing one carbon by one titanium yielded the second lowest minimum (singlet, +7.9 kcal·mol^{-1}).[154] A rhomboidal "kite" structure with a transannular C−C bond is lowest in energy at the B3LYP level (Table 7). It is important to note that this geometric conformation is associated with a *quintet* spin state. The triplet and the singlet states associated with the same structure are relatively high in energy (+26.3 and +47.6 eV, respectively), higher than the low-spin states characterized for the cyclic "square" and

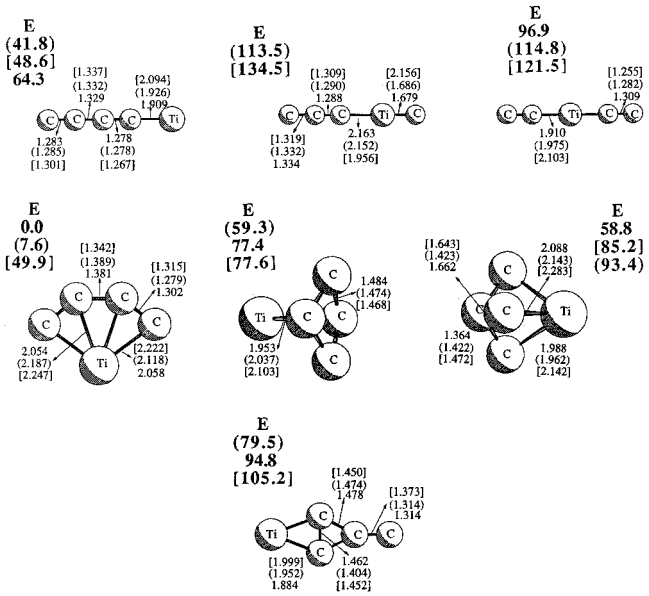

Figure 40. Optimal bond distances (Å) and relative energies (*E*, eV) obtained by Sumathi and Hendrickx for the singlet, (triplet), and [quintet] lowest energy states corresponding to various conformers of TiC_4 (from DFT/B3LYP calculations). Reprinted with permission from ref 28. Copyright 1998 American Chemical Society.

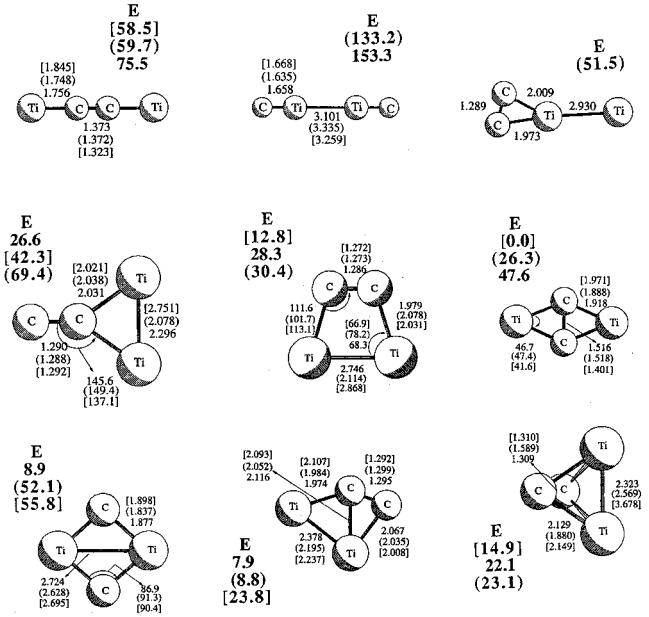

Figure 41. Optimal bond distances (Å) and relative energies (*E*, eV) obtained by Sumathi and Hendrickx for the singlet, (triplet), and [quintet] lowest energy states corresponding to various conformers of Ti_2C_2 (from DFT/B3LYP calculations). Reprinted with permission from ref 154. Copyright 1999 American Chemical Society.

"trapezoidal" forms and even for the unique nonplanar isomer (Figure 41). Although the spin state was not specified in the local density DFT calculations reported by Reddy and Khanna,[66,150] one can guess that the restriction to low-spin states explains why those authors found the "square" conformation as the most stable one with a total binding energy of 16.06 eV.

A large number of topologically distinct conformations, either linear, planar, or nonplanar, were investigated by SH for Ti_2C_3, optimized each in the singlet, triplet, and quintet states (Figure 42). Some of those isomers were characterized as minima at energies higher by ~100 kcal·mol^{-1} than that of the global minimum (Figure 43). SH noted however that the relative population of those species would be appreciable at the temperature of the plasma and that there is indeed a certain probability for them to play a role in the formation of met-cars. The global minimum found by SH for Ti_2C_3 is a fanlike structure similar to that of TiC_4 in which the second atom of the bent carbon chain has been replaced by a titanium. The state of lowest energy is a singlet, closely followed by a triplet with same conformation. Let us remark that this structure is reminiscent of the pentagonal face of dodecahedral met-cars. This similarity was taken by SH as an argument in favor of the T_h structure for M_8C_{12} clusters.[29] The other possible fanlike structure, in which the carbon atom of TiC_4 replaced by a titanium is in *terminal* position has a triplet configuration close enough in energy (Figure 43). Reddy and Khanna also carried out DFT calculations (but at the LDA level) on Ti_2C_3[66,150] and constrained the Ti−Ti axis to be either parallel or perpendicular to a preexistent C−C bond. Both optimization processes resulted in nonplanar conformations, one very similar to SH's pentagon of lowest energy but with Ti−Ti parallel to the C−C bond at the base and located above the plane containing the C atoms. This configuration is 0.3 eV higher than the other one, which has C_{2v} symmetry and can be described as a Ti_2C_2 butterfly with the two titanium wings connected to the third carbon atom. The total binding energy for this latter form is 24.54 eV. This isomer is reminiscent of the nonplanar form of lowest energy (XIV) optimized by SH (Figure 42). However, the Ti−C distances in the butterfly part of SH's cluster are longer than the distances between Ti and the isolated carbon, whereas the trend is quite opposite in the optimal structure of Reddy and Khanna.

For Ti_2C_4, Ge et al.[152] found at the DFT/LSDA level of theory two conformations with equivalent energy, both corresponding to planar six-atom cycles in which two opposite C_2 moieties are linked to titanium atoms. The linear conformer Ti−C_4−Ti is destabilized by 104 kcal·mol^{-1}.

C. Structure of Intermediate Size Clusters: From Ti_3C_8 to Ti_9C_{15}

The number of topologically distinct conformations associated with local minima of the five-atom cluster Ti_2C_3 (Figures 42 and 43) clearly shows that such a comprehensive investigation is impossible for higher nuclearity clusters. The most systematic way to solve this problem of global energy optimization would be to apply techniques developed over the past few years and based upon the concept of potential smoothing which consists of reducing the number of unique minima and the heights of the barriers.[155] However, the recent theoretical studies on Ti/C clusters with intermediate size have rather been grounded on a more empirical approach based on chemical or crystallographical intuition. The first DFT study on those clusters is due to Wang et al., who started from their

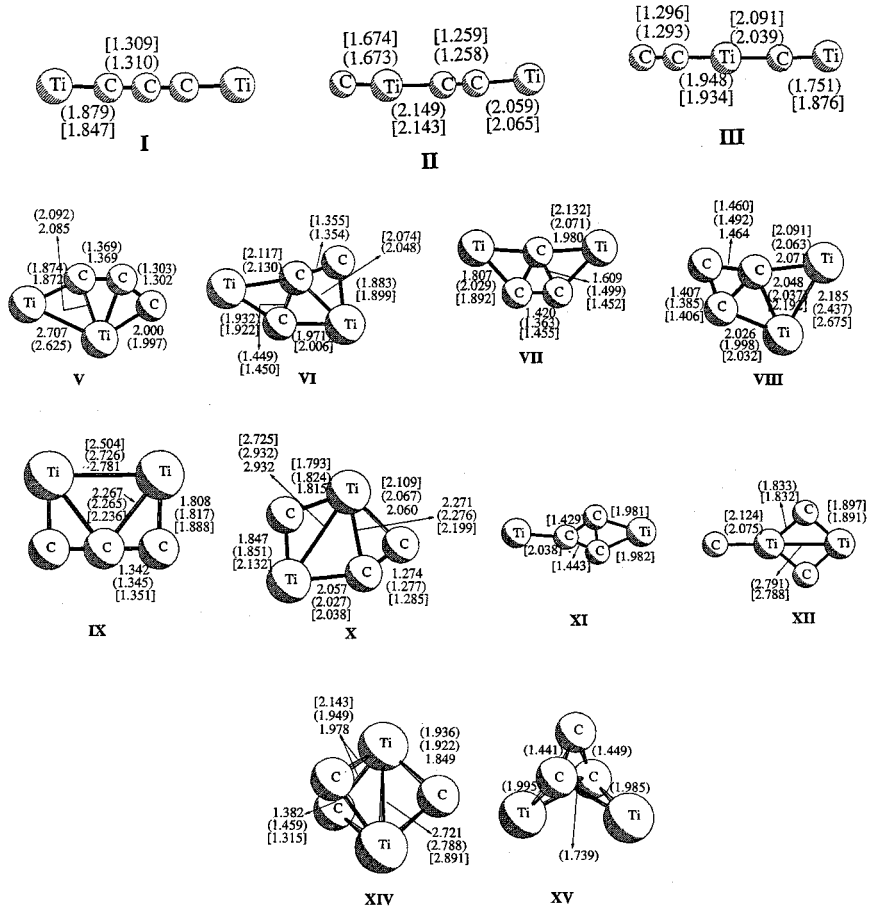

Figure 42. Optimal bond distances (Å) obtained by Sumathi and Hendrickx for the singlet, (triplet), and [quintet] lowest energy states corresponding to various conformers of Ti_2C_3 (from DFT/B3LYP calculations). Reprinted with permission from ref 29. Copyright 1998 American Chemical Society.

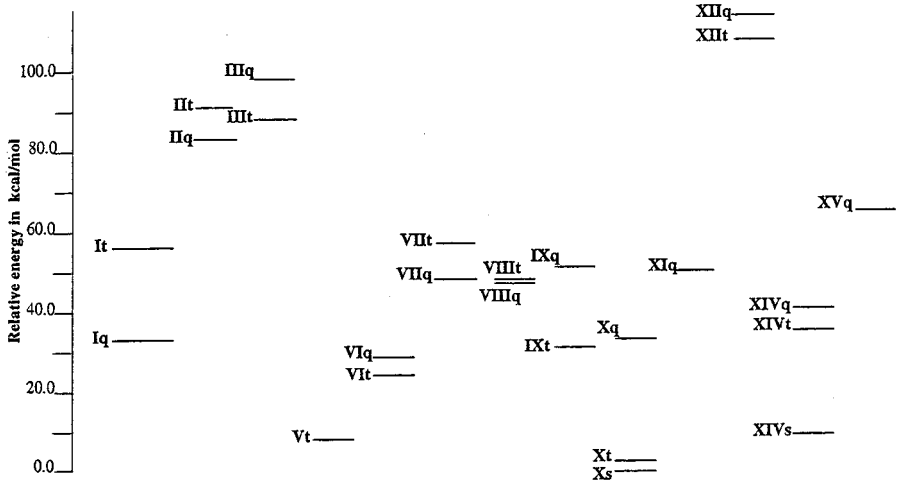

Figure 43. Relative energies (eV) obtained by Sumathi and Hendrickx for the singlet (s), triplet (t), and quintet (q) lowest energy states corresponding to various conformers of Ti_2C_3 (from DFT/B3LYP calculations). Reprinted with permission from ref 29. Copyright 1998 American Chemical Society.

experimental investigation on the $Ti_xC_y^-$ anions.[34] As can be noted from Figure 38, the peaks corresponding to $Ti_3C_8^-$, $Ti_4C_8^-$, $Ti_6C_{13}^-$, $Ti_7C_{13}^-$, and $Ti_9C_{15}^-$ dominate the mass spectrum and, accounting for the absence of $Ti_8C_{12}^-$, the corresponding cluster anions can be considered as the most probable intermediate steps toward the formation of the high-nuclearity systems $Ti_{13}C_{22}^-$ and $Ti_{14}C_{24}^-$. Wang et al. therefore carried out spin polarized, gradient-corrected DFT calculations on the whole series of above-mentioned clusters. Note that this calculation scheme yields exclusively closed-shell electronic structures for the neutral clusters. The selection of the initial structures for geometry optimization was made according to the following guidelines: (1) C_2 dimers play an important role in the carbon-rich clusters, and (2) the cubic structural motif as exemplified in the $3 \times 3 \times 3$ cubic $Ti_{14}C_{13}^+$ nanocrystal (Figure 34) and in the C_2-decorated cubic structure postulated for $Ti_{13}C_{22}$ (section VI.D.1) should be progressively assembling in

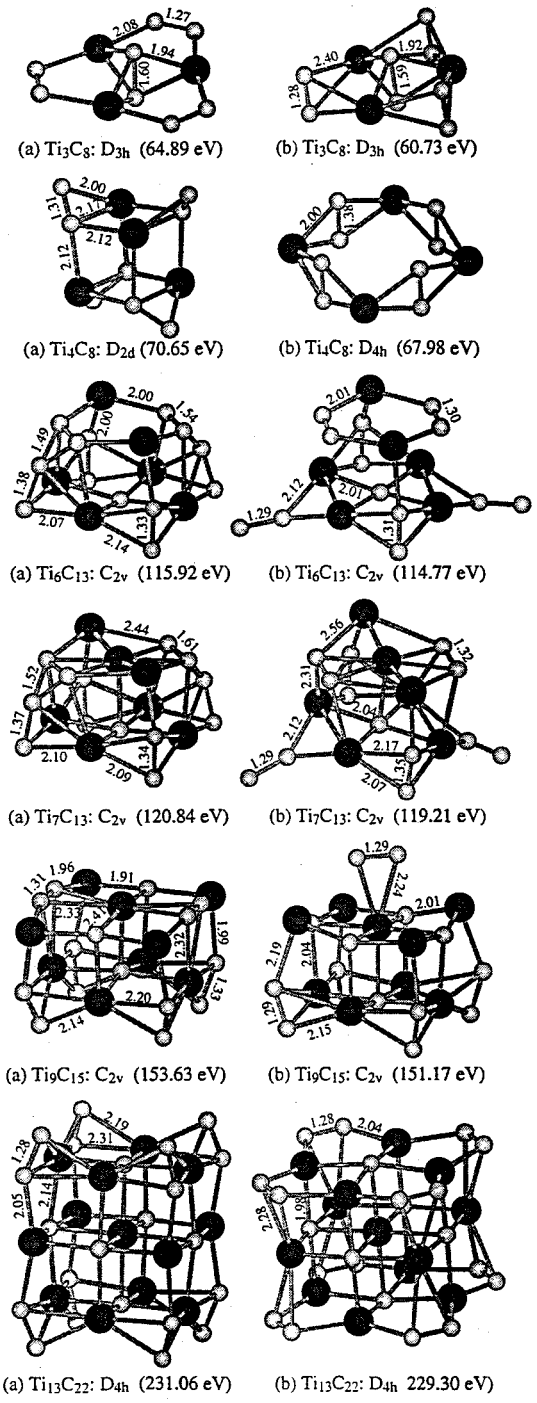

Figure 44. Structures optimized by Wang et al. by means of gradient-corrected DFT calculations for the Ti_3C_8, Ti_4C_8, Ti_6C_{13}, Ti_7C_{13}, Ti_9C_{15}, and $Ti_{13}C_{22}$ clusters, starting from conformations involving cubic structural motifs and various C_2 dimers. Reprinted with permission from ref 34. Copyright 1998 American Chemical Society.

the smaller structures.[34] For each considered stoichiometry, the two conformations of lowest energy obtained by Wang et al. assuming those prerequisites are displayed in Figure 44 together with their symmetries and the associated binding energies.[156]

Separate optimization processes have been carried out on the anionic species in order to obtain the adiabatic electron affinities. A comparison with the experimental values deduced from the photoelectron spectra shows that the difference with the computed EA's never exceeds 0.32 eV when the conformation of lowest energy is considered (Table 7).[34]

After this work had been published, Muñoz et al.[35] considered that the prerequisites introduced by Wang et al. for selecting the trial conformations were susceptible to introduce a bias in the optimization process. They argued that the topology of very small clusters may follow an erratic behavior, quite unrelated with the more regular growth path established for larger species. For species of intermediate size (Ti_6C_{13}, Ti_7C_{13}) they proposed as an initial guess for geometry optimization a structure derived from the T_d conformation of endohedral Ti_8C_{13}, assuming that the special stability of Dance's conformer should persist for stoichiometries that differ from the endohedral met-car by the substitution or by the loss of one or possibly two metal atoms. Gradient corrected DFT calculations carried out on such grounds with the ADF program and the binding energies of the optimal structures were compared to that of Wang's most stable conformation, reoptimized in the same computational conditions. Several conformers were proposed, displaying higher stability than Wang's cubiclike framework for all considered clusters (Ti_3C_8, Ti_4C_8, Ti_6C_{13}, Ti_7C_{13}) (Figure 45). The conformations of lowest energy obtained for Ti_3C_8 and Ti_4C_8 confirm that isolated carbon atoms and C_2 dimers are not the sole building blocks to be considered along the growth path of carbon-rich Ti/C clusters. Bent C_4 chains similar to the one characterized by Sumathi and Hendrickx in the most stable "fan" conformation of TiC_4 are ubiquitous in the most stable forms of Ti_3C_8 and Ti_4C_8. The conformer of lowest energy obtained for Ti_7C_{13} has the same topology as a tetrahedral met-car in which one capping metal atom has been substituted by a carbon, giving rise to a branched C_7 moiety (Figure 45). The same C_7 fragment is present in the optimal structure of Ti_6C_{13} which differs from Ti_7C_{13} by the loss of a metal atom belonging to the inner tetrahedron and opposite to the substituted site (Figure 45). Other conformations of Ti_6C_{13} and Ti_7C_{13} were obtained by removing one or two metal atoms from the *endohedral* conformation of Ti_8C_{13}. Let us finally note that the conformations of lowest energy obtained for Ti_4C_8 and Ti_6C_{13} correspond to triplet states.

Wang et al. validated the structures based upon a cubic framework of the Ti_xC_y clusters by the excellent agreement obtained with experiment for the computed adiabatic electron affinities (Table 7). For the four investigated clusters Ti_3C_8, Ti_4C_8, Ti_6C_{13}, and Ti_7C_{13}, the average gap between the experimental and the computed values did not exceed 0.21 eV. To assess their own structures, Muñoz et al. had therefore to prove that the agreement obtained by Wang could have been fortuitous and that an agreement of similar or even better quality was obtained with the structures of lowest energy. The values reproduced in Table 7 show that the average discrepancy between experiment and Muñoz's computed values amounts to 0.15 eV for the same series of four clusters. If this agreement is not sufficient by itself to fully assess the proposed structures—the proof was

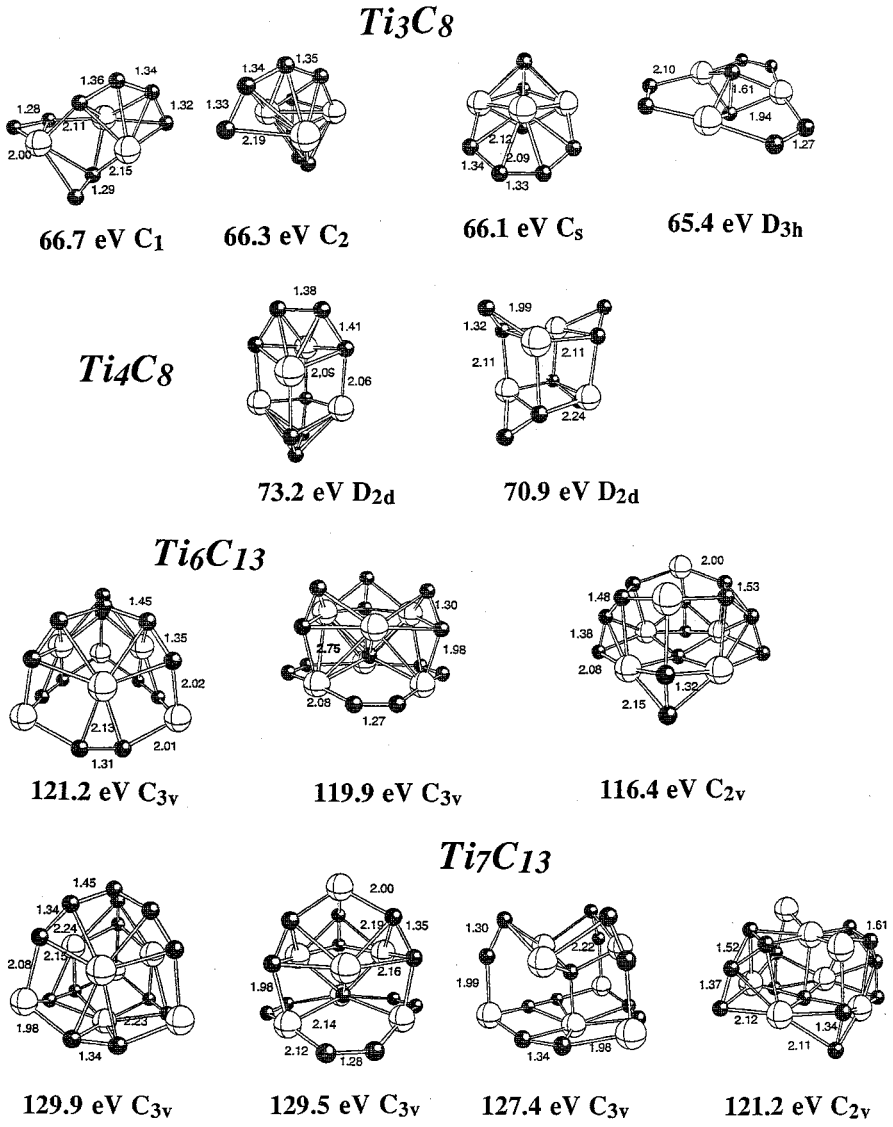

Figure 45. Conformations of lowest energies optimized by Muñoz et al. for Ti_3C_8, Ti_4C_8, Ti_6C_{13}, and Ti_7C_{13} (from gradient-corrected DFT calculations). The total binding energies (eV) are compared to those obtained for the best structure of Wang et al. (WWWC; see Figure 44), reoptimized within the same methodological conditions.

given that such an agreement can be fortuitous—it shows that the conformations optimized in that work are compatible with the presently available experimental data and that the indications provided by the relative binding energies should be considered seriously.

D. Large-Nuclearity Ti/C Clusters

1. Layered Cubic Structures

The discovery by Pilgrim and Duncan[25] that met-cars could coexist with higher nuclearity fcc nanocrystals has triggered experimental and theoretical investigations focused on their respective conditions of formation, on the relative stabilities of both types of structures, and on the pathways that were susceptible to connect one structural type to the other. The problem was made more complex by the existence, at least with zirconium and niobium, of stable, carbon-rich, high-nuclearity clusters that had been assigned by Wei and Castleman the structure of a multicage species composed of face-sharing dodecahedral met-cars, assuming in some cases the replacement of one metal by one carbon atom.[142,143] The recent investigation by Wang et al. of the mass spectrum characteristic of metal carbon cluster anions showed that stoichiometries characteristic of double-cage species, such as $M_{13}C_{22}^-$, were producing prominent peaks for M = Ti and V.[34] In relation with those experiments Wang and Cheng recently reconsidered the structure of the $Ti_{13}C_{22}$ cluster.[33] They noted that the nanocrystal $Ti_{14}C_{13}^+$ appears as a large peak in the mass spectrum of Ti/C cations, but the alternative $3 \times 3 \times 3$ structure $Ti_{13}C_{14}^+$ with eight carbon atoms at the cube corners has never been observed. Wang and Cheng noted however that replacing the eight corner C atoms with eight C_2 dimers naturally leads to the $Ti_{13}C_{22}$ cluster observed in the spectrum of anions. They carried out geometry optimizations with the DFT formalism on the two isomers represented in Figure 44 (bottom).[33] The geometries were optimized using the local spin density (LSD) approximation, and single-point cal-

culations of the energies incorporating gradient corrections were performed at the optimal geometries. Form a of Figure 44, which differs from form b by the close to vertical position of the C_2 dimers, was found more stable by 2.03 eV at the LSD level and by 1.76 eV at the gradient-corrected level. Wang and Cheng also carried out an optimization process starting from the double-cage topology advocated by Wei and Castleman. This double cage was made originally from two fused dodecahedra sharing a pentagonal face, with one metal atom substituted by a carbon. Interestingly, the optimization process yielded a deformation of the double cage eventually leading to a topology reminiscent of two fused Ti_7C_{13} clusters both in Dance's conformation of tetracapped tetrahedron (Figure 46). The energy of the latter structure

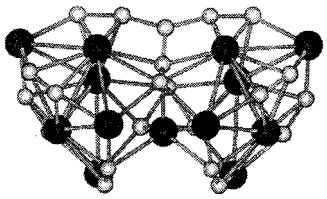

Figure 46. Double-cage structure optimized by Wang and Cheng for the $Ti_{13}C_{22}$ cluster. The stability of that conformation is intermediate between those of the two C_2-decorated cubic structures displayed at the bottom of Figure 44. Reprinted with permission from ref 33. Copyright 1997 American Physical Society.

was not computed at the gradient-corrected level, but the difference of the LSD energies is no more than 1.33 eV with respect to the C_2-decorated cubic conformer of Figure 44a.[33] Such an energy difference corresponding to 0.04 eV/atom is not sufficient at that level of calculation to rule out the double-cage structure. However, several arguments were suggested by Wang and Cheng to assess the cubiclike structure. First, the calculated electron affinities of the cubiclike forms exactly coincide with the experimental value of 3.0 ± 0.1 eV (Table 7). The density of states (DOS) spectrum associated with the three investigated conformations was simulated by convoluting a 0.2 eV width Gaussian function onto the single particle occupied energy levels of the anions. (Figure 47). The simulated spectrum correponding to conformer a (the cubic framework decorated with vertically oriented C_2 dimers) reproduces quite well the observed photoelectron spectrum, whereas the agreement is poor for a horizontal orientation of the dimers (conformer b) and still worse for the double cage (conformer c).

Then, a layer-by-layer growth pathway involving C_2 dimers at the periphery of a cubic structural framework was shown to account for most of the magic peaks previously assigned to multicage structures.[33] In the case of the carbon-rich $Ti_{13}C_{22}$ nanocrystal, the 3 × 3 × 3 structure of Figure 44a is composed of three layers: two layers of Ti_4C_9 (A) sandwiching a layer of Ti_5C_4 (B). A growth pathway in which the A and B layers are stacked alternatively yields the following clusters, either exactly corresponding to the stoichiometries assigned to magic

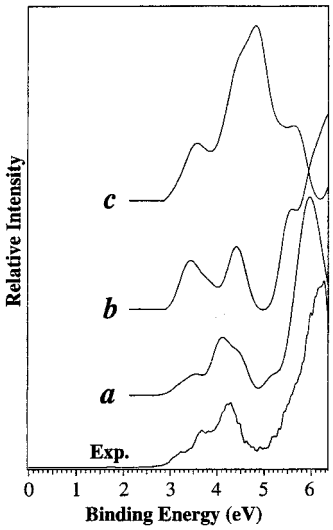

Figure 47. Photoelectron spectrum of the $Ti_{13}C_{22}^-$ cluster at 6.42 eV (Exp.), compared with simulated electronic density-of-state spectra corresponding (i) to the C_2-decorated cubic structures of Figure 44 (bottom) with vertical C_2 units (a) and with horizontal C_2 units (b) and (ii) to the double-cage structure of Figure 46 (c). Reprinted with permission from ref 33. Copyright 1997 American Physical Society.

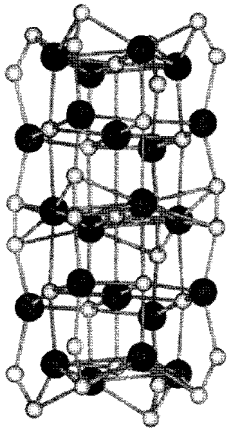

Figure 48. Optimized structure of a five-layer ABABA structure ($Ti_{22}C_{35}$) with a total binding energy of 379.7 eV (DFT, local density approximation). Reprinted with permission from ref 33. Copyright 1997 American Physical Society.

peaks or closely related to them:

$$AB \rightarrow M_9C_{13}\ (Ti_9C_{15}^-,\ V_9C_{15}^-)$$

$$ABA \rightarrow M_{13}C_{22}\ (Ti_{13}C_{22}^-,\ V_{13}C_{22}^-,\ Zr_{13}C_{22}^+,\ Zr_{14}C_{21}^+,\ Nb_{13}C_{22}^+)$$

$$ABAB \rightarrow M_{18}C_{26}\ (Zr_{18}C_{27}^+)$$

$$ABABA \rightarrow M_{22}C_{35}\ (Zr_{22}C_{35}^+)$$

The geometry of the five-layer ABABA structure corresponding to the $M_{22}C_{35}$ cluster was optimized by Wang and Cheng for M = Ti (Figure 48). The binding energy per atom is 6.66 eV after gradient corrections (Table 7), slightly higher than for $Ti_{13}C_{22}$ (ABA, 6.60 eV/atom).[33]

2. Fcc Nanocrystals

The structure of the high nuclearity "carbon poor" Ti/C V/C and Nb/C aggregates referred to as nanocrystals by Pilgrim and Duncan[25] did not generate any serious controversy concerning the structure of those clusters. The stoichiometries associated with the most prominent peaks clearly coincide with XxYxZ cubic structures, as previously observed and assigned for tantalum carbon aggregates.[143] The most intense mass peak associated with those crystallites corresponds to the $3 \times 3 \times 3$ nanocrystal $M_{14}C_{13}$ for M = Ti and V and to the $2 \times 3 \times 3$ structure M_9C_9 for M = Nb.[25] Several theoretical studies have been devoted to the $Ti_{14}C_{13}$ cluster considered as a prototypical molecule for the class of nanocrystals. All authors agree with the $3 \times 3 \times 3$ cubic conformation, with the exception of Khan, who rather advocates a C_{13} cluster encapsulated in a metal cage.[158] The ab initio SCF calculations of Rohmer et al. yielded a small distortion of the cubic framework from O_h to T_d symmetry induced by the localization of four metal d electrons at the apexes of a tetrahedron,[90] but this effect has not been confirmed by the DFT calculations carried out later by Dance.[27] The first DFT calculation on $Ti_{14}C_{13}$ was however reported by Reddy and Khanna,[66] who used the discrete variational method and constrained the nanocrystal to be perfectly cubic, with a unique Ti−C distance optimized at 2.04 Å. Dance's nonlocal DFT calculations[27] yielded a structure with O_h symmetry but Ti−C distances slightly longer for facial titanium atoms (2.17/2.18 Å) than for apical titanium atoms (2.05 Å). The distance from facial titanium atoms to the central carbon is 2.12/2.13 Å, depending on the used functional. This latter distance is the most relevant one for a comparison with the bond length observed in the face-centered cubic structure of titanium carbide, 2.16 Å. The electronic structure of the neutral cluster is that of a spin multiplet with three or four electrons accommodated in partially occupied, closely spaced, nonbonding orbitals.

The binding energy per atom calculated by Reddy and Khanna is quite high: 6.74 eV. The comparison with Ti_8C_{12} (6.1 eV) is biased since the dodecahedral structure was assumed for the met-car. A subsequent calculation carried out at the same methodological level with the D_{2d} structure[150] yielded a binding energy of 6.66 eV/atom for the met-car, very close to that of the nanocrystal. Comparisons were also carried out with the binding energies obtained for the neutral C_2 dimer (6.6 eV), for the C_2^- anion (10.4 eV), and for the TiC molecule (4.5 eV).[66] An investigation of less extended fcc crystallites showed that the binding energy per atom increases with the size of the nanocrystal, from 6.3 eV for Ti_6C_6 ($2 \times 2 \times 3$ fcc structure) to 6.6 eV for Ti_9C_9 ($2 \times 3 \times 3$) and finally to 6.74 eV for the $3 \times 3 \times 3$ cluster (Table 1).[150] Reddy and Khanna then explained the competition between met-cars and cubic structures by the dual ability of carbon atoms to be stabilized either through strongly energetic C_2^- bonds or through bonds between metal and single carbon atoms. Experimental conditions that generate beams rich in carbon will therefore displace the balance toward the formation of C_2^- bonds, and met-cars will then prevail; whereas beams rich in titanium will tend to form cubic structures which will reach sufficient stability for a relatively large size of the fcc structure. This situation is then compared to that of titanium *nitride* clusters Ti_nN_m for which no analogue of the met-car structure has been detected. Both the N−N bond (9.5 eV) and the Ti−N bond (5.9 eV) are computed to be more energetic than their carbon equivalents, but the propensity to stabilize a nitrogen-rich cluster through metal-to-N_2 donation vanishes because of the relatively low energy of the N−N bond in the N_2^- anion (8.0 eV).[150]

3. Decomposition Pathways to Met-Cars

In the context of two stable but chemically and topologically different types of Ti/C clusters, Pilgrim and Duncan deduced from the photodissociation experiment of $Ti_{14}C_{13}^+$ that pathways might exist that connect both types of species.[109] The fragmentation pattern of the $3 \times 3 \times 3$ nanocrystal, reproduced in Figure 36b, indicates a sequence of six metal atom losses, eventually leading to the most intense fragment: $Ti_8C_{13}^+$.[25a] A scenario suggested by Pilgrim and Duncan to explain the fragmentation of $Ti_{14}C_{13}^+$ into $Ti_8C_{13}^+$ is that the six metal atoms which are eliminated come from the six faces of the fcc cube. If carbon atoms located on opposite edges can then join to form six C_2 units spanning the metal-free faces of the cube, one is left with a cluster composed of eight metal atoms in a cubic arrangement surrounded by six C_2 units. Assuming that the extrusion of the metal atoms did not induce further structural rearrangements, the resulting $Ti_8C_{13}^+$ cluster can be easily identified with a dodecahedral met-car, with an additional carbon atom trapped at the center.[25a,109]

This hypothesis has triggered a first theoretical investigation of the endohedral met-car $C\subset Ti_8C_{12}$ by Lou and Nordlander, by means of the DFT formalism at the local density level of approximation.[67] This study reports and compares the optimal geometries and binding energies obtained for Ti_8C_{12} and for $C\subset Ti_8C_{12}$ in the T_h (dodecahedral), D_{2d}, and T_d (tetracapped) structures (Table 1). The results concerning Ti_8C_{12} have been discussed above (see section II.C). The addition of an endohedral carbon does not lead to a significant decrease of the average binding energy per atom, except for the T_h form which has a too large cavity for efficiently accommodating a single carbon atom.[27] The binding energy per atom even increases from 7.35 to 7.40 eV in the D_{2d} form. Since the average binding energy was already very high for Ti_8C_{12}, this means that the endohedral carbon is very strongly bonded to the cluster (7.7 eV for the T_d form, 8.4 eV for the D_{2d} form). The binding energies of the extra carbon obtained later by Dance[27] (5.4 or 5.1 eV for $C\subset Ti_8C_{12}$ depending on the exchange-correlation potential) and by Muñoz et al.[21] (5.77 eV for $C\subset Ti_8C_{12}$; 6.35 eV for $C\subset Zr_8C_{12}$), both assuming the T_d conformation, are somewhat smaller, but they account for the gradient corrections, which always tend to decrease the bonding energies (Table 1).[159] All three calculations show that the endohedral carbon is bonded to the four metal atoms of the inner tetrahedron in the T_d form, with Ti−C distances of 1.84[67] or 1.88/1.90 Å[27] (Figure 49c).

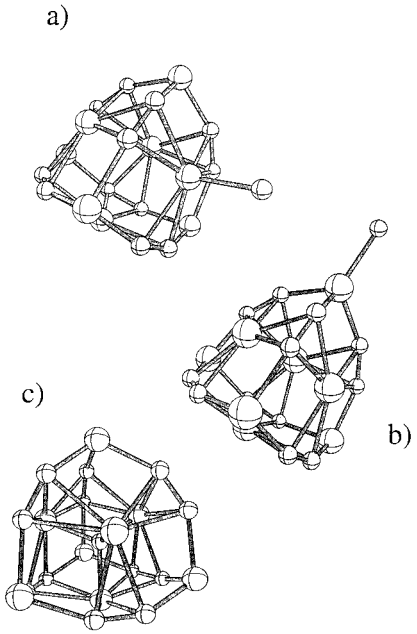

Figure 49. The three possible conformations of the 21-atom met-car cluster Ti_8C_{13}: (a) exohedral, C attached to an atom of the inner tetrahedron (binding energy 3.39 eV); (b) exohedral, C attached to an atom of the capping tetrahedron (BE, 3.66 eV); (c) endohedral (BE, 5.77 eV). From gradient-corrected DFT calculations by Muñoz et al.[21]

Those distances tend to increase by 0.02/0.03 Å when the cluster is ionized.[27] The encapsulation of a carbon atom also yields a spectacular increase of the HOMO−LUMO gap, at least in the T_d form (1.17 eV according to Lou and Nordlander[67] or 1.02 eV according to Dance[27] between the $(t_2)^6$ HOMO and the t_2 LUMO, instead of 0.23 eV[67] for Ti_8C_{12}) and an increase of the ionization potential. At variance with the "empty" met-car, for which the sequence of orbital energies favors the electronic configuration of the double cation, the neutral form of the encapsulated cluster $C\subset Ti_8C_{12}$ is definitely a stable closed-shell singlet. Those results can be easily rationalized within the orbital scheme associated with the high-spin state of lowest energy obtained from Hartree−Fock calculations[96] (see section III.C). The four singly occupied orbitals of that quintet state are d_{z^2}-like combinations centered on the metal atoms of the inner tetrahedron and pointing toward the center of the cluster (Figure 20). They are therefore ideally suited to give four covalent bonds with a sp^3-hybridized carbon atom occupying the central position. The price to pay for establishing those bonds is the loss of the metal−metal overlap involving the four atoms of the inner tetrahedron and occurring through orbital $1a_1$ (Figure 20).

The results of Lou and Nordlander, showing that the most stable structure for $C\subset Ti_8C_{12}$ is the tetra-capped tetrahedron as for Ti_8C_{12}, suggest that the loss of the metal atoms induces a complex rearrangement of the cluster structure with a 45° rotation of the newly formed C_2 dimers. Dance[27] has investigated by means of the gradient-corrected DFT formalism the transformation of the $3 \times 3 \times 3$ fcc nanocrystal induced by the successive extrusion of six metal atoms (Figure 50). In agreement with the hypothesis of Brock and Duncan, the starting point for the optimization of the first intermediate, $Ti_{13}C_{13}$ was generated by the removal of one metal atom at the center of a cubic face (number 9 in Figure 50) and movement of the two adjacent C atoms in the direction shown in diagram 14/13 (Figure 50). When the optimization process was carried out with the minimal constraints of the C_2 point group in order

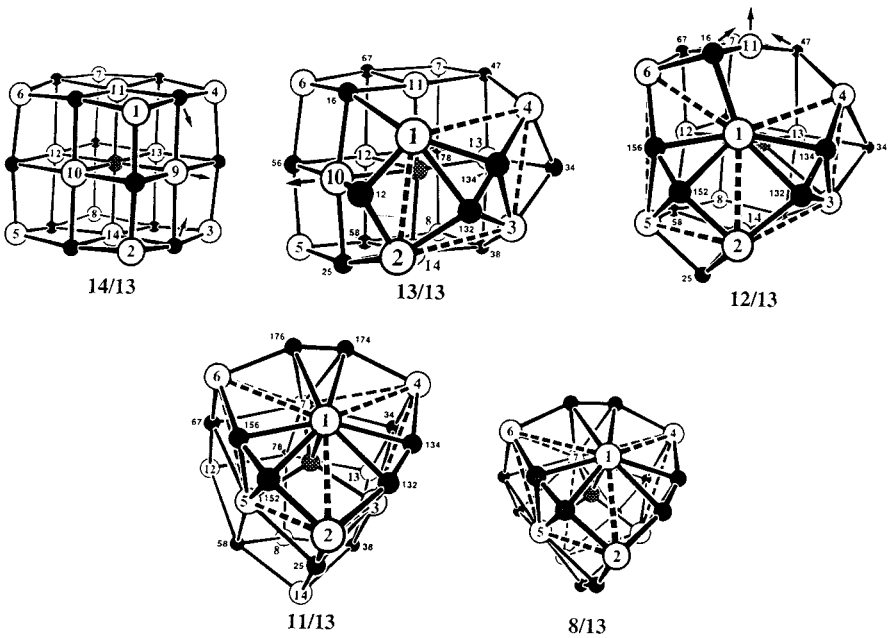

Figure 50. Mechanism of the dissociation reaction $Ti_{14}C_{13} \rightarrow Ti_8C_{13}$ by successive extrusion of six metal atoms. Structures of the reactant, intermediate, and product clusters were optimized by Dance. Open circles represent Ti atoms; filled circles represent surface carbon atoms; the central carbon atom is stippled. Ti atoms retain the number labels of **14**/**13** throughout the sequence of structures. Carbon atoms are labeled C_{xy} or C_{xyz}, where x, y, and z represent the labels of the Ti atoms at bonding distance. The arrows show the movement of atoms in the progression to the next intermediate. Reprinted with permission from ref 27. Copyright 1996 American Chemical Society.

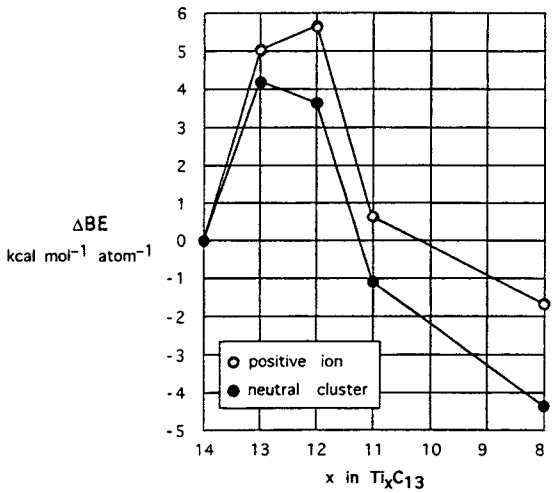

Figure 51. Energy profile of the dissociation reaction $Ti_{14}C_{13} \rightarrow Ti_8C_{13}$, calculated by Dance at the gradient-corrected DFT level. Comparative binding energies (ΔBE, kcal·mol^{-1}·atom^{-1}) for the reactant, intermediate, and product clusters. Closed circles are neutral clusters, and open circles are positive ions. Reprinted with permission from ref 27. Copyright 1996 American Chemical Society.

not to impede the displacement of the carbon atoms, it eventually yielded the 13/13 cluster of Figure 50, characterized by the expected rotation of the two C atoms with respect to the four surrounding metals.[160] The acetylenic conformation of the dicarbon fragment ($d_{C-C} = 1.36$ Å), coordinated end-on to titanium atoms 2 and 4 and side-on to Ti atoms 1 and 3, is obviously reminiscent of the T_d structure of met-cars. In the optimal structure of $Ti_{13}C_{13}$, the two metal atoms Ti(10) and Ti(13) have moved away from the central carbon, indicating that the next metal extrusion process will most probably affect one of those atoms. This process yields the $Ti_{12}C_{13}$ cluster of Figure 50, in which the reorganization has extended to the whole cluster, making it the least symmetrical intermediate in the transformation from highly symmetrical $Ti_{14}C_{13}$ to highly symmetrical Ti_8C_{13}. No symmetry constraint has been imposed either in this transformation step or in the next one leading to $Ti_{11}C_{13}$. However, after the extrusion of Ti(11), the structure of $Ti_{11}C_{13}$ spontaneously evolves toward a conformation with 3-fold symmetry in which the environment of the opposite metal atoms Ti(1) and Ti(8) is already characteristic of the inner and outer tetrahedral sites, respectively, of the met-cars in T_d symmetry. The final intermediates $Ti_{10}C_{13}$ and Ti_9C_{13} were predicted to arise from extrusion processes carried out along similar guidelines and were not optimized.[27]

If the energy *barriers* associated with each metal extrusion have not been explicitely calculated by Dance, the graph displaying the variation of the binding energy per atom (ΔBE, kcal·mol^{-1}·atom^{-1}) for each intermediate shows that $Ti_{13}C_{13}$ and $Ti_{12}C_{13}$ and their cations, which are the least symmetric species, are also the least stable ones (Figure 51).[161] As for $Ti_{14}C_{13}$ itself, the electronic structure of the two first intermediates is characterized by closely spaced, partially occupied orbitals at the Fermi level. The HOMO−LUMO gap thereafter increases to 0.67 in $Ti_{11}C_{13}$ and then to more than 1 eV in Ti_8C_{13} as symmetry is restored and as tetrahedral coordination of the central carbon to four titanium atoms becomes possible.

Table 8. Metal−Ligand Bond Lengths (Å) and Binding Energies (BE, kcal·mol^{-1}) from DFT Calculations[a] and Corresponding to the Addition of *n* Molecules of L (L = HCN, CO, NH3, Cl, *n* = 6, 8) to $Ti_{14}C_{13}$ and $V_{14}C_{13}$ (O_h Symmetry)

L	*n*	site	d_{Ti-L}	BE	d_{V-L}	BE
HCN	8	apex			2.11	157
	6	face			2.21	3
CO	8	apex	2.32	131	2.16	169
	6	face	2.25	51	2.08	79
NH_3	8	apex	2.34	173	2.24	187

[a] Calculations carried out using the Becke−Perdew functional by means of the ADF program.[76]

The gas-phase reactivity of the vanadium cluster $V_{14}C_{13}^+$ with respect to water and acetonitrile has been studied experimentally by Byun et al.[162] Sequential reactions with up to 8 H_2O molecules result in the formation of $V_{14}C_{13}(OH)_2(H_2O)_6^+$ and $V_{14}C_{13}(OH)_4(H_2O)_4^+$ by loss of H_2 or attachment of H_2O. Reaction with acetonitrile yielded the attachment of up to 8 CH_3CN molecules. Those results were interpreted as providing evidence for the $3 \times 3 \times 3$ cubic structure where the 8 coordinatively unsaturated metals in the corners are the active binding sites.[162] Preliminary DFT calculations by Muñoz and Poblet on the reactivity of neutral $Ti_{14}C_{13}$ and $V_{14}C_{13}$ with respect to HCN, CO, and NH_3 confirm those trends (Table 8).

At the DFT level, the attachment of eight molecules to the vanadium atoms in the apical position is calculated to be exothermic by 157 kcal·mol^{-1} for HCN to 187 kcal·mol^{-1} for NH_3, whereas the binding of six molecules of CO to the metal atoms in facial position is only moderately favorable (79 kcal·mol^{-1}). The facial vanadium atoms are practically nonbonding with respect to HCN. The calculated trends are similar when vanadium is replaced by titanium, but the binding energies with respect to CO and NH_3 are slightly lower and the metal-to-ligand equilibrium distances are longer by 0.10−0.16 Å (Table 8).

E. Theoretical Investigations on Other Metal−Carbon Clusters

1. Molybdenum Carbon Clusters: Reassessment of Experimental Results

Some structural and theoretical information is available about other transition metal carbide clusters directly related to met-cars or to fcc nanocrystals. The method most widely used to generate those clusters is the laser-induced plasma technique first described by Castleman et al. for the generation of met-cars involving transition metals of groups 3 and 4.[3,7] The same method has been successfully applied to characterize $Cr_8C_{12}^+$, $Mo_8C_{12}^+$, and $Fe_8C_{12}^+$.[8] For the less reactive later transition metals or main group metals (Ni, Co, W, Ag, Cu, Bi, Sb), Reddic and Duncan[163] rather advocate the vaporization of pure metal/carbon mixtures. Composite samples made of carbon rods coated with a thin film of metal yielded novel carbide clusters with the metals listed above.

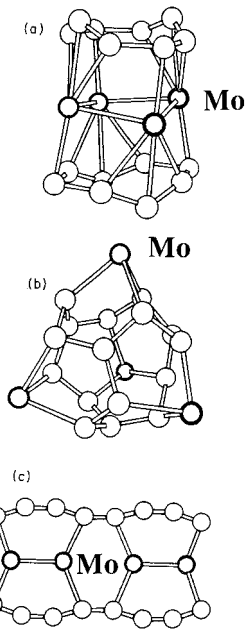

Figure 52. Geometries optimized by Wei and Yang for Mo_4C_{16} and $Mo_4C_{16}^-$ from DFT/LSD calculations. Bold circles represent Mo atoms. (a) D_{2d} symmetry, BE/atom: 6.93 eV (neutral); 7.05 eV (anion). (b) T_d symmetry, BE/atom: 6.82 eV (neutral); 6.91 eV (anion). (c) D_{2h} symmetry, BE/atom: 6.80 eV (neutral); 7.00 eV (anion). Reprinted with permission from ref 32. Copyright 1995 American Physical Society.

Still another technique was used for producing ultrafine M_nC_m particles (M = Cr, Mo, W). It consists of exposing gas-phase carbonyls of transition metals such as $M(CO)_6$ to XeCl laser radiation.[164,165] However, the case of molybdenum carbide clusters reminds one that the assignment of mass peaks should always be carried out with extreme caution. The negative ion Fourier transform mass spectra revealed abundant cluster anions which were interpreted first as having the stoichiometry $Mo_nC_{4n}^-$ with $n = 1-4$.[165] A met-car-like structure of pentagonal dodecahedron was considered for what was thought to be the 20-atom cluster Mo_4C_{16}. An alternative structure consisting of four $Mo(C_2)_2$ subunits bound together by four Mo−Mo bonds in the same plane seemed however more probable to Jin et al.[165] However, the authors soon after realized that the samples had been contaminated by small amounts of molybdenum oxide and, because of the large electron affinity of MoO_3, the masses observed in at least 95% of the laser photolysis samples correspond to $Mo_n(O_3)_n^-$ instead of the expected $Mo_n(C_4)_n^-$.[166] In the meantime, DFT/LSD calculations had been carried out by Wei and Yang on the series of neutral and negatively charged clusters Mo_nC_{4n} ($n = 1-4$).[32] Despite the misinterpretation of the mass spectrum, those calculations present a real interest since they show that the met-car-like cage structure of the carbon-rich cluster Mo_4C_{16} is not characterized by a special stability with respect to other three-dimensional or even planar conformations. Three conformers were found relatively close in energy for Mo_4C_{16} and for its anion (Figure 52). The most stable one (6.93 eV/atom for the neutral form) approximately corresponds to the structure advocated by Jin et al. (Figure 52a). The four shortest Mo−Mo distances (2.40 Å) are probably underestimated due to the LSD approximation but confirm anyhow the existence of metal−metal bonds. At variance with the structure postulated by Jin et al., the Mo_4 framework is not square planar, but distorted, and the carbon atoms are not organized into separate C_2 dimers, but condensed in two boatlike C_8 cycles (Figure 52a). Next in energy for the cluster anion comes a planar form obtained by cutting and unfolding the previous conformation (Figure 52c). Finally, the conformation displayed in Figure 52b has T_d symmetry and corresponds to a "met-car-like" structure with 12 distorted pentagons containing each one metal atom. This "met-car" form of $Mo_4C_{16}^-$ is destabilized by ~2.8 eV (0.14 eV/atom) with respect to conformation a.

Wei and Yang constructed the series of the Mo_nC_{4n} clusters from a MoC_4 fragment composed of two C_2 dimers either parallel or perpendicular and opposite with respect to the metal atom.[32] However, DFT calculations carried by Yang et al.[31] on MoC_4 suggest that three conformations at least are more stable, namely the linear chain with the metal bound at one end (total binding energy, 29.4 eV), the fanlike form (BE. 29.1 eV), and a three-dimensional structure in which the metal is bound to a rectangular C_4 cluster (BE, 28.7 eV).

2. ScC_2, LaC_2, and Small Yttrium Carbon Clusters: Similarities and Differences with Ti_nC_m

Carbon clusters doped with one or two transition metal atoms have been extensively studied experimentally in the past decade. When the cluster carbons are larger than C_{34}, the isomer distribution of the MC_n clusters is dominated by metallofullerenes,[167] which have also been the subject of several recent theoretical investigations.[168−170] Carbon clusters of sizes comprised between 12 and 30 are generally monocyclic when annealed,[171] monocyclic or bicyclic otherwise.[172] When monocyclic rings are considered, the metal atom may be either inserted in the ring for an even number of carbon atoms or remain external to it for even or odd numbers of carbons.[173] Although a number of MC_n and M_2C_n clusters ($n < 12$) have been experimentally observed and studied, little reliable information is available about the molecular structure of these species. Consistent values for thermodynamic data were measured by the Knudsen effusion technique combined with mass spectrometry,[174] always assuming that MC_n clusters consist of linear or bent carbon chains with the metal attached at one end (with the exception of MC_4 for which the dicarbide C_2-M-C_2 structure has also been considered).[175−178] However, other experiments suggest that even for a small number of carbon atoms, ringlike structures are preferred.[179] The series of ab initio and DFT calculations recently reported by Roszak and Balasubramanian on mono- and dimetallic yttrium/carbon clusters[180−182] as well as on ScC_2,[183] LaC_2,[184] and $YIrC_2$,[185] provide interesting information on the structure of small clusters comparable and complementary to the results of the similar investigation recently carried out by Sumathi and Hendrickx on small titanium/carbon clus-

ters[28,29,147,154] (see section VI.B). Ab initio calculations were carried out using relativistic core potentials on metal atoms and triple-ζ basis sets for the valence shells of metal and carbon. The basis set of carbon atoms was supplemented with one d-type polarization function. The effect of f-type polarization functions on yttrium ($\zeta = 0.206$) was tested on Y_2C_2 and found negligible. Geometry optimizations for the MC_2 systems and for $YIrC_2$ were carried out at the CASSCF and at the single-configuration-MP2 levels. The CASSCF active space for MC_2 was made of 12 orbitals, populated with 7 electrons. Various physical and thermodynamic properties (dissociation energies into M and C_2; atomization enthalpies, ionization potentials, Gibbs energy functions, heat content functions) were then computed at the same levels of theory and also by means of first-order CI (FOCI)[186] and multireference singles-and-doubles CI (MRSDCI) based upon a preliminary CASSCF treatment. Relativistic CI calculations were carried out on LaC_2 to estimate the spin−orbit contribution to the atomization energies, but the energy lowering assigned to spin−orbit-induced mixing between the lowest electronic configurations with different space symmetry and spin multiplicity was no more than 1 kJ·mol^{-1}.[185] Geometry optimizations on larger systems (YC_n, $n = 2-6$,[181] and Y_2C_n, $n = 2,8$[182]) were carried out by means of ab initio MP2 and nonlocal DFT calculations using the BLYP functional for exchange and correlation.[72a,75]

The MC_2 molecules (M = Sc, Y, La) are formed from the ^{2}D ground state of the atomic metal combined with one of the two low-lying electronic states of the C_2 fragment, singlet or triplet.[187] Doublet and quartet states were therefore systematically investigated and optimized for the triangular as for the linear unsymmetrical conformations of MC_2. As for TiC_2,[147] the low-spin states are more stable than the high-spin ones and the T-shape more stable than the linear conformation at all levels of calculation and for the three considered metals.[180,183,184] Inclusion of the dynamic correlation through perturbational or CI approaches systematically increases the energy gap between the triangular and the linear conformations. Those results rule out the hypothesis of a linear unsymmetrical conformation for MC_2 molecules that had been assumed for the experimental determination of the bond energies and of the thermodynamic functions.[176−178] However, the corrections to the experimental evaluations induced by a change of the assumed geometry remain small but lead to a better agreement with the theoretical results.[180,183,184] The bonding between the early transition metal and the C_2 moiety is interpreted in terms of a predominantly ionic bonding between M^{2+} and $(C{\equiv}C)^{2-}$. The Mulliken charge on the metal is +0.915 e for Sc, +0.978 e for Y, and +1.092 e for La. However, in YIrC and $YIrC_2$, there is a strong covalent bonding between iridium and carbon even resulting in a slightly negative net charge on iridium for the ground state of YIrC.[185] Figure 53 reproduces the electron difference map obtained at the CASSCF level between ScC_2 in its ground state and the fragments Sc + C_2 in the molecular plane.

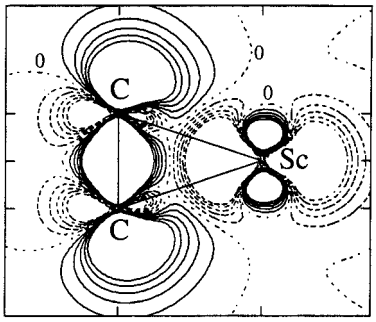

Figure 53. Electron density difference map between ScC_2 in its $^2A_1$ ground-state configuration and the (Sc + C_2) fragments in the molecular plane (from the CASSCF natural orbitals). Contour interval: 0.005 e.bohr^{-3}. Solid lines are for positive contours (density accumulation); dashed lines are for zero and negative contours. Reprinted with permission from ref 183. Copyright 1997 American Physical Society.

The geometries of the YC_n ($n = 3-6$)[181] and Y_2C_n ($n = 2,8$)[182] clusters have been optimized at the ab initio MP2 level for the monometallic species and at the nonlocal DFT/BLYP level for the dimetallic clusters, using the same basis set as for YC_2.[180] As for YC_2 and for the same reasons, the doublet and the quartet spin states were systematically investigated for the monometallic species, but at variance with TiC_n,[28] the low-spin configuration was found more stable for all structures and all values of n. Since the carbon cluster always interacts in its singlet state to give YC_n, the investigations concerning the spin state of the bimetallic clusters were restricted to the spin coupling between two yttrium atoms in their ^{2}D ground state. Only singlet and triplet electronic states were therefore considered for Y_2C_n clusters.[182] The number of distinct topologies for the smallest species is limited, and the same conformations that were displayed in Figures 39−42 for TiC_n and Ti_2C_n clusters are present, although with occasional differences in the energy sequence. For instance, the kite shape represents the conformation of lowest energy for YC_3 instead of the fan shape for TiC_3. The linear form comes third in both cases, and the nonplanar forms are destabilized by more than 50 kcal·mol^{-1}. The sequence computed for TiC_4, fan < nonsymmetric linear < pyramidal < kite (Figure 40), is barely modified for YC_4 except for an interversion between the two forms of highest energy. Besides, the nonplanar form is not a local minimum for YC_4 and the optimization process goes back to the fan conformation when the symmetry constraints are lifted. For YC_5, the linear and the kite structures are close in energy, but the linear form definitely becomes most stable for YC_6. The evolution of the molecular topology of the YC_n clusters is analyzed[181] in terms of a competition between the stabilization induced by the charge density transfer from the metal to the nearest carbon neighbors, which favors nonlinear structures, and the trend of middle-sized carbon clusters to organize into linear chains.[188]

Three isomers of Y_2C_2 were found quasi-degenerate at the DFT level: the linear Y−C−C−Y form in the singlet spin state, the rhombic conformation with a C−C bond (triplet spin state), and a C-shaped structure with the metal atoms at both ends (triplet

state).[182] If the two last forms were among the most stable ones for Ti_2C_2, the linear form of the dititanium cluster was destabilized by more than 2 eV (Figure 41). The nonplanar isomer, which was among the low-energy local minima for Ti_2C_2, does not appear for Y_2C_2. The optimization processes carried out at the MP2 level on the mixed-metal cluster $YIrC_2$[185] are possibly more in keeping with the results obtained for the dititanium cluster: the rhombic form (singlet spin state) is definitely the most stable one, followed by the linear form Y−C−C−Ir (+1.85 eV, singlet) and by the T-shaped Y−Ir−C_2 isomer (+2.04 eV, singlet). The large energy differences obtained by interverting the metal positions in the linear and in the T-shaped forms stress the importance of the covalent bonding between Ir and C_2 in the stabilization of the cluster. For five-atom, bimetallic clusters, the planar pentagon with separated metal atoms was found most stable with yttrium[182] as with titanium,[29] but the energy sequences of the other isomers appear quite unrelated. At variance with the titanium case, the forms that contain a direct Y−Y bond, and more specifically the nonplanar isomers, were found to be unstable.[182] Not all possible topologies were considered by Roszak and Balasubramanian for dimetallic clusters with higher values of *n*. On the basis of the results computed for Y_2C_3, a planar monocyclic, a linear, and a bent form were only considered for Y_2C_4 and Y_2C_5. The planar monocycle, with maximal metal−metal separation, was found most stable in both cases. In the cyclic isomer of Y_2C_4, one yttrium atom is bound side-on to the two C_2 fragments, whereas the other metal atom is bound end-on to the same fragments. With two ligands instead of three, this bonding mode is quite reminiscent of that observed in the tetrahedral conformation of met-cars.

3. Iron Carbon Clusters

Iron carbon cluster anions $Fe_nC_m^-$ have been generated by laser vaporization of a mixed carbon−iron rod, and the structures of mass-selected clusters, corresponding to $n = 1$, 2, and 3 and $m = 2-8$, have been studied using gas-phase ion chromatography.[189]

The two iron atom clusters are pure monocyclic rings with the two metal atoms nearest neighbors. The three iron species are three-dimensional. The situation is less clear-cut for the one metal atom clusters FeC_n^- ($n = 4-8$). Only the linear isomer of FeC_4^- is observed, and for FeC_7^-, only a cyclic isomer is seen. Two mobility peaks are resolved for FeC_5^- and for FeC_6^-, assigned to the linear and to the cyclic isomers. Three peaks could be characterized for FeC_8^-.[189] Preliminary ab initio calculations have been reported for some FeC_n, Fe_2C_5, and Fe_3C_6 structures, but no theoretical explanation has been given yet for the enhanced propensity for the $Fe_nC_4^-$ clusters in the mass spectrum.[189]

The anion photoelectron spectroscopy technique has been applied by Wang et al. to monometallic cluster ions FeC_n^- ($n = 2-5$).[190−192] The photoelectron spectrum of FeC_2^- is characterized by two prominent bands at 1.91 and 2.9 eV. Both features are interpreted in terms of an electron detachment transition with both the anion and the neutral species assumed in a conformation with $C_{\infty v}$ symmetry (linear-to-linear transition).[191,192] This structural assignment is however questioned by several recent ab initio and DFT calculations. The first ab initio study, due to Cao,[193] assigns a triangular conformation to both FeC_2^- and FeC_2^{2-} on the basis of CISD calculations including Davidson's correction for quadruples[194] and carried out from UHF orbitals obtained with a moderate size basis set. The energy values displayed at the correlated level for various electronic states in both the linear and the triangle conformations are however extremely puzzling and difficult to reconcile with the author's conclusions.[193] Very recently, Arbuznikov et al. reported DFT/B3LYP, CASSCF, and CASSCF/CASPT2 calculations carried out with large ANO basis sets[149] including polarization functions on both iron and carbon.[195] Although CASSCF alone is not able to assign the correct electronic configuration for the ground state, all three methodological approaches agree to rule out the linear form, destabilized with respect to the triangle conformation by 20 kcal·mol^{-1} at least (12 kcal·mol^{-1} at the DFT/B3LYP level).[195] The CASPT2 treatment, which includes a perturbational estimate of the dynamic correlation, is in agreement with the DFT/B3LYP framework to assign $^5A_2$ as the ground state, with another quintet ($^5A_1$) very close in energy. The FeC_2 complex in its ground state can be formally regarded as an ionic $Fe^{2+}-C_2^{2-}$ complex resulting from the transfer of the two 4s electrons of iron to the $3\sigma_g$ orbital of the C_2 ligand.[195]

DFT calculations, either at the LDA level or using Becke's nonlocal corrections, have been carried out by Nash et al. on FeC, FeC_2, and FeC_3 with basis sets including polarization functions on carbon but not on iron.[196] The geometry of FeC_2 was also optimized by means of ab initio Hartree−Fock + MP4 calculations. The geometrical parameters of the cyclic ground state obtained for FeC_2 at the HF-MP4 level ($d_{C-C} = 1.30$ Å; $d_{Fe-C} = 1.93$ Å) are practically identical with those optimized later by Arbuznikov et al.[195] from DFT/B3LYP calculations ($d_{C-C} = 1.292$ Å; $d_{Fe-C} = 1.921$ Å). Both studies also agree to assign the ground state to be a quintet at the most accurate levels of calculation. The atomization energy reported by Nash for FeC_2 is 11.58 eV, at both the DFT(NL) and the ab initio HF-MP4 levels. The optimal linear structure is destabilized by as much as 3.1 eV with respect to the cyclic form (HF-MP4),[196] a gap considerably larger than the 20 kcal·mol^{-1} obtained by Arbuznikov et al. at the CASSCF/CASPT2 level.

Information on the respective structures of FeC_n^- and FeC_n ($n = 3-5$) could be obtained by interpreting the vibrational features in the photoelectron spectra of the cluster anions. The well-resolved spectrum of FeC_3^- was interpreted as was that of FeC_2^- in terms of a linear-to-linear transition,[191] but the DFT calculations by Nash et al. favor a cyclic structure for neutral FeC_3 as for FeC_2. However, the energy difference with respect to the linear conformation has been reduced to 0.5 eV for FeC_3.[196] The spectrum of FeC_4^- is unusually diffuse, indicating a large geometry change from the anion to the neutral.[191,192] Since the ion mobility experiments of von Helden et al. are consistent with a linear structure for the anion,[189] it

was suggested that neutral FeC_4 could have a cyclic conformation.[191,192] The PES spectrum of FeC_5^- shows both sharp and diffuse features,[191] suggesting the coexistence of isomers, in agreement with the ion mobility experiments.[189]

The DFT calculations reported by Fan, Lou, and Wang on FeC_3, FeC_4, and their anions are more ambiguous and do not totally support those conclusions.[192] In fact, geometry optimization carried out in the local approximation found the ring form to be most stable for both iron carbide clusters, either neutral or anionic. However, incorporation of Becke's nonlocal exchange potential systematically reverses the trend, and linear structures become more stable with energy differences ranging from 0.21 eV (FeC_3) to 1.11 eV (FeC_4).[192] The result concerning FeC_3 is therefore at variance with that of Nash,[196] and further work at a high level of ab initio theory is clearly needed to rationalize the conflicting information concerning the structure of FeC_n^- and FeC_n clusters.

4. Nickel Carbon Clusters

Most of the experimental[197] and theoretical[198] studies concerning nickel/carbon systems have been focused on the strong interaction occurring between nickel and graphite and resulting in ferromagnetic monolayers of metal atoms above the graphite surface. The reactivity of nickel and other transition metals with C_{60} and C_{70} resulting either in $M_n(C_{60})_m$ systems or in the MC_{59-2n} and MC_{69-2n} ($n = 0, 1, 2, ...$) cluster series has also been investigated.[141,167k,170b] It is not until recently that laser vaporization of composite nickel carbide samples has been successfully used to generate and detect by a mass spectrometer small Ni_xC_y cluster cations ($x = 1, 2$; $y = 3-16$).[163] No peak corresponding to NiC^+ or to NiC_2^+ was detected; the distribution begins at NiC_3^+. The most abundant carbide masses correspond to clusters having the formula NiC_x^+ with enhanced peaks at $x = 3$ and, to some extent, at $x = 10$. Clusters corresponding to $Ni_2C_x^+$ have also been detected, especially $Ni_2C_3^+$, $Ni_2C_6^+$, and $Ni_2C_{11}^+$.[163] The structure of such small NiC_x ($x = 3, 4$) and Ni_2C_x ($x = 4-6$) clusters was recently optimized[199] by means a newly developed tight-binding molecular dynamics method[200] and checked by DFT calculations. The most stable structures were found to be the following: a kite conformation for NiC_3; a rhombic pyramid, with Ni as the apex, for NiC_4; a square bipyramid for Ni_2C_4; still a bipyramid, with a planar C_5 basis, for Ni_2C_5; a strongly ruffled C_6 ring bicapped by the metal atoms for Ni_2C_6.[199] Cluster models were also proposed to represent the hole and top positions of a Ni atom interacting with a graphite surface simulated by a planar assembly of 22 or 37 atoms, respectively.[199]

5. Niobium Carbon Clusters

For niobium−carbon as for Ti/C and V/C clusters, two types of stoichiometries, corresponding to met-cars and to fcc crystallites, are observed to be especially abundant.[10,25c,134,138] For small niobium−carbon cluster cations, the $Nb_nC_n^+$ species ($n = 2-4$) were found to be the prominent ions in the mass spectrum.[10,25c,30] Abstraction reaction observed between $Nb_4C_4^+$ and water, or methanol (cf. section V.E), suggest the following estimates for the bond energies between the cluster and the abstracted species:

$$D_e(Nb_4C_4^+-OH) \leq D_e(H-OH) = 119 \text{ kcal·mol}^{-1}$$

$$D_e(Nb_4C_4^+-OCH_3) \sim D_e(H-OCH_3) = 104 \text{ kcal·mol}^{-1}\ ^{30}$$

Ab initio RHF and MP2 calculations were carried out on Nb_4C_4 and $Nb_4C_4^+$ by assuming the topology of a NaCl type lattice with imposed T_d symmetry.[30] The Nb−C distance was optimized at 2.013 Å, and the structure was that of a slightly distorted cube with C−Nb−C angles of 85.0°. The ground-state configuration is a closed-shell singlet at the MP2 level and, therefore, appears stable with respect to a Jahn−Teller distortion. The removal of an electron to give $Nb_4C_4^+$ results in a doublet state with configuration $(2e)^3$, which is expected to undergo Jahn−Teller distortion to symmetries lower than T_d. The Nb_4C_2 cluster and its cation, which results from the reaction of $Nb_4C_4^+$ with O_2, were calculated to have the structure of a bicapped tetrahedron (C_{2v} symmetry). The neutral cluster has a singlet ground state and metal−metal distances comprised between 2.72 and 2.86 Å. Calculations carried out at the MP2 level with double-ζ valence basis sets showed that the reactions of the neutral and ionic species with O_2,

$$Nb_4C_4 + O_2 \rightarrow Nb_4C_2 + 2CO \quad (11)$$

$$Nb_4C_4^+ + O_2 \rightarrow Nb_4C_2^+ + 2CO \quad (12)$$

are nearly thermoneutral.[30]

Apart from the peaks corresponding to the met-car cation $Nb_8C_{12}^+$, to $Nb_4C_4^+$, and to fcc nanocrystals with higher nuclearity, a local maximum in the mass spectra obtained by Pilgrim, Brock, and Duncan et al. was assigned the stoichiometry $Nb_6C_7^+$.[25c] Byun et al. reported ab initio RHF calculations on Nb_5C_6, Nb_6C_7, and their cations, completed by an investigation of the reactivity of $Nb_6C_7^+$ that gives a consistent view of the cluster structure.[201] The structure previously optimized for Nb_4C_4[30] was used as a building block for Nb_5C_6, obtained by adding a NbC_2 unit atop of the distorted cube. Starting from this conformation (Figure 54a) several structures were investigated for Nb_6C_7, the most reasonable one from the criterion of the charge distribution being that of a double cube sharing one face, with D_{2h} symmetry and one carbon at the exact inversion center of the cluster (Figure 54b).

The total binding energy computed with respect to isolated atoms (1.3489 hartree) corresponds to a binding energy per atom of 2.82 eV, which appears extremely low when compared to the values higher than 6 eV/atom usually found from DFT calculations on met-cars and nanocrystals. Part of the difference should be assigned to the neglect of correlation energy in those ab initio RHF calculations. In the D_{2h}

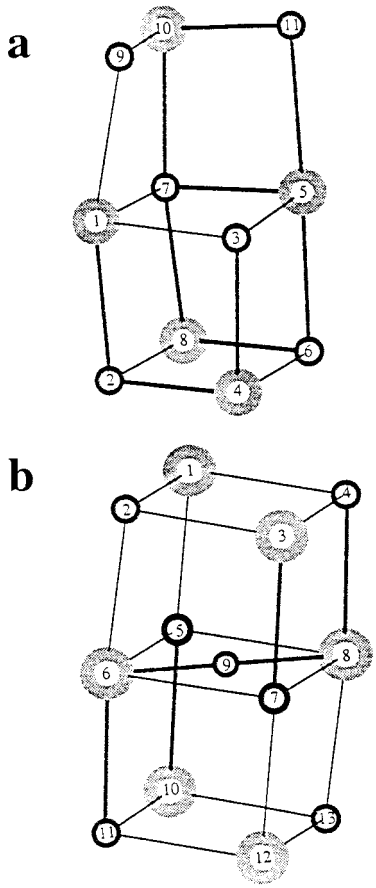

Figure 54. Geometries optimized at the ab initio Hartree−Fock level for (a) Nb_5C_6 and (b) Nb_6C_7. Reprinted with permission from ref 201. Copyright 1996 American Chemical Society.

structure of Figure 54b, four of the six niobium atoms are mutually equivalent but different from the other two. Those four metal atoms are more coordinatively unsaturated and are therefore expected to be more reactive, despite a smaller positive Mulliken net charge. This prediction is consistent with the reactivity pattern oberved between $Nb_6C_7^+$ and polar and nonpolar molecules, namely H_2O, NH_3, CH_3OH, CH_3CN, and C_6H_6.[201] For each of these ligands, sequential attachment reactions occur leading to the initial truncation products $Nb_6C_7L_4^+$. Minor amounts of $Nb_6C_7L_5^+$ and $Nb_6C_7L_6^+$ are observed for polar molecules, but they grow in slowly.

6. Extension of the Met-Car Structural Principles to High-Nuclearity Clusters

Yamada and Castleman reported in 1993 the formation of copper carbide cluster cations by heating metallic copper in the presence of C_2H_2.[202] The dominant peaks in the mass spectra were assigned to the series $Cu_{2n+1}C_{2n}^+$, $n = 1-10$. The structure of those clusters was assumed first to resemble that of solid copper acetylide Cu_2C_2, a face-centered tetragonal lattice made of copper atoms and C_2 dimers.[202] Just after having discovered the structure most stable for M_8C_{12}, the tetracapped tetrahedron, Dance applied the same structural principles, assessed with DFT/LSD calculations, to propose compact, met-car-like structures for the $Cu_{2n+1}C_{2n}$ clusters.[203,204] Essential to Dance's argument is the $Cu_{13}C_{12}$ cluster, since the 13 metal atoms can be arranged into a centered cuboctahedron which is the building block for the cubic close packed system of bulk copper. As the cube, the cuboctahedron has six square faces that can accommodate six C_2 groups, accounting for the observed composition (Figure 55). The optimal conformation calculated with DFT showed a slight deformation toward concavity of the Cu_4 faces, similar to, but less conspicuous than, that observed in the tetracapped tetrahedron structure of met-cars.[203] At variance with met-cars however, the twelve outer metal atoms of the distorted cuboctahedron remain equivalent and bonded each to two dicarbons, one coordinated end-on and the other one side-on. This conformation was compared with two other structures. One is also based upon a cuboctahedral copper framework, but the C_2 units are parallel to the edges of the underlying Cu_4 faces. This structure is therefore equivalent to the *dodecahedral* conformation of met-cars. The energy difference in favor of the conformation of Figure 55 is relatively weak however: 71 kcal·mol^{-1}. Another conformation, with Cu-centered, hexagonal prism structure is ∼180 kcal·mol^{-1} higher. No comparison has been reported however with the fcc tetragonal crystallites advocated by Yamada and Castleman. A cluster growth pathway was proposed along the same guidelines from the met-car-like $Cu_{13}C_{12}$ cluster toward higher members of the $Cu_{2n+1}C_{2n}$ series.[204]

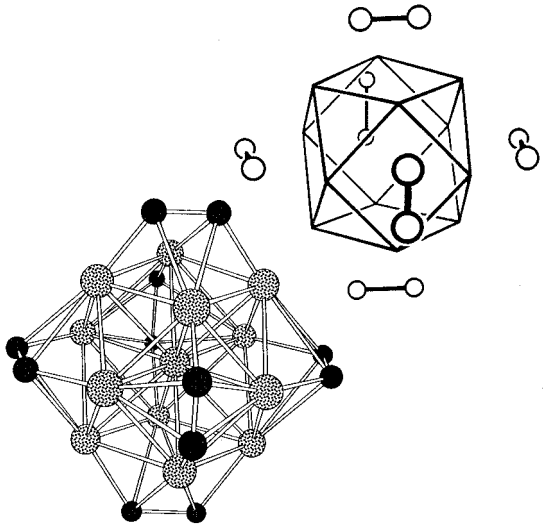

Figure 55. Schematic and ball-and-stick representations of the met-car-like structure advocated by Dance for $Cu_{13}C_{12}^+$. Reprinted with permission from refs 203 and 204. Copyright 1993 American Chemical Society and The Royal Society of Chemistry.

Let us come to an end with a more speculative hypothesis inspired by the beauty of the 5-fold symmetry. As an alternative to the multicage growth path proposed by Wei and Castleman[9,142,143] for high-nuclearity, carbon-rich Zr/C clusters, Dance imagined a $M_{30}C_{45}$ cluster formed by cyclic fusion of five dodecahedral M_8C_{12} units (Figure 56).[205] The central motif of that supercluster is a carbon pentagon, but all other carbon atoms are retained in C_2 units. The symmetry is D_{5h}, and the pentagon is the only polygon occurring in that molecule, which can un-

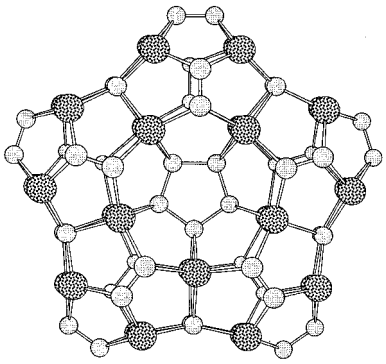

Figure 56. Superpentagonal structure proposed by Dance for a hypothetic $M_{30}C_{45}$ cluster composed of five fused dodecahedral met-car cages. Reprinted with permission from ref 205. Copyright 1993 Australian Academy of Sciences.

dergo large distance variations without significant strain.[205] Note that the layer-by-layer cubic growth pathway advocated by Wang and Cheng for large carbon-rich metal carbide clusters[33] predicts a stoichiometry of $M_{31}C_{48}$ for the seven-layer ABABABA structure (see section VI.D.1). If a competition could be considered between both conformations, it would be that of a unique, "magic" form with specific, topology-dependent orbital interactions, against the increasing stability offered by the extension of a regular structure eventually growing to infinity. The case of met-cars offers a striking example that the stability of some isolated, specific cluster shapes can overcome that of standard crystal fragments. The competition for such "magic" clusters however becomes increasingly difficult as the destabilizing edge effects in the crystallite with equivalent size become negligible with respect to the bulk properties.

VII. Concluding Remarks

The emphasis of this article has been to highlight the close interrelation that exists since the very beginning of the met-car story between experimental information and the predictive and interpretative arguments of computational quantum chemistry. Structure was a key issue into that debate since it is not readily accessible to experiment but however represents the ultimate explanation to the specific properties of met-cars and in particular to their stability. From a purely statistical point of view, it was an impossible task to single out from scratch the topology most probable for a system made of 20 atoms. It was an achievement of chemical intuition to guess from the early beginning that a hollow cage structure only could account for the "supermagic" character of titanium met-cars cations.[3] It was the ability of computational chemistry to refine the initial model by quantitatively accounting for the fact that tetravalent titanium does not behave exactly the same way as tetravalent carbon. The 8-year long story of quantum chemical calculations on met-cars however shows how much computational chemistry remains dependent on the accumulation of experimental knowledge. Dance[27] recently pointed out that 15 isomers at least had been proposed and evaluated for the Ti_8C_{12} molecule. Most of those isomers—with the notable exception of the pentagonal dodecahedron[49,88]—are local minima of the potential energy hypersurface. This represents however a negligible proportion of all energy minima that should exist given a collection of 12 carbon and 8 titanium atoms—and possibly a small proportion of the Ti_8C_{12} isomers that are effectively present in the plasma source. There is indeed no mathematical evidence that the structure of tetracapped tetrahedron, lowest in energy among the above 15, represents the global minimum. If experimentalists and theoreticians presently agree to consider that the form with T_d symmetry represents the most abundant isomer of Ti_8C_{12} and other met-cars,[105] it is mainly because the topological, physical, and chemical properties specific to that cluster shape explain or agree with the experimental information presently available. Let us summarize the main points of agreement:

(i) The presence of two types of metal sites, each occurring four times, explains the sharp truncation at $n = 4$ of some association series, especially with nonpolar molecules having a π-bonding system.[61,129,131] Calculations however confirm that *polar* molecules can fix on both types of metal sites.[23]

(ii) The diversity in the response of met-car cations toward halide abstraction can be nicely correlated with the number of upper valence, weakly coupled metal electrons accommodated in a slightly antibonding set of metal orbitals.

(iii) Calculations suggest that the substitution of Ti by Zr yielding binary metal met-cars $Ti_{8-x}Zr_xC_{12}$ ($x = 1-5$) can occur on either type of metal site with nearly identical probability, thus explaining the regular evolution of the peak intensities from $x = 0$ to $x = 5$.[21]

(iv) The particularly low values experimentally determined for the ionization potential and the electron affinity of Ti_8C_{12} and Zr_8C_{12}[105,126] are well reproduced by DFT calculations.[21,27,35,67]

(v) The Monte Carlo simulation of the ion mobility assuming the structure of tetracapped tetrahedron is in reasonable agreement with the measured value.[84]

The experimental information is more scattered however concerning the metal carbide clusters with non-met-car stoichiometries that appear with a certain prominence in the mass spectra of neutral or anionic species. For that reason, some structures that have been optimized from DFT calculations remain more controversial. It appears however that three main types of structures are encountered with a relative abundance depending upon the experimental conditions:

(1) "Carbon-poor" clusters, with 1:1 metal carbon ratio, are easily rationalized in terms of face-centered cubic crystal fragments. This structural aspect has been comfirmed by the calculations that have been carried out on the prototypical systems Nb_2C_2[30] and $Ti_{14}C_{13}$.[27,66,90]

(2) "Carbon-rich" clusters are characterized by a metal carbon ratio close to 1:1.5. Met-cars belong to that category, but this structure apparently represents an isolated peak of stability in the 20-atom region. The stability of met-cars however extends to 21-atom systems by encapsulation of an additional

carbon.[21,27,67] It can also persist for stoichiometries that differ from M_8C_{12}/M_8C_{13} by the substitution or the loss of one and even of two atoms: Ti_7C_{13} and Ti_6C_{13} are predicted to have a met-car-like structure.[21]

(3) The structure of high-nuclearity, carbon-rich clusters is presently difficult to predict with certainty. The stability of some specific stoichiometries such as $M_{13}C_{22}$ or $M_{18}C_{27}$ has been tentatively explained by an extension of the met-car topological properties resulting from the fusion of two or more dodecahedral cages.[9,142] The fact that met-cars are eventually not dodecahedral makes fused cages more difficult to conceptualize, but they do exist as local minima and they apparently retain most of the stability of met-cars.[33] A binding energy of ~6.5 eV/atom was remarkable for a 20-atom system, but the same value is less exceptional for a 35-atom cluster which can take advantage of the size effect eventually favorable to the ordered structures. That is the reason why the C_2-decorated layered cubic structures of Wang and Cheng which can be extended in linear wires to infinity could account for the magic peaks at very high masses.[33] From a purely energetical viewpoint, the case of $Ti_{13}C_{22}$ remains ambiguous, but the agreement obtained between the photoelectron spectrum of $Ti_{13}C_{22}^-$ and the electronic density of states spectrum calculated from the cubic form represents a strong argument in favor of that structure.[33]

If chemical reasoning, known crystal structures, and designed growth pathways can provide useful guidelines to picture the topologies most probable for large clusters, they are of little help for small and intermediate size systems. The comprehensive scanning strategy reaches its limits beyond five or six atoms.[29] We therefore think that progress in the computational investigation of clusters will require in the near future the systematic use of techniques for global optimization.[155]

Note Added in Proof. In a quite recent report, the quantum chemical investigations on the structure of E_8C_{12} clusters have been extended to the carbides of main group elements with four valence electrons (E = Si, Ge, Sn). By means of ab initio RHF, MCSCF, MCQDPT2, and MP2 calculations, Bode and Gordon (*J. Chem. Phys.* **1999**, *111*, 8778−8784) show that the conformations preferred for the homologues of C_{20} are the dodecahedral form (for E = Si) and, for E = Sn and Ge, a new cage conformation with D_{2h} symmetry and no more than 16 bonds between the E atoms and acetylenic dicarbons characterized by very short C−C bond lengths.

VIII. References and Notes

(1) (1) See for instance: Ebbesen, T. W. *Acc. Chem. Res.* **1998**, *31*, 558−566.

(2) Kroto, H. W.; Heath, J. R.; O'Brien, S. C.; Curl, R. F.; Smalley, R. E. *Nature* **1985**, *318*, 162−163.

(3) Guo, B. C.; Kerns, K. P.; Castleman, A. W., Jr. *Science* **1992**, *255*, 1411−1413.

(4) C_{20} is expected to remain hypothetical because of the high strain assigned to the presence of fused pentagonal rings but also because of the open-shell character of the π system leading to Jahn−Teller distortion.[5] The smallest fullerene characterized to date as bulk samples is C_{36}, composed of 12 pentagons and 8 hexagons.[6] However, a very recent work by Hata et al. reports the selective formation of C_{20}^+ cluster cations by field evaporation from carbon nanotubes. C_{20}^+ appears as a prominent peak in the mass spectrum, and its structure is tentatively assigned to be icosahedral. See: Hata, K.; Ariff, M.; Tohji, K.; Saito, Y. *Chem. Phys. Lett.* **1999**, *308*, 343−346.

(5) (a) Klein, D. J.; Seitz, W. A.; Schmalz, T. G. *Nature* **1986**, *323*, 703−706. (b) Fowler, W. P.; Woolrich, J. *Chem. Phys. Lett.* **1986**, *127*, 78−83. (c) Martin, J. M. L.; François, J. P.; Gijbels, R.; Almlöf, J. *Chem. Phys. Lett.* **1991**, *187*, 367−374. (d) Bakowies, D.; Thiel, W. *J. Am. Chem. Soc.* **1991**, *113*, 3704−3714. Note that some derivatives of the elusive C_{20} have been characterized, the most famous one being Paquette's dodecahedrane $C_{20}H_{20}$ (Paquette, L. A.; Ternansky, R. J.; Balogh, D. W.; Kentgen, G. *J. Am. Chem. Soc.* **1983**, *105*, 5446−5450). Two organometallic derivatives of $C_{20}H_{20}$ have been recently synthesized, where 8 hydrogens have been substituted either by two $Pt(PPh_3)_2$ and two organic CO_2CH_3 groups or by four $Fe(CO)_4$ ligands (Oswald, T.; Keller, M.; Prinzbach, H. communication at the XXXIII International Conference on Coordination Chemistry, Florence, Italy, 1998). Isoelectronic with $C_{20}H_{20}$ would be the dodecahedral N_{20} molecule, which has been calculated to be a relative minimum on its potential energy hypersurface, although destabilized by ~1000 kcal·mol^{-1} with respect to 10 N_2 molecules (Blyzniuk, A. A.; Shen, M.; Schaefer, H. F., III *Chem. Phys. Lett.* **1992**, *198*, 249−252).

(6) Piskoti, C.; Yarger, J.; Zettl, A. *Nature* **1988**, *393*, 771−774. The special stability of C_{36} in the solid state has been assigned to the diradical character of the isolated cage, which allows this lower fullerene to overcome the strain by forming covalent bonds with other C_{36} molecules in a tightly bound solid. See: (a) Fowler, P. W.; Mitchell, D.; Zerbetto, F. *J. Am. Chem. Soc.* **1999**, *121*, 3218−3219. (b) Jagadeesh, M. N.; Chandrasekhar, J. *Chem. Phys. Lett.* **1999**, *305*, 298−302.

(7) (a) Guo, B. C.; Wei, S.; Purnell, J.; Buzza, S.; Castleman, A. W., Jr. *Science* **1992**, *256*, 515−516. (b) Wei, S.; Guo, B. C.; Purnell, J.; Buzza, S.; Castleman, A. W., Jr. *J. Phys. Chem.* **1992**, *96*, 4166−4168.

(8) Pilgrim, J. S.; Duncan, M. A. *J. Am. Chem. Soc.* **1993**, *115*, 6958−6961.

(9) (a) Castleman, A. W., Jr.; Guo, B. C.; Wei, S.; Chen, Z. Y. *Plasma Phys. Contr. Fusion* **1992**, *34*, 2047−2051. (b) Castleman, A. W., Jr. *Z. Phys. D* **1993**, *26*, 159−161.

(10) Wei, S.; Guo, B. C.; Deng, H. T.; Kerns, K.; Purnell, J.; Buzza, S.; Castleman, A. W., Jr. *J. Am. Chem. Soc.* **1994**, *116*, 4475−4476.

(11) Referred to by: Baum, R. *Chem. Eng. News* **1992**, March 16, 4−5.

(12) Fowler, P. W. *Philos. Trans. R. Soc. London* **1993**, *A343*, 39−52.

(13) Dance, I. *J. Chem. Soc., Chem. Commun.* **1992**, 1779−1780.

(14) Lin, Z.; Hall, M. B. *J. Am. Chem. Soc.* **1993**, *115*, 11165−11168.

(15) Rohmer, M.-M.; Bénard, M.; Henriet, C.; Bo, C.; Poblet, J.-M. *J. Chem. Soc., Chem. Commun.* **1993**, 1182−1185.

(16) Reddy, B. V.; Khanna, S. N.; Jena, P. *Science* **1992**, *258*, 1640−1643.

(17) Grimes, R. W.; Gale, J. D. *J. Phys. Chem.* **1993**, *97*, 4616−4620.

(18) Li, Z. Q.; Gu, B. L.; Han, R. S.; Zheng, Q. Q. *Z. Phys. D* **1993**, *27*, 275−279.

(19) Lou, L.; Nordlander, P. Unpublished, referred to in ref 22.

(20) Dance, I. Unpublished, referred to in ref 22.

(21) Muñoz, J.; Pujol, C.; Bo, C.; Poblet, J.-M.; Rohmer, M.-M.; Bénard, M. *J. Phys. Chem. A* **1997**, *101*, 8345−8350.

(22) Brock, L. R.; Duncan, M. A. *J. Phys. Chem.* **1996**, *100*, 5654−5659.

(23) Poblet, J.-M.; Bo, C.; Rohmer, M.-M.; Bénard, M. *Chem. Phys. Lett.* **1996**, *260*, 577−581.

(24) Rubio, A.; Alonso, J. A.; López, J. M. *An. Fis.* **1993**, *89*, 174−179.

(25) (a) Pilgrim, J. S.; Duncan, M. A. *J. Am. Chem. Soc.* **1993**, *115*, 9724−9727. (b) Pilgrim, J. S.; Duncan, M. A. *Int. J. Mass Spectrom. Ion Processes* **1994**, *138*, 283−296. (c) Pilgrim, J. S.; Brock, L. R.; Duncan, M. A. *J. Phys. Chem. A* **1995**, *99*, 544−550.

(26) Sakurai, H.; Castleman, A. W., Jr. *J. Phys. Chem. A* **1997**, *101*, 7695−7698.

(27) Dance, I. *J. Am. Chem. Soc.* **1996**, *118*, 2699−2707.

(28) Sumathi, R.; Hendrickx, M. *J. Phys. Chem. A* **1998**, *102*, 4883−4889.

(29) Sumathi, R.; Hendrickx, M. *J. Phys. Chem. A* **1998**, *102*, 7308−7313.

(30) Yeh, C. S.; Byun, Y. G.; Afzaal, S.; Kan, S. Z.; Lee, S.; Freiser, B. S.; Hay, P. J. *J. Am. Chem. Soc.* **1995**, *117*, 4042−4048.

(31) Yang, J.; Toigo, F.; Wang, K. *Chem. Phys. Lett.* **1994**, *228*, 279−283.

(32) Wei, P.; Yang, W. *Phys. Rev. B* **1995**, *51*, 7224−7230.

(33) Wang, L.-S.; Cheng, H. *Phys. Rev. Lett.* **1997**, *78*, 2893−2896.

(34) Wang, L.-S.; Wang, X.-B.; Wu, H. Cheng, H. *J. Am. Chem. Soc.* **1998**, *120*, 6556−6562.

(35) Muñoz, J.; Rohmer, M.-M.; Bénard, M.; Poblet, J.-M. *J. Phys. Chem. A* **1999**, *103*, 4762−4768.

(36) Cartier, S. F.; Chen, Z. Y.; Walder, G. J.; Sleppy, C. R.; Castleman, A. W., Jr. *Science* **1993**, *260*, 195−196.
(37) Selvan, R.; Pradeep, T. *Chem. Phys. Lett.* **1999**, *309*, 149−156.
(38) Pradeep, T.; Manoharan, P. T. *Curr. Sci.* **1995**, *68*, 1017−1026.
(39) Lin, Z.; Hall, M. B. *J. Am. Chem. Soc.* **1992**, *114*, 10054−10055.
(40) Hay, P. J. *J. Phys. Chem.* **1993**, *97*, 3081−3083.
(41) Liu, J.-N.; Gu, B. L. *J. Phys.: Condens. Matter* **1993**, *5*, 4785−4792.
(42) Xia, H. B.; Tian, D. C.; Jin, Z. Z.; Wang, L. L. *J. Phys.: Condens. Matter* **1994**, *6*, 4269−4276.
(43) Xiao, C.-Y.; Deng, K. M. *Commun. Theor. Phys.* **1996**, *26*, 263−272.
(44) Grimes, R. W.; Gale, J. D. *J. Chem. Soc., Chem. Commun.* **1992**, 1222−1224.
(45) Lou, L.; Guo, T.; Nordlander, P.; Smalley, R. E. *J. Chem. Phys.* **1993**, *99*, 5301−5305.
(46) Rantala, T. T.; Jelski, D. A.; Bowser, J. R.; Xia, X.; George, T. F. *Z. Phys. D* **1993**, *S26*, 255−257.
(47) Han, R.; Wang, S.; Yin, D. L.; Zheng, Q. Q.; Pan, W. *Solid State Commun.* **1993**, *86*, 313−315.
(48) Muñoz, J.; Poblet, J.-M. Unpublished results.
(49) Chen, H.; Feyereisen, M.; Long, X. P.; Fitzgerald, G. *Phys. Rev. Lett.* **1993**, *71*, 1732−1735.
(50) Methfessel, M.; van Schilfgaarde, M.; Scheffler, M. *Phys. Rev. Lett.* **1993**, *70*, 29−32.
(51) Srinivas, G. N.; Srinivas, H.; Jemmis, E. V. *Proc. Indian Acad. Sci. (Chem. Sci.)* **1994**, *106*, 169−181.
(52) Mingos, D. M. P. *Acc. Chem. Res.* **1984**, *17*, 311−319.
(53) In that sense, the bonding interactions in dodecahedral Ti_8C_{12}, V_8C_{12}, and isoelectronic met-cars are not strikingly different from those obtained for the d^0 clusters Sc_8C_{12} or Y_8C_{12}. However, the stability of met-cars made from group 3 metals seems much reduced, since no such cluster cation could be characterized as a "magic" peak,[54] except for mixed Ti−Y species involving at most two yttrium atoms.[55]
(54) Kan, S. Z.; Lee, S. A.; Freiser, B. S. *J. Mass. Spectrom.* **1996**, *31*, 62−68.
(55) Cartier, S. F.; May, B. D.; Castleman, A. W., Jr. *J. Am. Chem. Soc.* **1994**, *116*, 5295−5297.
(56) For a discussion on the correlation between the weighted HOMO−LUMO gap and the kinetic stability of fullerene and fullerene-like systems, see: Yoshida, M.; Aihara, J. *PCCP* **1999**, *1*, 227−230.
(57) Dunlap, B. I.; Brenner, D. W.; Mintmire, J. W.; Mowrey, R. C.; White, C. T. *J. Phys. Chem.* **1991**, *95*, 8737−8741.
(58) Scuseria, G. E. *Chem. Phys. Lett.* **1991**, *176*, 423−427.
(59) Guo, B. C.; Kerns, K. P.; Castleman, A. W., Jr. *J. Am. Chem. Soc.* **1993**, *115*, 7415−7418.
(60) Byun, Y. G. Lee, S. A.; Kan, S. Z. Freiser, B. S. *J. Phys. Chem.* **1996**, *100*, 14281−14288.
(61) Deng, H. T.; Kerns, K. P.; Castleman, A. W., Jr. *J. Am. Chem. Soc.* **1996**, *118*, 446−450.
(62) Deng, H. T.; Guo, B. C.; Kerns, K. P.; Castleman, A. W., Jr. *J. Phys. Chem.* **1994**, *98*, 13373−13378.
(63) Kerns, K. P.; Guo, B. C.; Deng, H. T.; Castleman, A. W., Jr. *J. Am. Chem. Soc.* **1995**, *117*, 4026−4029.
(64) Ceulemans, A.; Fowler, P. W. *J. Chem. Soc., Faraday Trans.* **1992**, *88*, 2797−2798.
(65) (a) Fowler, P. W.; Woolrich, J. *Chem. Phys. Lett.* **1986**, *127*, 78−83. (b) Stollhoff, G. *Phys. Rev. B* **1991**, *44*, 10998.
(66) Reddy, B. V.; Khanna, S. N. *Chem. Phys. Lett.* **1993**, *209*, 104−108.
(67) Lou, L.; Nordlander, P. *Chem. Phys. Lett.* **1994**, *224*, 439−444.
(68) Khanna, S. N. *Phys. Rev. B* **1995**, *51*, 10965−10967.
(69) (a) Hedin, L.; Lundqvist, B. I. *J. Phys. C* **1971**, *4*, 2064. (b) von Barth, U.; Hedin, L. *J. Phys. C* **1972**, *5*, 1629.
(70) von Barth, U.; Hedin, L. *J. Phys. C* **1964**, *136*, 864.
(71) Andzelm, J.; Wimmer, E. *J. Chem. Phys.* **1992**, *96*, 1280−1303.
(72) (a) Becke, *Phys. Rev. A* **1988**, *38*, 3098. (b) Perdew, J. *Phys. Rev. B* **1986**, *33*, 8822.
(73) (a) Ellis, D. E. *Int. J. Quantum Chem.* **1968**, *2*, 35. (b) Ellis, D. E.; Painter, G. P. *Phys. Rev. B* **1970**, *2*, 2887.
(74) Vosko, S. H.; Wilk, L.; Nusair, M. *Can. J. Phys.* **1980**, *58*, 1200−1211.
(75) Lee, C.; Yang, W.; Parr, R. G. *Phys. Rev. B* **1988,** *37*, 785.
(76) (a) Baerends, E. J.; Ellis, D. E.; Ros, P. *Chem. Phys.* **1973**, *2*, 41. (b) te Velde, G.; Baerends, E. J. *J. Comput. Phys.* **1992**, *99*, 84.
(77) (a) Ceulemans, A.; Fowler, P. W. *Phys. Rev. A* **1989**, *39*, 481. (b) Ceulemans, A.; Vanquickenborne, L. G. *Struct. Bonding (Berlin)* **1989**, *71*, 125.
(78) Pauling, L. *Proc. Natl. Acad. Sci. U.S.A.* **1992,** *89*, 8175−8176.
(79) Culberson, J.; Knappe, P.; Rösch, N.; Zerner, M. C. *Theor. Chim. Acta* **1987**, *71*, 21−39.
(80) Khan, A. *J. Phys. Chem.* **1993**, *97*, 10937−10941; **1995**, *99*, 4923−4928.
(81) 4.3 eV/atom, compared to 5.9 eV/atom for a monocyclic chain. Those values were obtained from single-point energy calculations at the MP2/6-31G* level.[80]
(82) Cartier, S. F.; May, B. D.; Castleman, A. W., Jr. *J. Phys. Chem.* **1996**, *100*, 8175−8179.
(83) Khanna, S. N.; Jena, P. *Phys. Rev. B* **1995**, *51*, 13705−13716.
(84) Bowers, M. T. *Acc. Chem. Res.* **1994**, *27*, 324−332.
(85) Cotton, F. A. *Chemical Applications of Group Theory*, 2nd ed.; Wiley-Interscience: New York, 1971; p 60, Exercises 3.16 and 3.17.
(86) Rohmer, M.-M.; de Vaal, P.; Bénard, M. *J. Am. Chem. Soc.* **1992**, *114*, 9696−9697.
(87) The application of gradient-corrected, nonlocal density functionals reduces the attractive interatomic potential and therefore yields a slightly expanded equilibrium geometry for the T_d isomer of Ti_8C_{12} (Ti^i-Ti^i = 2.94 Å; Ti^o-Ti^o = 4.94 Å; Ti^i-Ti^o = 2.96 Å; Ti^i-C = 2.28 Å; Ti^o-C = 2.01 Å; C−C = 1.35 Å).[27]
(88) Dance, I. *J. Am. Chem. Soc.* **1996**, *118*, 6309−6310.
(89) The transformation pathways from T_h to either T_d or D_{2d} require intermediate loss of mirror symmetry, thus explaining why the geometry optimization processes carried out with the D_{2h} or C_{2v} constraints could not get out of the dodecahedral topology.
(90) Rohmer, M.-M.; Bénard, M.; Bo, C.; Poblet, J.-M. *J. Am. Chem. Soc.* **1995**, *117*, 508−517.
(91) See for instance: For the general problem of core electron delocalization and hole states: (a) Snyder, L. C. *J. Chem. Phys.* **1971**, *55*, 95−99. (b) Cederbaum, L. S.; Domcke, W. *J. Chem. Phys.* **1977**, *66*, 5084−5086. (c) Cederbaum, L. S.; Tarantelli, F.; Sgamellotti, A.; Schirmer, J. *J. Chem. Phys.* **1986**, *85*, 6513−6523; **1987**, *86*, 2168−2175. (d) Schwarz, W. H. E.; Chang, T. C.; Seeger, U.; Hwang, K. H. *Chem. Phys.* **1987**, *117*, 73−89. (e) Backsay, G. B.; Bryant, G.; Hush, N. S. *Int. J. Quantum Chem.* **1987**, *31*, 471−487. For the specific case of transition metal complexes and clusters: (f) Newton, M. D. *Chem. Phys. Lett.* **1982**, *90*, 291−295. (g) Bénard, M. *Chem. Phys. Lett.* **1983**, *96*, 183−191. (h) Granozzi, G.; Mougenot, P.; Demuynck, Bénard, M. *Inorg. Chem.* **1987**, *26*, 2588−2594. (i) Quelch, G. E.; Hillier, I. H. *Chem. Phys. Lett.* **1988**, *144*, 153−157. (j) Clark, D. L.; Green, J. C.; Redfern, C. N.; Quelch, G. E.; Hillier, I. H. *Chem. Phys. Lett.* **1989**, *154*, 326−329.
(92) Still shorter Ti−Ti bonds (2.70, 2.74 Å) have been optimized for the D_{2d} isomer of the endohedral met-car $C\subset Ti_8C_{12}$.[67]
(93) Poblet, J.-M.; Rohmer, M.-M.; Bénard, M. *Inorg. Chem.* **1996**, *35*, 4073−4075.
(94) (a) Park, Y.; DeGroot, D. C.; Schindler, J.; Kannewurf, C. R.; Kanatzidis, M. G. *Angew. Chem., Int. Ed. Engl.* **1991**, *30*, 1325−1328. (b) Zhang, X.; Park, Y.; Hogan, T.; Schindler, J. L.; Kannewurf, C. R.; Seong, S.; Albright, T.; Kanatzidis, M. G. *J. Am. Chem. Soc.* **1995**, *117*, 10300−10310.
(95) Hollander, F. J.; Coucouvanis, D. *J. Am. Chem. Soc.* **1974**, *96*, 5646−5648; **1977**, *99*, 6268−6280. It is however interesting to note that in some metal chalcogenide clusters encapsulating a sulfur atom, such as $S\subset Cd_8(SR)_{12}X_4$ the metal framework has the structure of a tetracapped tetrahedron similar to that calculated for the endohedral met-car $C\subset Ti_8C_{12}$. No calculations have been carried out on those clusters. See: (a) Dance, I. G. *Aust. J. Chem.* **1985**, *38*, 1391−1411. (b) Lee, G. S. H.; Fisher, K. J.; Craig, D. C.; Scudder, M. L.; Dance, I. G. *J. Am. Chem. Soc.* **1990**, *112*, 6435−6437. (c) Dance, I. G.; Fisher, K. J. *Prog. Inorg. Chem.* **1994**, *41*, 637−803.
(96) Bénard, M.; Rohmer, M.-M.; Poblet, J.-M.; Bo, C. *J. Phys. Chem.* **1995**, *99*, 16913−16924.
(97) The same trends are observed for Zr_8C_{12}, but the effect of singlet coupling is still more important due to the larger overlap between the 4d orbitals of Zr. The optimal Zr^i-Zr^i distances are decreased from 3.43 to 3.31 Å from the quintet to the singlet-coupled state. Still shorter Zr^i-Zr^i distances of 3.175 [96] or 3.24 Å [14] are optimized when considering a RHF closed-shell state in which the metal−metal bonding $1a_1$ orbital is populated with two electrons. The computed energy difference between the quintet and the singlet-coupled states amounts to 18.4 kcal·mol^{-1}.[96]
(98) (a) Heisenberg, W. *Z. Physik* **1926**, *38*, 411; **1928**, *49*, 619. (b) Hay, P. J.; Thibeault, J. C.; Hoffmann, R. *J. Am. Chem. Soc.* **1975**, *97*, 4884−4899.
(99) A scanning of the RHF orbital energies of the singly occupied MOs obtained for Ti_8C_{12} ($1a_1$, −4.16 eV; $2a_1$, −1.85 eV; $2t_2$, −1.55 eV; $3t_2$, −1.55 eV) clearly shows that the stabilization of the lowest quintet state should be exclusively assigned to the population of the $1a_1$ orbital, Since $1a_1$ has nearly pure metal character, as have $2a_1$ and the triply degenerate, singly occupied MOs, the 78 kcal·mol^{-1} stabilization of the lowest $^5A_2$ state associated with the frontier orbitals of Figure 20 should be unambiguously assigned to the metal−metal bonding interactions.
(100) (a) Bader, R. F. W. *Atoms in Molecules, a Quantum Theory*; Clarendon Press: Oxford, U.K., 1990. (b) Bader, R. F. W.; MacDougall, P. J.; Lau, C. D. H. *J. Am. Chem. Soc.* **1984**, *106*, 1594−1605.
(101) Bader, R. F. W.; Slee, T. S.; Cremer, D.; Kraka, E. *J. Am. Chem. Soc.* **1983**, *105*, 5061−5068.

(102) (a) Bo, C.; Sarasa, J.-P.; Poblet, J.-M. *J. Phys. Chem.* **1993**, *97*, 6362−6366. (b) Bo, C.; Poblet, J.-M.; Bénard, M. *Chem. Phys. Lett.* **1990**, *169*, 89−96. (c) Costas, M.; Poblet, J.-M.; Rohmer, M.-M.; Bénard, M. *Inorg. Chem.* **1995**, *34*, 176−183.

(103) Bader, R. F. W.; Nguyen-Dang, T. T. *Adv. Quantum Chem.* **1981**, *14*, 63.

(104) Maclagan, R. G. A. R.; Scuseria, G. E. In *Advances in Metal and Semiconductor Clusters, Cluster Materials*; Duncan, M. A., Ed.; JAI Press: Stamford, CT, 1998; Vol. 4, pp 253−261.

(105) Sakurai, H.; Castleman, A. W., Jr. *J. Phys. Chem. A* **1998**, *102*, 10486−10492.

(106) Armentrout, P. B.; Sunderlin, L. S.; Fisher, E. R. *Inorg. Chem.* **1989**, *28*, 4436−4437 and references therein.

(107) (a) Siegbahn, P. E. M. In *Advances in Chemical Physics*; Prigogine, I., Rice, S. A., Eds.; John Wiley & Sons: New York, 1996; Vol. XCIII. (b) Bauschlicher, C. W., Jr.; Partridge, H.; Sheehy, J. A.; Langhoff, S. R.; Rosi, M. *J. Phys. Chem.* **1992**, *96*, 6969−6973.

(108) Siegbahn, P. E. M. *J. Am. Chem. Soc.* **1994**, *116*, 7722−7728.

(109) Duncan, M. A. *J. Cluster Sci.* **1997**, *8*, 239.

(110) Cartier, S. F.; May, B. D.; Castleman, A. W., Jr. *J. Chem. Phys.* **1994**, *100*, 5384−5386.

(111) Cartier, S. F., May, B. D.; Castleman, A. W., Jr. *J. Phys. Chem.* **1996**, *100*, 8175−8179.

(112) Iñiguez, M. P.; López, M. J.; Alonso, J. A.; Soler, J. M. *Z. Phys. D* **1989**, *11*, 163.

(113) Hertel, I. V.; Steger, H.; de Vries, J.; Weisser, B.; Menzel, C.; Kamke, B.; Kamke, W. *Phys. Rev. Lett.* **1992**, *68*, 784.

(114) May, B. D.; Cartier, S. F.; Castleman, A. W., Jr. *Chem. Phys. Lett.* **1995**, *242*, 265−272.

(115) Kooi, S. E.; Castleman, A. W., Jr. *J. Chem. Phys.* **1998**, *108*, 8864−8869.

(116) Cartier, S. F.; May, B. D.; Castleman, A. W., Jr. *J. Chem. Phys.* **1996**, *104*, 3423−3432.

(117) (a) Leisner, T.; Athanassenas, K.; Kreisle, D.; Recknagel, E.; Echt, O. *J. Chem. Phys.* **1993**, *99*, 9670−9680. (b) Leisner, T.; Athanassenas, K.; Echt, O.; Kandler, O., Kreisle, D.; Recknagel, E. *Z. Phys. D* **1991**, *20*, 127. (c) Collings, B. A.; Amrein, A. H.; Rayner, D. M.; Hackett, P. A. *J. Chem. Phys.* **1993**, *99*, 4174−4180.

(118) (a) Nieman, G. C.; Parks, E. K.; Richtsmeier, S. C.; Liu, K.; Pobo, L. G.; Riley, S. J. *High Temp. Sci.* **1986**, *22*, 115. (b) Athanassenas, K.; Leisner, T.; Frenzel, U.; Kreisle, D. *Ber. Bunsen-Ges. Phys. Chem.* **1992**, *96*, 1192−1194.

(119) Amrein, A.; Simpson, R.; Hackett, P. *J. Chem. Phys.* **1991**, *95*, 1781−1800.

(120) (a) Campbell, E. E. B.; Ulmer, G.; Hertel, I. V. *Phys. Rev. Lett.* **1991**, *67*, 1986. (b) Ding, D.; Huang, J.; Compton, R. N.; Klots, C. E.; Haufler, R. E. *Phys. Rev. Lett.* **1994**, *73*, 1084−1087. (c) Lin, H.; Han, K.-L.; Bao, Y.; Gallogly, E. B.; Jackson, W. M. *J. Phys. Chem.* **1994**, *98*, 12495−12500.

(121) The value of 6.62 eV taken from Reddy et al.[16] and often referred to in the discussion concerning the mechanism of the atomic ion emission of Ti_8C_{12}[114,116] corresponds to an average stabilization energy per atom and cannot be assimilated to the difference between the energy of Ti_8C_{12} in its ground state and optimized geometry and the energy of Ti_7C_{12} in a similar situation.

(122) *Handbook of Chemistry and Physics*, 70th ed.; CRC: Boca Raton, FL, 1989.

(123) Lee, S.; Gotts, N. G.; von Helden, G.; Bowers, M. T. *Science* **1995**, *267*, 999−1001.

(124) Kerns, K. P.; Guo, B. C.; Deng, H. T.; Castleman, A. W., Jr. *J. Chem. Phys.* **1994**, *101*, 8529−8534.

(125) Kerns, K. P.; Guo, B. C.; Deng, H. T.; Castleman, A. W., Jr. *J. Phys. Chem.* **1996**, *100*, 16817−16821.

(126) Wang, L.-S.; Li, S.; Wu, H. *J. Phys. Chem.* **1996**, *100*, 19211−19214.

(127) Li, S.; Wu, H.; Wang, L.-S. *J. Am. Chem. Soc.* **1997**, *119*, 7417−7422.

(128) The difference of 0.17 eV between the adiabatic IP′ values of Ti_8C_{12} reported in refs 21 and 35 and both computed with the ADF package[76] is due to a change in the description of the core electrons. In ref 21, all calculations, including those on Ti_8C_{12}, have been carried out with the relativistic core provided by ADF, for the purpose of compatibility with the calculations carried out on clusters involving heavier metals. In ref 35, a standard nonrelativistic core has been used for titanium. The same reason explains the slight difference between the computed electron affinities reported in the two papers.

(129) Yeh, C. S.; Afzaal, S.; Lee, S. A.; Byun, Y. G.; Freiser, B. S. *J. Am. Chem. Soc.* **1994**, *116*, 8806−8807.

(130) (a) Feng, J. K.; Tian, W. Q.; Huang, X. R.; Ge, M. F.; Li, Z. R. *Acta Chim. Sin.* **1998**, *56*, 631−635. (b) Ge, M. F.; Feng, J. K.; Tian, W. Q.; Li, Z. R.; Huang, X. R.; Sun, C. C. *Chem. Phys. Lett.* **1998**, *282*, 54−58.

(131) Byun, Y. G.; Freiser, B. S. *J. Am. Chem. Soc.* **1996**, *118*, 3681−3686.

(132) Sakurai, H.; Castleman, A. W., Jr. *J. Chem. Phys.* **1999**, *111*, 1462−1466.

(133) Deng, H. T.; Kerns, K. P.; Castleman, A. W., Jr. *J. Chem. Phys.* **1996**, *104*, 4862−4864.

(134) Deng, H. T.; Kerns, K. P.; Bell, R.; Castleman, A. W., Jr. *Int. J. Mass Spectrom. Ion Processes* **1997**, *167*, 615−625.

(135) Ahlrichs, R.; Bär, M.; Häser, M.; Horn, H.; Kölmel, C. *Chem. Phys. Lett.* **1989**, *162*, 165−169.

(136) Pilgrim, J. S.; Duncan, M. A. *J. Am. Chem. Soc.* **1993**, *115*, 4395−4396.

(137) Wei, S.; Guo, B. C.; Purnell, J.; Buzza, S. A.; Castleman, A. W., Jr. *J. Phys. Chem.* **1993**, *97*, 9559−9561.

(138) Purnell, J.; Wei, S.; Castleman, A. W., Jr. *Chem. Phys. Lett.* **1994**, *229*, 105−110.

(139) May, B. D.; Kooi, S. E.; Toleno, B. J.; Castleman, A. W., Jr. *J. Chem. Phys.* **1997**, *106*, 2231−2338.

(140) Lu, W.; Huang, R.; Ding, J.; Yang, S. *J. Chem. Phys.* **1996**, *104*, 6577−6581.

(141) Tast, F.; Malinowski, N.; Frank, S.; Heinebrodt, M.; Billas, I. M. L.; Martin, T. P. *Phys. Rev. Lett.* **1996**, *77*, 3529−3532; *Z. Phys. D* **1997**, *40*, 351−354.

(142) Wei, S.; Guo, B. C.; Purnell, J.; Buzza, S.; Castleman, A. W., Jr. *Science* **1992**, *256*, 818−820.

(143) Wei, S.; Castleman, A. W., Jr. *Chem. Phys. Lett.* **1994**, *227*, 305−311.

(144) Yu, H.; Huber, M. G.; Froben, F. W. *Appl. Surf. Sci.* **1995**, *86*, 74−78.

(145) Hack, M. D.; Maclaglan, R. G. A. R.; Scuseria, G. E.; Gordon, M. S. *J. Chem. Phys.* **1996**, *104*, 6628−6630.

(146) Note that a negative dissociation energy (D_e) value (−1.24 eV) was obtained at the HF level, whereas local spin density calculations overestimated D_e at 6.06 eV.[104] Local density calculations by Reddy and Khanna yielded a D_e value of 4.51 eV.[66,150] Rather unexpectedly, similar LDA calculations by Reddy and Khanna yielded for the ground state of the T-shaped TiC_2 a binding energy of 12.21 eV only, less than the B3LYP value (13.5 eV) and very close to the experimental dissociation energy (11.8 eV).[151] Very recently, DFT calculations in the local spin density approximations were carried out by Ge et al. on a series of Ti_nC_{2n} clusters (n = 1, 6) with LANL2DZ basis sets.[152] The T-shaped structure was also found lowest in energy with a total binding energy of 14.3 eV, but at that level of approximation, the sequence of the electronic states appeared strikingly different from that found by SH. The state of lowest energy was found by Ge et al. to be the $^1A_1$ state, which was destabilized by 28 kcal·mol^{-1} in the calculations by SH. The lowest triplet state, probably corresponding to SH's ground state, appears at +45.8 kcal·mol^{-1}. A similar interversion between the lowest singlet and triplet states was found for the linear form with $C_{\infty v}$ symmetry.[152]

(147) Sumathi, R.; Hendrickx, *Chem. Phys. Lett.* **1998**, *287*, 496−502.

(148) Wachters, A. J. H. *J. Chem. Phys.* **1970**, *52*, 1033−1036.

(149) Pierloot, K.; Dumez, B.; Widmark, P.-O.; Roos, B. O. *Theor. Chim. Acta* **1995**, *90*, 87−114.

(150) Reddy, B. V.; Khanna, S. N. *J. Phys. Chem.* **1994**, *98*, 9446−9449.

(151) Stearns, C. A.; Kohl, F. J. *High Temp. Sci.* **1970**, *2*, 274; **1974**, *6*, 284.

(152) Ge, M. F.; Feng, J. K.; Yang, C.; Li, Z. R.; Sun, C. C. *Int. J. Quantum Chem.* **1999**, *71*, 313−318.

(153) Wang, X. B.; Ding, C. F.; Wang, L. S. *J. Phys. Chem. A* **1997**, *101*, 7699−7701.

(154) Sumathi, R.; Hendrickx, M. *J. Phys. Chem.* **1999**, *103*, 585−591.

(155) For a review on global optimization methods and on the state of the art concerning potential energy smoothing: see Pappu, R. V.; Hart, R. K.; Ponder J. W. *J. Phys. Chem. B* **1998**, *102*, 9725−9742. See also (a) Cvijovic, D.; Klinowski. *Science* **1995**, *267*, 664−666. (b) Hartke, B.; Schütz, M.; Werner, H.-J. *Chem. Phys. Lett.* **1998**, *239*, 561−572 and references therein. (c) Klepeis, J. L.; Floudas, C. A. *J. Chem. Phys.* **1999**, *110*, 7491−7512.

(156) For Ti_4C_8, two conformations with structures similar to forms (a) and (b) from Wang et al.[34] but somewhat more constrained concerning form (a) were obtained by Ge et al. using DFT/LSD calculations.[152] The total binding energies are consistently higher than those obtained by Wang et al., a straightforward consequence of the lack of gradient corrections (Table 7).

(157) Hendrickx, M.; Sumathi, R. Private communication.

(158) Khan, A. *Chem. Phys. Lett.* **1995**, *247*, 447−453.

(159) The prediction of an endohedral structure for $Ti_8C_{13}^+$ seems in contradiction with the ion mobility experiments of Lee et al.,[123] which yield a poor agreement with the encapsulated conformation but an excellent accord with a conformer displaying an *exohedral* carbon. This has been assigned to the difference in the experimental conditions, which could favor in the plasma source the fixation of an exohedral carbon to an already existing met-car cluster. The calculations by Muñoz et al.[21] confirm that the endohedral form is *thermodynamically* more stable for neutral Ti_8C_{13} (by 2.11 eV) as for neutral Zr_8C_{13} (by 2.54 eV). The computed binding energies of the exohedral carbon are 3.39 or 3.66 eV for the titanium cluster, according to the site of fixation, instead of 5.77 eV for an encapsulated carbon.[21]

(160) The structure of $Ti_{13}C_{13}$ constrained by symmetry in order to keep the C_2 dimer parallel to the edges of the Ti(1)−Ti(2)−Ti(3)−Ti(4) rectangle is 21 kcal·mol^{-1} higher in energy than the optimal conformation of Figure 50.
(161) To eliminate the bias due to the changing ratio of light and heavy atoms, Dance also introduces the normalization of the binding energy according to the total number of electrons, BE/ΣZ.[27] The profile of the curve in BE/ΣZ is however similar to that of the curve in ΔBE reproduced in Figure 51.
(162) Byun, Y. G.; Yeh, C. S.; Xu, Y. C.; Freiser, B. S. *J. Am. Chem. Soc.* **1995**, *117*, 8299−8303.
(163) Reddic, J. E.; Duncan, M. A. *Chem. Phys. Lett.* **1997**, *264*, 157−162.
(164) (a) Dem'yanenko, A. V.; Puretzky, A. A. *Spectrochim. Acta Part A* **1990**, *46*, 509. (b) Dem'yanenko, A. V.; Puretzky, A. A. *Sov. J. Quantum Electron.* **1990**, *20*, 1437.
(165) Jin, C.-M.; Haufler, R. E.; Hettich, R. L.; Barshick, C. M.; Compton, R. N.; Puretzky, A. A.; Dem'yanenko, A. V.; Tuinman, A. A. *Science* **1994**, *263*, 68−71.
(166) Jin, C.-M.; Haufler, R. E.; Hettich, R. L.; Barshick, C. M.; Compton, R. N.; Puretzky, A. A.; Dem'yanenko, A. V.; Tuinman, A. A. *Science* **1995**, *267*, 440−441.
(167) For *endohedral* metallofullerenes, see: (a) Chai, Y.; Guo, T.; Jin, C.; Haufler, R. E.; Chibante, L. P. F.; Fure, J.; Wang, L.; Alford, J. M.; Smalley, R. E. *J. Phys. Chem.* **1991**, *95*, 7564−7568. (b) Pradeep, T.; Kulkarni, G.; Kannan, K.; Row, T. G.; Rao, C. *J. Am. Chem. Soc.* **1992**, *114*, 2272−2273. (c) Bethune, D. S.; Johnson, R. D.; Salem, J. R.; de Vries, M. S.; Yannoni, C. S. *Nature* **1993**, *366*, 123−128. (d) Takata, M.; Umeda, B.; Nishibori, E.; Sakata, M.; Saito, Y.; Ohno, M.; Shinohara, H. *Nature* **1995,** *377*, 46−49. (e) Tomioka, Y.; Kajimara, H.; Ishibashi, M.; Taniguchi, Y. *Mol. Cryst. Liq. Cryst.* **1995**, *267*, 347. (f) Rübsam, M.; Plüschau, M.; Schweitzer, P.; Dinse, K.-P.; Fuchs, D.; Rietschel, H.; Michel, R. H.; Benz, M.; Kappes, M. M. *Chem. Phys. Lett.* **1995**, *240*, 615−621. See also refs 2−13 in ref 27. For *networked*, or *substitutional* metallofullerenes, see: (g) Clemmer, D. E.; Jarrold, M. F. *J. Am. Chem. Soc.* **1995**, *117*, 8841−8850. (h) Shelimov, K. B.; Clemmer, D. E.; Jarrold, M. F. *J. Phys. Chem.* **1994**, *98*, 12819−12821. For *exohedral* or *coated* fullerenes, see: (i) Nakajima, A.; Nagao, S.; Takeda, H.; Kurikawa, T.; Kaya, K. *J. Chem. Phys.* **1997**, *107*, 6491−6494. (j) Nagao, S.; Kurikawa, T.; Miyajama, K.; Nakajima, A.; Kaya, K. *J. Phys. Chem. A* **1998**, *102*, 4495−4500. (k) Branz, W.; Billas, I. M. L.; Malinowski, N.; Tast, F.; Heinebrodt, M.; Martin, T. P. *J. Chem. Phys.* **1998**, *109*, 3425−3430. (l) Zimmermann, U.; Malinowski, N.; Burckhardt, A.; Martin, T. P. *Carbon* **1995**, *33*, 995.
(168) For reviews, see: (a) Nagase, S.; Kobayashi, K.; Akosaka, T. *Bull. Chem. Soc. Jpn.* **1996**, *69*, 2131. (b) Nagase, S.; Kobayashi, K.; Akosaka, T. *J. Comput. Chem.* **1998**, *19*, 232−239.
(169) For theoretical works on *endohedral* metallofullerenes, see: (a) Schulke, J.; Böhm, M. C.; Dinse, K.-P. *J. Mol. Struct. (THEOCHEM)* **1998**, *427***,** 279−292 and references therein. (b) Aree, T.; Kerdcharoen, T.; Hannongbua, S. *Chem. Phys. Lett.* **1998**, *285*, 221−225. (c) Sarasola, C.; Elorza, J. M.; Ugalde, J. M. *Chem. Phys. Lett.* **1998**, *285*, 221−225. (d) Bol, A.; Scott, M. J.; Alonso, J. A. *Physica B* **1997**, *240*, 154. (e) Kobayashi, K.; Nagase, S. *Chem. Phys. Lett.* **1997**, *274*, 226−230. (f) Kobayashi, K.; Nagase, S. *Chem. Phys. Lett.* **1998**, *282*, 325−329. (g) Kobayashi, K.; Nagase, S. *Chem. Phys. Lett.* **1999**, *302*, 312−316. (h) Gou, T.; Odom, G. K.; Scuseria, G. E. *J. Phys. Chem.* **1994**, *98*, 7745−7747. (i) Wang, Y.; Tomanek, D.; Ruoff, R. S. *Chem. Phys. Lett.* **1993**, *208*, 79−85.
(170) For theoretical works on *exohedral* and on *substitutional* metallofullerenes, see: (a) Lichtenberg, L.; Wright, L.; Gruhn, N. E.; Rempe, M. *J. Organomet. Chem.* **1994**, *478*, 213−221. (b) Poblet, J. M.; Muñoz, J.; Winkler, K.; Cancilla, M.; Hayashi, A.; Lebrilla, C. B.; Balch, A. L. *J. Chem. Soc., Chem. Commun.* **1999**, 493−494.
(171) (a) Hunter, J.; Fye, J.; Jarrold, M. F. *J. Phys. Chem.* **1993**, *97*, 7, 3460−3462. (b) von Helden, G.; Gotts, N. G.; Bowers, M. T. *J. Am. Chem. Soc.* **1993**, *115*, 4363−4364.
(172) von Helden, G.; Hsu, M.-T.; Kemper, P. R.; Bowers, M. T. *J. Chem. Phys.* **1991**, *95*, 3835−3837.
(173) Clemmer, D. E.; Shelimov, K. B.; Jarrold, M. F. *J. Am. Chem. Soc.* **1994**, *116*, 5971−5972.
(174) (a) Gingerich, K. A. *J. Chem. Phys.* **1968**, *49*, 14−18. (b) Gingerich, K. A. In *Current Topics in Materials Science*; Kaldis, E., Ed.; North-Holland, Amsterdam, 1980; Vol. 6, pp 347−462. (c) Gupta, S. K.; Kingkade, J. E., Jr.; Gingerich, K. A. *Adv. Mass Spectrom.* **1980**, *8*, 445−451.
(175) (c) Kingcade, J. E., Jr.; Cocke, D. L.; Gingerich, K. A. *High Temp. Sci.* **1983**, *16*, 89−109.
(176) For ScC_2: (a) Haque, R.; Gingerich, K. A. *J. Chem. Phys.* **1981**, *74*, 6407−6414. (b) Kohl, K. A.; Stearns, C. A. *J. Chem. Phys.* **1971**, *54*, 1414−1416. (c) Drowart, J.; Verhaegen, G.; Simoes, S. *Annu. Conf. Mass Spectrom. Allied Top.* **1963**, *11*, 329−335.
(177) For YC_2: (a) Pelino, M.; Haque, R.; Bencivenni, L., Gingerich, K. A. *J. Chem. Phys.* **1988**, *88*, 6534−6539. (b) De Maria, G.; Guido, M.; Malaspina, M.; Pesce, B. *J. Chem. Phys.* **1965**, *43*, 4449−4452. (c) Kohl, K. A.; Stearns, C. A. *J. Chem. Phys.* **1970**, *52*, 6310−6315.
(178) (a) Gingerich, K. A.; Pelino, M.; Haque, R. *High Temp. Sci.* **1981**, *14*, 137−151. (b) Gingerich, K. A.; Haque, R.; Pelino, M. *J. Chem. Soc., Faraday Trans. 1* **1982**, *78*, 341−346. (c) Chupka, W. A.; Berkowitz, J.; Giese, C. F.; Inghram, M. G. *J. Phys. Chem.* **1958**, *62*, 611−614. (d) Stearns, C. A.; Kohl, F. J. *J. Chem. Phys.* **1971**, *54*, 5180−5187.
(179) (a) McElvany, S. W.; Cassady, C. J. *J. Phys. Chem.* **1990**, *94*, 4, 2057−2062. (b) Cassady, C. J.; McElvany, S. W. *J. Am. Chem. Soc.* **1990**, *112*, 4788−4797.
(180) Roszak, S.; Balasubramanian, K. *Chem. Phys. Lett.* **1995**, *246*, 20−25.
(181) Roszak, S.; Balasubramanian, K. *J. Phys. Chem.* **1996**, *100*, 8254−8259.
(182) Roszak, S.; Balasubramanian, K. *J. Phys. Chem. A* **1998**, *102*, 6004−6009.
(183) Roszak, S.; Balasubramanian, K. *J. Phys. Chem. A* **1997**, *101*, 2666−2669.
(184) Roszak, S.; Balasubramanian, K. *J. Phys. Chem.* **1996**, *100*, 11255−11259.
(185) Roszak, S.; Balasubramanian, K. *Chem. Phys. Lett.* **1996**, *254*, 274−280.
(186) The FOCI expansion includes (i) all configurations of the CASSCF treatment and (ii) all configurations generated by distributing all active electrons but one in the CASSCF active space and one electron in the external space.
(187) (a) Maier, J. P. *J. Phys. Chem. A* **1998**, *102*, 3462−3469. (b) Brown, S. T.; Rienstra-Kiracofe, J. C.; Schaefer, H. F. **1999**, *103*, 4065−4077.
(188) Watts, J. D.; Bartlett, R. J. *J. Chem. Phys.* **1992**, *96*, 6073−6084.
(189) von Helden, G.; Gotts, N. G.; Maitre, P.; Bowers, M. T. *Chem. Phys. Lett.* **1994**, *227*, 601−608.
(190) Fan, J.; Wang, L.-S. *J. Phys. Chem.* **1994**, *98*, 11814−11817.
(191) Wang, L.-S. *Surf. Rev. Lett.* **1996**, *3*, 423−427.
(192) Fan, J.; Lou, L.; Wang, L.-S. *J. Chem. Phys.* **1995**, *102*, 2701−2707.
(193) Cao, Z. *J. Mol. Struct. (THEOCHEM)* **1996,** *365***,** 211−214.
(194) (a) Langhoff, S. R.; Davidson, E. R. *Int. J. Quantum Chem.* **1974**, *8*, 61−72. (b) Davidson, E. R.; Silver, D. W. *Chem. Phys. Lett.* **1977**, *52*, 403−406.
(195) Arbuznikov, A. V.; Hendrickx, M.; Vanquickenborne, L. G. *Chem. Phys. Lett.* **1999**, *310*, 515−522.
(196) Nash, B. K.; Rao, B. K.; Jena, P. *J. Chem. Phys.* **1996**, *105*, 11020−11023.
(197) (a) Binns, C.; Baker, S. H.; Keen, A. M.; Mozley, S. N.; Norris, C.; Derbyshire, H. S.; Bayliss, S. C. *Phys. Rev. B* **1996**, *53*, 7451. (b) Baumer, M.; Libuda, J.; Freund, H.-J. *Surf. Sci.* **1995**, *327*, 321.
(198) (a) Kruger, P.; Rakotomahevitra, A.; Parlebas, J.-C.; Demangeat, C. *Phys. Rev. B* **1998**, *57*, 5276. (b) Duffy, D. M.; Blackman, J. A. *Phys. Rev. B* **1998**, *58*, 7443.
(199) Andriotis, A. N.; Menon, M.; Froudakis, G. E.; Lowther, J. E. *Chem. Phys. Lett.* **1999**, *301*, 503−508.
(200) (a) Andriotis, A. N.; Menon, M. *Phys. Rev. B* **1998**, *58*, 7443. (b) Lathiotakis, N. N.; Andriotis, A. N.; Menon, M. *J. Chem. Phys.* **1996**, *104*, 992−1003.
(201) Byun, Y. G.; Kan, S. Z.; Lee, S. A.; Kim, Y. H.; Miletic, M.; Bleil, R. E.; Kais, S.; Freiser, B. S. *J. Phys. Chem.* **1996**, *100*, 6336−6341.
(202) Yamada, Y.; Castleman, A. W., Jr. *Chem. Phys. Lett.* **1993**, *204*, 133−138.
(203) Dance, I. *J. Chem. Soc., Chem. Commun.* **1993**, 1306−1308.
(204) Dance, I. *J. Am. Chem. Soc.* **1993**, *115*, 11052−11053.
(205) Dance, I. G. *Aust. J. Chem.* **1993**, *46*, 727−730.

CR9803885